COMPUTATIONAL HEMODYNAMIC ANALYSIS OF STENOSED CORONARY ARTERY

SARFARAZ KAMANGAR

FACULTY OF ENGINEERING

UNIVERSITY OF MALAYA

KUALA LUMPUR

2016

COMPUTATIONAL HEMODYNAMIC ANALYSIS OF STENOSED CORONARY ARTERY

SARFARAZ KAMANGAR

THESIS SUBMITTED IN FULFILMENT OF THE REQUIREMENTS FOR THE DEGREE OF DOCTOR OF PHILOSOPHY

FACULTY OF ENGINEERING

UNIVERSITY OF MALAYA

KUALA LUMPUR

2016

UNIVERSITI MALAYA

ORIGINAL LITERARY WORK DECLARATION

Name of Candidate: Sarfaraz Kamangar C/Passport No:

Registration/Matric No: KHA130108

Name of Degree: Ph.D Engineering

Title of Project Paper/Research Report/Dissertation/Thesis ("this Work"):

COMPUTATIONAL HEMODYNAMIC ANALYSIS OF STENOSED CORONARY ARTERY

Heat Transfer

I do solemnly and sincerely declare that:

(1) I am the sole author/writer of this Work;
(2) This Work is original;
(3) Any use of any work in which copyright exists was done by way of fair dealing and for permitted purposes and any excerpt or extract from, or reference to or reproduction of any copyright work has been disclosed expressly and sufficiently and the title of the Work and its authorship have been acknowledged in this Work;
(4) I do not have any actual knowledge nor do I ought reasonably to know that the making of this work constitutes an infringement of any copyright work;
(5) I hereby assign all and every rights in the copyright to this Work to the University of Malaya ("UM"), who henceforth shall be owner of the copyright in this Work and that any reproduction or use in any form or by any means whatsoever is prohibited without the written consent of UM having been first had and obtained;
(6) I am fully aware that if in the course of making this Work I have infringed any copyright whether intentionally or otherwise, I may be subject to legal action or any other action as may be determined by UM.

Candidate's Signature Date

Subscribed and solemnly declared before,

Witness's Signature Date

Name:
Designation:

ABSTRACT

The coronary artery disease is a leading cause of death all over the world. The primary cause of coronary artery disease is the arthrosclerosis. There are various causes of stenosis formation primarily linked to food habits. There has been continuously growing interest to understand the blood flow behaviour in Atherosclerosis condition due to its serious impact on human life. It is believed that hemodynamic plays an important role in further progression of these coronary artery diseases. In this study, an investigation of variation in hemodynamic and diagnostic parameters in the left coronary artery was carried out based on idealistic and realistic patient specific models of left coronary arteries in diseased and normal condition during hyperthermia. The CT scan images of suspected patients of coronary artery disease were acquired to reconstruct the 3D models of realistic left coronary models. Computational fluid dynamics is used to reflect the in vivo cardiac hemodynamic. The wall pressure, velocity flow pattern, and wall shear stress were calculated during the cardiac cycle. To investigate the effect of shapes of stenosis on hemodynamic and diagnostic parameters, three different shapes of stenosis models (elliptical, trapezoidal and triangular) are studied. The highest level of pressure drop was observed for trapezoidal shape of stenosis followed by elliptical and then by triangular shaped stenosis. The increase in percentage area stenosis, increases the velocity profile inside the blockage region. The variation in FFR in the region of 76.5-82.7% AS could lead to the misdiagnosis of intermediate stenosis to decide upon coronary intervention around the clinically used cut-off value of 0.75. The influence of angle of curvature of artery i.e. 30^0, 60^0, 90^0 and 120^0 on hemodynamic parameters was investigated. It is found that the blood flow

behaviour is substantially affected by the combined effect of stenosis and the curvature of artery. The presence of curvature provides low blood flow region at the lower wall of artery creating a potential stenotic region. The effect of different degree of stenosis on various locations in patient's specific left coronary artery on hemodynamic parameters have been studied by using CT scan images during hyperemic conditions. The decrease in pressure was found downstream to the stenosis as compared to the coronary artery without stenosis. The velocity increases with the increase in the percentage area stenosis. The result also shows that the re-circulation zone was observed immediate to the stenosis and highest wall shear stress was observed across the stenosis. The maximum pressure drop was found for the models having stenosis of 70% and 90% at the left main stem and left circumflex branch respectively. Thus it can be conveniently said that the case of 70% AS located at left main stem and 90% AS at left circumflex is the most severe condition among 10 models being investigated.

ABSTRAK

penyakit arteri koronari adalah penyebab utama kematian di seluruh dunia. Punca utama penyakit arteri koronari adalah arthrosclerosis itu. Terdapat pelbagai sebab pembentukan stenosis terutamanya dikaitkan dengan tabiat makanan. Terdapat minat terus berkembang untuk memahami tingkah laku aliran darah dalam keadaan Aterosklerosis disebabkan kesan yang serius terhadap kehidupan manusia. Adalah dipercayai bahawa hemodynamic memainkan peranan yang penting dalam perkembangan selanjutnya penyakit-penyakit arteri koronari. Dalam kajian ini, siasatan variasi parameter hemodynamic dan diagnostik dalam arteri koronari kiri telah dijalankan berdasarkan model tertentu pesakit idealistik dan realistik arteri koronari kiri dalam keadaan berpenyakit dan biasa pada hyperthermia. CT imej scan pesakit yang disyaki penyakit arteri koronari telah dibeli untuk membina semula model 3D realistik model koronari kiri. Pengiraan dinamik bendalir digunakan untuk mencerminkan in vivo hemodynamics jantung. Tekanan dinding, corak aliran halaju, dan tekanan dinding ricih dikira semasa kitaran jantung. Untuk mengkaji kesan bentuk stenosis pada parameter hemodynamic dan diagnostik, tiga bentuk yang berbeza daripada model stenosis (elips, trapezoid dan segi tiga) sedang dikaji. Tahap tertinggi kejatuhan tekanan diperhatikan untuk bentuk trapezoid stenosis diikuti oleh elips dan kemudian oleh stenosis berbentuk segi tiga. Peningkatan kawasan peratusan stenosis, meningkatkan profil halaju di dalam rantau yang tersumbat. Perubahan dalam FFR di kawasan 76.5-82.7% AS boleh membawa kepada misdiagnosis stenosis perantaraan untuk membuat keputusan ke atas campur tangan koronari sekitar nilai cut-off secara klinikal digunakan sebanyak 0.75. Pengaruh sudut kelengkungan iaitu 30^0, 60^0, 90^0 dan 120^0 pada parameter hemodynamic disiasat. Ia didapati bahawa kelakuan aliran darah dengan ketara terjejas oleh kesan gabungan stenosis dan kelengkungan arteri. Kehadiran

kelengkungan menyediakan kawasan aliran darah rendah pada dinding yang lebih rendah daripada arteri mewujudkan rantau stenotic yang berpotensi. Kesan daripada tahap yang berbeza stenosis di pelbagai lokasi di tertentu arteri koronari kiri pesakit pada parameter hemodynamic telah dikaji dengan menggunakan CT imej imbasan semasa keadaan hyperemic. Penurunan tekanan ditemui hiliran untuk stenosis berbanding arteri koronari tanpa stenosis. halaju meningkat dengan peningkatan dalam kawasan peratusan stenosis. Hasil kajian juga menunjukkan bahawa zon edaran semula diperhatikan segera untuk stenosis dan paling tinggi tekanan dinding ricih diperhatikan seluruh stenosis. Penurunan tekanan maksimum didapati untuk model masing-masing mempunyai stenosis sebanyak 70% dan 90% pada batang utama kiri dan cawangan sirkumfleks kiri. Oleh itu, ia boleh ditemui dengan mudah berkata, kes itu sebanyak 70% AS terletak di batang utama kiri dan 90% pada sirkumfleks kiri adalah keadaan yang paling teruk di kalangan 10 model sedang disiasat.

ACKNOWLEDGEMENT

First of all, I would like to thank Almighty ALLAH Subhana Watalah for giving me strength, determination and ability to complete this thesis. After that, I would like to express my sincerest gratitude to my supervisors Associate Professor Dr. Irfan Anjum Magami, Dr. Ahmad Badarudin Bin Mohamad Badry and Associate Professor Dr. Nik Nazri Bin Nik Ghazali for their excellent guidance and constant encouragement throughout this work.

Furthermore, I would like to express gratitude to my colleagues Dr. Govindaraju and Dr. Salman Ahmed khan and for their assistance, suggestions and help during this course.

I would also like to thank University of Malaya for the research funding support through University Malaya research grant (UMRG) and Post graduate research grant (PPP).

Lastly, I would like to thank my parents and family for their affection and continuous encouragement to accomplish this course.

TABLE OF CONTENTS

LIST OF FIGURES

LIST OF TABLES

LIST OF ABBREVIATION AND SYMBOLS

LCA	Left Coronary Artery
RCA	Right Coronary Artery
LAD	Left Anterior Descending
LCX	Left circumflex
CAD	Coronary artery disease
CCTA	Coronary computed tomographic angiogram
IVUS	Intravascular ultrasound
CFD	Computational Fluid Dynamic
FFR	Fractional Flow Reserve
MRI	Magnetic resonance imaging
SST	Shear Stress Transport
AS	Area Stenosis
DICOM	Digital Imaging and Communications in Medicine
CT	Computed Tomography
HU	Hounsfield Units
CDP	Pressure Drop Coefficient
LFC	Lesion Flow Coefficient
LMS	Left Main Stem
LDL	Low-density Lipoproteins
NURD	Non-uniform rotational distortion
WPSG	Wall pressure stress gradient
IEL	Internal elastic lamina
MI	Myocardial infarction

3D	Three Dimensional
2D	Two Dimensional
m/s	Meter per Second
Pa	Pascal
ml/min	Milliliters Per Second
Kg/m^3	Kilogram per cubic meter
ρ	Density
v	Three dimensional velocity
p	Pressure
τ	Stress tensor
μ	Blood viscosity
μ_0	Low shear viscosity
μ_∞	High shear viscosity
λ	Time constant
t	Time
Re_T	Turbulence Reynolds number
k	Turbulence kinetic energy
ω	Turbulent frequency
ε	Turbulence eddy dissipation
$\Delta\tilde{p}$	Time average pressure drop
Re	Reynolds number

CHAPTER 1: INTRODUCTION

1.1 Background

Human knowledge has been progressing since centuries but last few decades have seen an explosion of knowledge in almost every aspect of life. In-spite of such an advancement of knowledge, there are few fields which are still as new as it could have been to the stone-age people. One such field of study is the human body which is such a complex and fascinating system to study. There are many individual subsystems in human body which collectively work together as one organic entity. There are various important organs in the human body among which the heart can be argued to be the most important organ because of its function of circulating blood to all body parts. Typically human heart weighs about is 250 - 350 gm though diseased heart can have much higher weight. The dimension of an adult heart could be 12cm x8cm x6cm. Heart is primarily comprised of 4 chambers namely left atrium, left ventricle, right atrium and right ventricle. The left side chambers handle the oxygenated blood whereas the right side chambers processes deoxygenated blood. The deoxygenated blood from right side of the heart flows to lungs, where it is loaded with oxygen and returns to the left side of the heart. The oxygenated blood from the left side of the heart flows to all tissues of the body (with the exception of the heart and lungs). Some of the facts of heart are truly mind boggling. For instance, it is estimated that the heart beats about 2.65 billion times and pumps about 194 million liters of blood in 70 years of life span.

This is similar to an amount of blood contained in a swimming pool of dimension 1km long, 100m wide and 2m depth. Supply of blood to body parts is such a crucial requirement for nourishment and functioning of that particular part. Like all other organs which require blood supply for function, heart itself needs adequate

oxygen and nourishment supplied through blood circulation to heart muscles for keeping itself in active state of pumping.

1.2 Coronary arteries

It is estimated that 4-6% of total blood supplied by heart is fed to heart muscles (Myer, 2003) through coronary arteries that are responsible to channel the blood to heart tissues. The main function of the coronary arteries is to supply the oxygenated blood and nutrient to the cardiac muscle. The coronary arteries are small arteries of diameter about 3 to 5mm originating from top of the aorta. There are two main coronary arteries called Left coronary artery (LCA) and Right coronary artery (RCA) that further subdivide into branches as depicted in figure 1.1. The initial segment of the left coronary artery (LCA) branches into two smaller arteries namely (Figure 1.2) left anterior descending artery (LAD) and left circumflex coronary artery (LCX) (Waite & Fine, 2007).

- Left Circumflex artery (LCX) that supplies blood to the left atrium, side and back of the left ventricle

- Left Anterior Descending artery (LAD) that supplies the front and bottom of the left ventricle and the front of the septum

The right coronary artery branches into

- Right marginal artery

- Posterior descending artery

The right side of human heart is smaller than left side. The right side of heart receives blood from right coronary artery which is active in pumping the blood to lungs for oxygenation, which pumps blood to the lungs. The rest of the right coronary artery and its main branch, the posterior descending artery, together with the branches of the

circumflex artery, run across the surface of the heart's underside, thus making sure that the bottom portion of the left ventricle and back of the septum are supplied with adequate blood. The left coronary artery (LCA) supplies blood to approximately 75% of the cardiac muscle. The remaining portion of the heart receives blood from right coronary artery (RCA). The coronary arteries are known to have significant tortuosity (twist/bend) and tapering after the branching from aorta. There is turbulence in blood flow inside the coronary arteries because of high flow rate and tortuosity. The non-dominant right coronary artery and their branches are shown in figure 1.3.

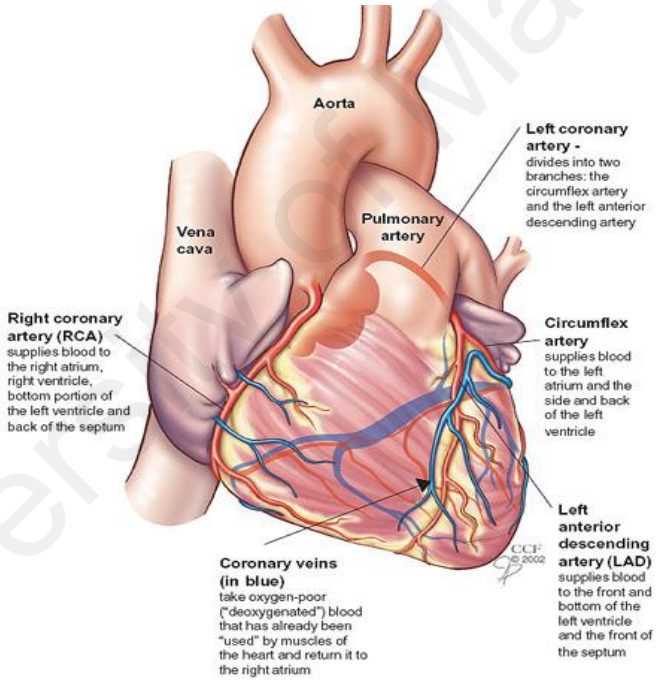

Figure 1.1: Coronary arteries of heart (http://my.clevelandclinic.org)

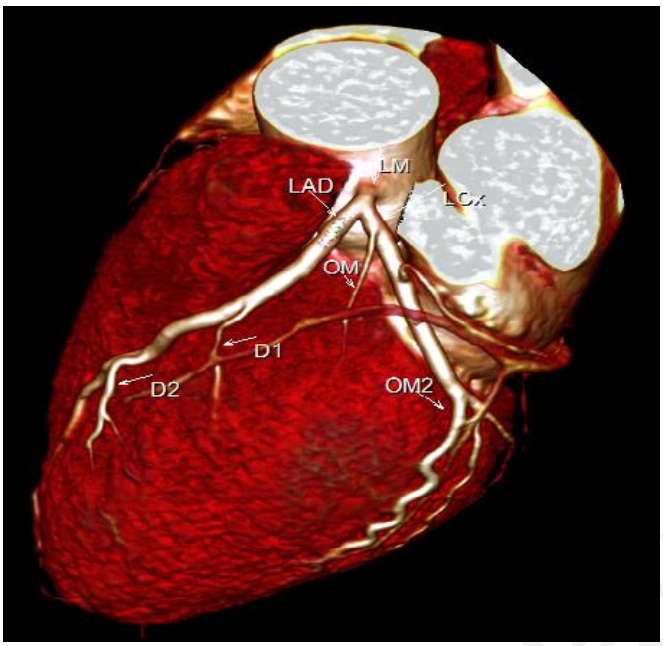

Figure 1.2: Volume-rendered image of the left coronary artery (LCA)

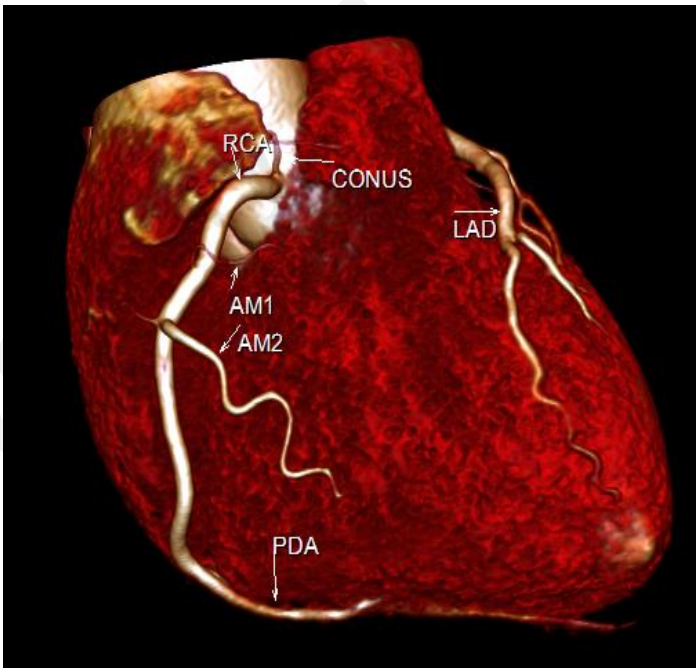

Figure 1.3: Volume-rendered image of the right coronary artery (RCA)

The supply of blood to the heart muscles can get hindered leading to very serious diseases such as atherosclerosis. The atherosclerosis is characterized by thickening of

arterial wall due to deposition of undesirable materials such as cholesterol, fatty substances, cellular waste products, calcium and fibrin (a clotting material in the blood) etc. as shown in figure 1.4. This is a condition in which plaque builds up inside the arteries which reduces the effective blood flow area of artery that eventually reduces the blood supply to heart muscles. The Coronary Artery Disease (CAD) is the leading cause of death across all over the world which has claimed millions of lives.

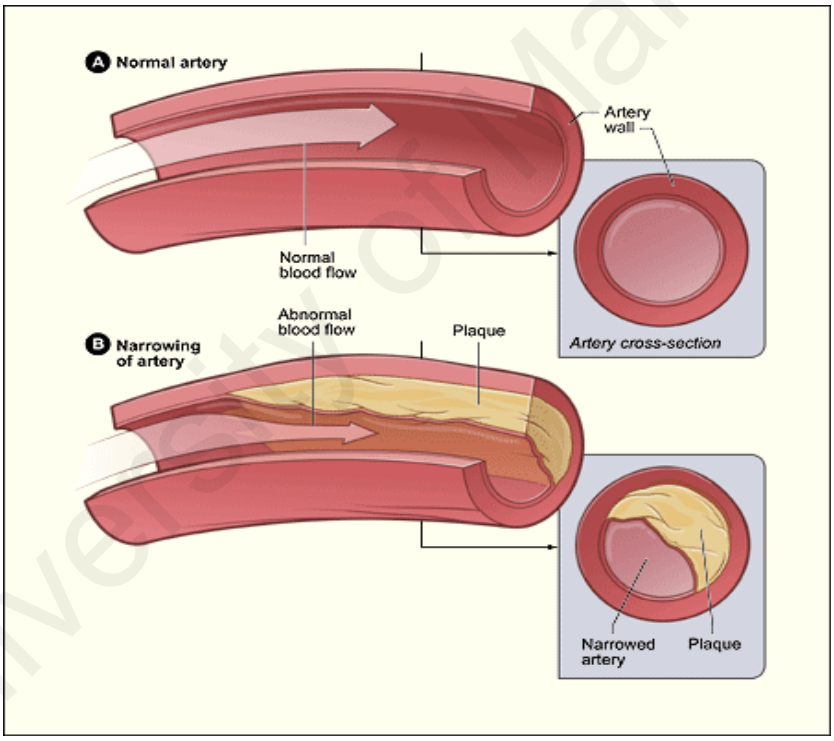

Figure 1.4: Thickening of artery (http://cardiac.surgery.ucsf.edu/)

According to the World Health Organization (WHO) fact sheet, ischeamic heart disease which is a result of reduced blood flow, has caused the death of 7.4 million people (figure 1.5) in the year 2012 alone (www.who.int) , constituting about 25% of total diseased death recorded. There are various diagnostic tools being used to identify

the narrowing of arteries due to plaques which includes the coronary angiography, Coronary computed tomographic angiogram (CCTA), intravascular ultrasound (IVUS) etc. These techniques are handy in identifying the anatomical significance of stenosis but do not provide any idea about functional significance of the stenosis. Thus a technique based on fluid dynamics analysis namely Computational Fluid Dynamic (CFD) is gaining popularity in assessing the flow dynamics of blood inside the arteries which is proving to be a useful tool in clinical decision making.

For instance, the fractional flow reserve (FFR) is one of the important parameter in assessing the functional severity of stenosis which is nothing but the ratio of maximum myocardial flow in artery having stenosis to the maximum myocardial flow had the stenosis been absent. This flow ratio is also expressed as the ratio of the distal coronary pressure to the aortic pressure (N. H. Pijls et al., 1995; N. H. J. Pijls & Sels, 2012). Thus FFR has a value of 1 for normal person without stenosis. The measurement of FFR in a clinical setting is carried out by inserting a guide wire in the vicinity of stenotic area. However, it influences the measured value due to resistance offered by guide wire. Here comes the advantage of using computational fluid dynamics that can assess the required FFR without affecting the blood flow behavior.

It is believed that the blood flow behavior has more to offer in terms of understanding of further thickening of stenosis and to indicate the vulnerable areas for the formation of fresh stenosis which is difficult to assess with direct measurement techniques. The detailed study of the gradual narrowing or bulging of the artery will help in understanding the underlying mechanisms for such unusual behavior (Fung, 1984; Nichols, 1998). It has been found that the fluid mechanical forces due to the interaction of the blood flow and the arterial wall have a strong influence on the initiation and progression of narrowing or bulging of the artery (Alberto Figueroa C., 2006). Clinical observations assisted by imaging techniques such as angiography,

computed tomographic angiogram (CTA), Magnetic resonance angiography (MRA) or duplex scanning does not provide sufficient and elaborated detailed insight into the mechanisms of formation and development of stenosis (Bernsdorf & Wang, 2009). The available imaging techniques today have their own limitations though they are useful for primary investigation.

These techniques are very useful in understanding the anatomy of various abnormalities taken place on arteries but fail to give realistic blood flow behavior specially in terms of secondary variables such as shear stress, gradients and also in identifying the fluid circulation regions that are crucial to predict the futuristic development of such abnormalities or in predicting the functional severity of those abnormalities. Thus an alternate route that of computational fluid dynamics is followed by many researchers to study the hemodynamic (blood dynamics) characteristics under various conditions. It is important to note that the CFD is completely noninvasive technique that can answer many questions related to hemodynamic behavior. The beauty of CFD lies in answering many what if scenarios arising from questions related to geometric changes in abnormalities (such as stenosis) or the physical condition that the patient may come across during the lifetime. It provides a clear picture of hemodynamic that in conjunction with the imaging techniques can prove to be a great asset in diagnosis and treatment of coronary artery or any other artery disease. It is observed from current state of literature in the field of hemodynamic of coronary artery that there is not enough information available pertaining to specific area stenosis size such as 70%, 80% and 90%. These area stenosis sizes can be fatal to patients and poses huge dilemma to clinicians to decide about the treatment process to be adopted.

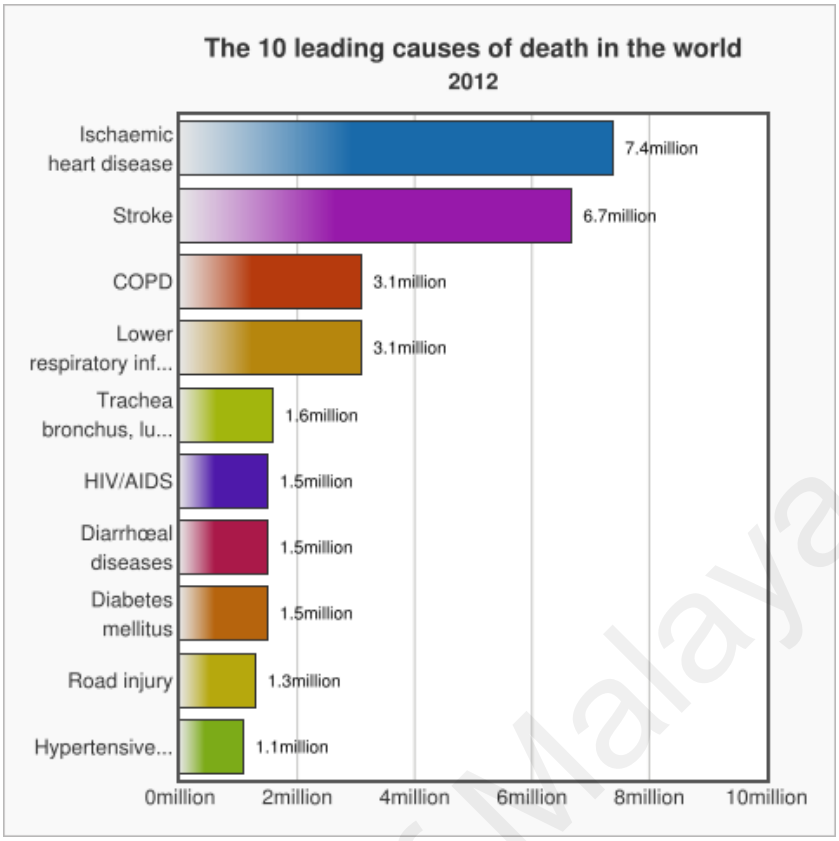

Figure 1.5: Leading causes of death (WHO)

1.3 Computational fluid dynamics for blood flow analysis

Computational fluid dynamics (CFD) has emerged as a major tool in analyzing the fluid flow problems ranging from weather forecast to aerodynamic flow, river flow, many complex industrial flow problems etc. CFD is a branch of fluid mechanics that uses numerical methods and algorithms to tackle complex flow problems. CFD has established itself as one of reliable tool in predicting the complex flow behavior including the fluid flow in human body. Recent time has witnessed increased use of computational fluid dynamic to understand the blood flow behavior such as flow in arteries and veins. The CFD technique allows for the analysis of different clinical situations. This technique eliminates the complicated and expensive in vivo measurements enabling quantification of the hemodynamic of healthy and diseased blood vessels. In many cases CFD has been applied successfully to provide missing data

that cannot be obtained by experimental means such as Wall Shear Stress (WSS) distribution and many other hemodynamic parameters that has led to improved clinical decision-making

1.4 Aims and Objectives

In the light of available literature explained in chapter 2, the following objectives are set to investigate the hemodynamic of coronary artery disease.

1. To investigate the effect of different geometrical shapes of stenosis in coronary artery on the hemodynamics and diagnostic parameters.

2. To study the influence of angle of curvature in coronary artery on the hemodynamic parameters such as wall pressure, pressure gradient, velocity and wall shear stress.

3. To study the effect of stenosis in a realistic patient left coronary artery on the blood flow behavior.

4. To investigate the effect of different degree of stenosis on hemodynamic parameters in left coronary artery.

5. To study the influence of multi stenosis on the hemodynamic parameters in realistic left coronary artery.

1.5 Scope of Study

The current work is focused to investigate the hemodynamic characteristics of blood flow in a diseased left coronary artery (LCA) using computational fluid dynamics. The present research work initially started with an idealized computer aided

design model of 3D coronary artery which was subjected to various shapes of stenosis (Elleptical, Trapezoidal and triangular), as well as the curvature angles (30^0 60^0 , 90^0 and 120^0). Further, the research continues to evaluate the hemodynamic behavior as well as diagnostic parameters of blood inside a patient specific realistic artery subjected to various higher degrees of stenosis i.e. 70%, 80% and 90% area stenosis, created in the main left coronary artery. Further investigation is carried out to judge the effect of multiple stenosis in various degrees along the sub branches of left coronary artery. A total of 10 models of multi-stenosis are investigated. The scope of study is limited to higher degree of area stenosis i.e. 70%, 80% and 90% subjected to hyperemic condition.

1.6 Organization of Thesis

This thesis has been presented in 5 chapters that systematically explain the objectives of this thesis research. The description of each chapter is as follows:

The first chapter describes a comprehensive background about the physiological functions, anatomy and diseases of coronary artery. The objectives and scope are also presented in the introduction chapter.

Chapter 2 provides an extensive background of this study with reviewing literature of most relevant literature in this field.

In the third chapter governing equation of blood flow in left coronary artery, with the modeling of realistic coronary artery model by CT scan data and solution methodology obtained in detail.

Chapter 4 is important part of this thesis describes the detailed investigation of blood flow in coronary artery with different shapes of stenosis, varying the angle of

curvature, and various degrees of stenosis were presented. Chapters 5, provides the conclusion and recommendations for the future works.

CHAPTER 2: LITERATURE REVIEW

2.1 Introduction

The immense research in the field of hemodynamic during the last few decades shows its importance as evident by extensive amount of research carried out by eminent researchers. The purpose of this chapter is to provide some of the related information regarding the research being carried out pertaining to blood flow analysis in various arteries by different researchers across the world.

Human heart is extremely important organ in the human body that supplies the blood throughout the body that in turn carries the oxygen and other nutrition vital for the development and sustenance of human body. Heart is typically made up of four chambers such as right atrium, left atrium, right ventricle and left ventricle (Myer, 2003).

There are two distinct mode of heart pumping namely systole and diastole. The systole and diastole takes place with perfect synchronisation for a normal heart. Contraction of the ventricular myocardium ejects blood into the aorta and pulmonary arteries. The heart has many valves that regulate the flow in one direction from one chamber to another and between chambers and arteries. In diastole phase, the arterial contracts that results into blood being pumped from left and right atrium to the left and right ventricles whereas in the systolic phase, ventricles contract causing the blood to be pumped from right ventricle to lungs through pulmonary artery and left ventricle to aorta. During systole, the blood flows to different organs through aorta. However, flow to coronary arteries is blocked by aortic valve during systole thus flow to these arties is achieved during diastole phase of cardiac cycle. The heart itself is comprised of tissues like other body parts and it too requires blood supply to keep functioning. The interruption of blood supply to the heart leads to serious consequences leading to death of the person in

most of the cases. Myocardial infarction which is known as heart failure in layman terminology is caused by blockages in the coronary arteries and this is major fatal disease in the world.

Coronary arteries are the main arteries that are responsible to supply blood to heart muscle (Myer, 2003), There are two main coronary arteries namely left coronary artery (LCA) and right coronary artery (RCA) that further subdivides into branches as shown in figure 2.1. The two arteries together envelop the entire heart with left coronary artery covering larger area and right coronary artery comparatively lesser area of heart.

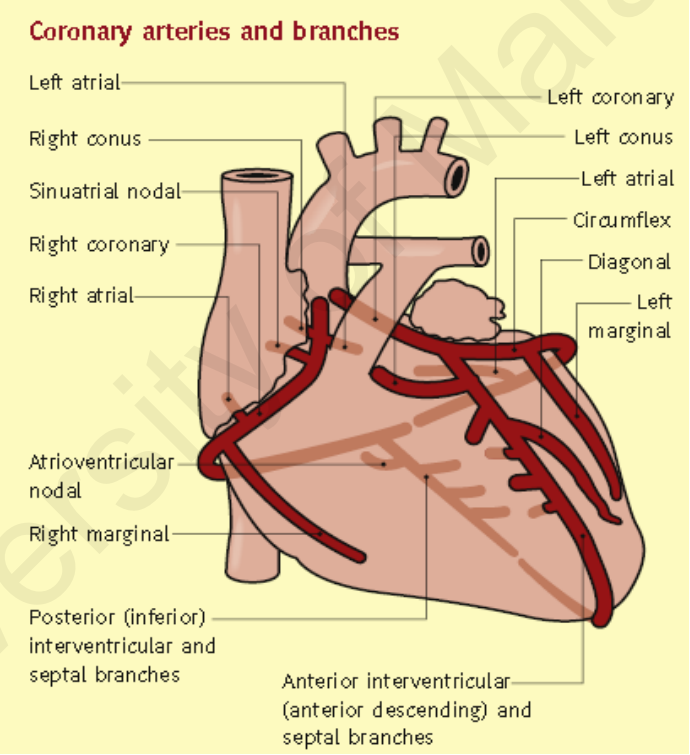

Figure 2.1: Coronary arteries

The arteries carrying blood from heart are normally straight that results into efficient transport various organs. However, it is possible that the arteries may become tortuous leading to vascular disease. Tortuous or twisted arteries and veins are commonly seen in humans and animals from common angiographic findings (Han, 2012). The

hemodynamic analysis of flow in the arteries has been a quite involved task due to such a complex geometry and flow mechanism of heart. There are many Computational fluid dynamics models being developed over the years to deal with hemodynamic of arteries. Several finite-element structural models were also developed in order to address the nonlinearities arising due to material and geometry of valves etc, (D Bluestein & Einav, 1993; Danny Bluestein, Einav, & Hwang, 1994). The following sections further elaborate the research being dedicated to study the hemodynamic of heart.

2.2 Numerical methods of blood flow in arteries

Numerical study has become an essential part of any research activity covering a wide range of human knowledge. This is particularly true for the case of scientific studies that are plagued by too much complexity in geometry involved or the difficult boundary conditions of complex problems. Hemodynamic is one such field that has been immensely benefitted by employing the techniques originating from numerical mathematics. Numerical Study is extensively used in biomechanics in recent years to have a better understanding of blood flow in the human body due to the intricacy involved in the vessel geometry as well as the complex hemodynamic mechanism (Botar et al., 2009; Brosig et al., 2014; Byun & Rhee, 2004; Jhunjhunwala, et al, 2015; Jung & Hassanein, 2008; Leuprecht, et al. 2002; Lorenzini & Casalena, 2008). Among the numerical techniques, finite volume method is most popular and adopted technique for hemodynamic study. These techniques deal with the governing Navier Stokes equations which are too difficult to solve thus most of the numerical studies being carried out revolve around the sophisticated software that has helped immensely in tackling such complex phenomenon. These techniques essentially require that the actual domain be divided into a number of smaller segments generally known as elements. The governing equations are applied to these small segment of the whole domain and the

continuous solution is obtained over entire set of elements that provide continuity at the nodal points. These numerical techniques are well coded into a number of software tools. Among the available software, it can be concluded that the most popular are ANSYS CFX (Alishahi, et al. 2011; Chaichana, et al., 2011, 2013a, 2014; George et al., 2008; Toloui, et al. 2012) and Fluent (Andersson, et al., 2000; Botar et al., 2009; Byun & Rhee, 2004; Keshavarz-Motamed & Kadem, 2011; Li, Beech-Brandt, et al., 2007; Paul & Larman, 2009; Sinha Roy, et al., 2006; Soulis, et al., 2006; Su et al., 2014; Zhang et al., 2012). Apart from the CFX and Fluent, there are other codes such as Comsol Multi-physics (Lorenzini & Casalena, 2008). Few researchers have developed simplified mathematical models to address a specific issue of blood flow in the artery. For instance a mathematical model is developed by Ai and Vafai (Ai & Vafai, 2006) that low-density lipoproteins (LDL), in the blood stream and in the arterial walls by making use of coupled analysis of the transport of macromolecules, This was made possible by using the advection–diffusion equations of porous media to model the species field in the arterial wall layers. The model is used to simulate the LDL transport in a stenosed artery with various area reductions and stenosis numbers. It is claimed that the above model has advantage of reliable results. There are other efforts also to evaluate the blood flow in artery such as that of Ikbal (Ikbal, 2012) to develop a two-dimensional mathematical model of viscoelastic fluid characterised by generalised Oldroyd-B fluid. Mustapha et al. (Mustapha, Mandal, Johnston, & Amin, 2010) developed a mathematical model of blood flow through an arterial segment with a couple of stenosis having surface irregularities. The governing equations of motion were solved by MAC (Marker and Cell) method.

2.2.1 Anatomy of arteries

The human vessels are too complex when it comes to analysing the geometrical aspect. Though the vessels are nearly cylindrical in geometry but, processes a huge web

of tiny cylindrical passages that allows the blood to flow efficiently to all required regions. In general, the main coronary arteries of heart have a diameter of roughly 1.5 to 4.5 mm (Zeev Vlodaver 2012). The normal arterial wall consists of endothelium, intima, internal elastic lamina (IEL), media and adventitia (Ai & Vafai, 2006) as shown in figure 2.2 . It is believed that the permeability of endothelium wall increases with deposition of cholesterol due to the damaged or inflamed arterial wall.

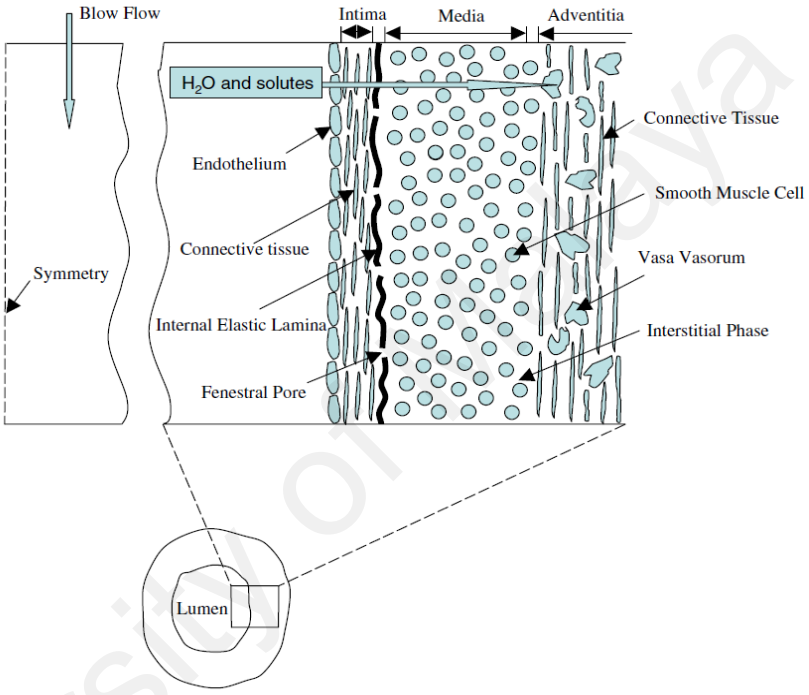

Figure 2.2: Cross section of blood vessel wall (Ai & Vafai, 2006)

The coronary arteries are main arteries that supply blood to heart. The amount of blood to be supplied is basically dictated by human activities that in turn lead the heart to pump higher or reduced flow rate because of oxygen requirement to supply adequate energy to heart muscles to function accordingly. Major portion of blood to heart is supplied by left coronary artery which encompasses larger area of heart and the rest is supplied by right coronary artery. The blood supply to heart is accordingly divided by left and right coronary artery. The left lateral portion of the left ventricle and the anterior (front) portion of the ventricular septum receive blood from the Left coronary

artery. Whereas the right ventricle, the posterior wall of the left ventricle and posterior third of the septum is supplied by right coronary artery (Ramanathan & Skinner, 2005). The blood flow to heart muscles get hindered due to reducing of artery flow area caused by deposition of undesirable material thus forming a block or stenosis (Ahmed, 1998; Chaichana, et al., 2012; Chaichana et al., 2013a, 2014; Chakravarty & Mandal, 2000; Liu, 2007; Long, Xu, et al., 2001; Melih Guleren, 2013; Mustapha et al., 2010; Zeev Vlodaver 2012). The human heart has an alternate flow mechanism known as collateral flow. The collateral flow is a bypass flow that helps the heart to get blood when main arteries are plagued by the presence of stenosis. (Christian Seiler, 2003). The presence of myocardial ischemia stimulates the coronary collateral flow (Takeshita, et al., 1982). The stimulus is result of low pressure at distal of stenosis. It has been established that the collateral flow is directly related to the severity of blockage i.e. when blockage area increases the collateral flow also increases to substitute itself as an alternate blood flow supplier. Thus the collateral flow rate is a good indicator of Coronary artery disease (Seiler, et al., 2013).

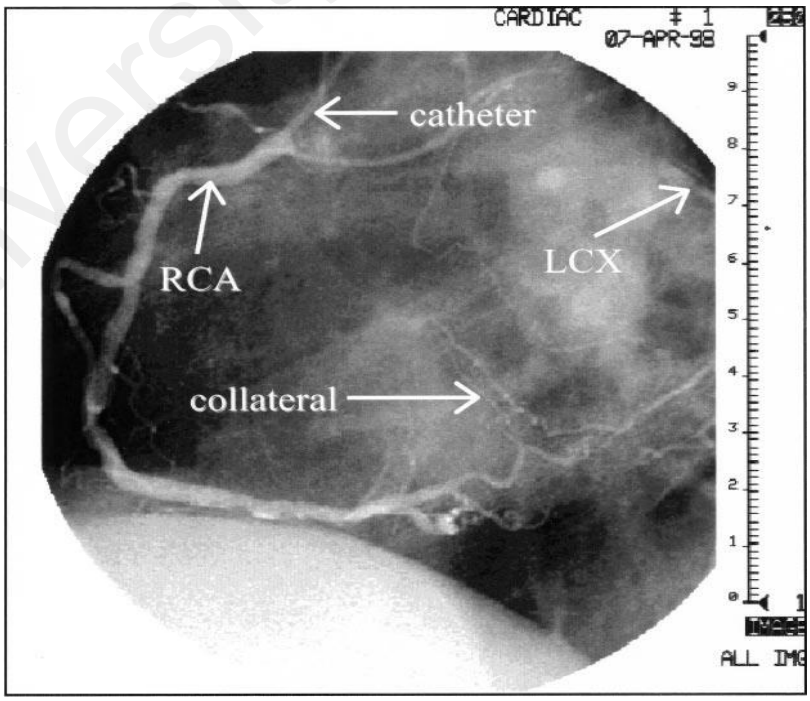

Figure 2.3: Collateral flow (Koerselman, van der Graaf, de Jaegere, & Grobbee, 2003)

Assessment of Stenosis:

Coronary angiography and CCTA

The presence of stenosis in coronary artery or any other vessel can be assessed using various techniques. Coronary angiography is a radiological study and the most common technique used to study coronary artery disease. Angiography is supposed to be a minimal invasive method that is commonly employed by physicians to test and diagnose to treat medical conditions. It provides a 2D image representation of the 3D vascular lumen of the arterial wall. Angiography uses one of three imaging technologies such as X-rays with catheters, Computed tomography (CT), Magnetic resonance imaging (MRI). In catheter angiography, a catheter which is a thin plastic tube, is inserted into an artery through a small incision in the skin. Once the catheter is guided to the area to be examined, a contrast material such as Iodixanol, Iohexol etc. is injected through the tube that highlights the interested vessels during imaging using x-rays.

There are few limitation of this technique such as it cannot provide the functional or physiological significance of lesion especially those of intermediate stenosis whose diameter is between 45% - 70% with normal artery (Meijboom et al., 2008; Tobis, et al., 2007). Therefore, this is still a gray area for assessment of an intermediate coronary artery stenosis severity for cardiologists (Tobis et al., 2007).

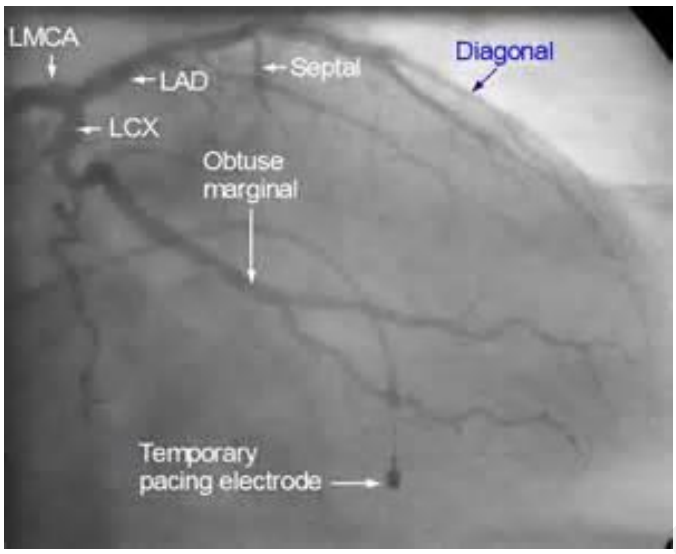

Figure 2.4: Coronary angiography (http://coronary-angiography.purzuit.com/)

The abnormal change in the anatomy of arteries medically termed as lesions or stenosis can have differing geometries and possibly they can be eccentric in nature having maximum and minimum diameters. These two diameters can differ significantly. On top of eccentricity, the artery may possess multiple stenosis that makes it extremely difficult to assess the severity of the stenosis, Further, the techniques solely relies on visual images obtained through imaging techniques, there is greater chance that the coronary angiogram techniques overestimate or underestimate the severity of the stenosis.

The 64-slice cardiac computed tomography angiography, commonly termed as CCTA has the ability to acquire the images of the complete coronary artery tree as shown in figure 2.5. The CCTA requires further processing after getting the images where Quantitative coronary angiography (QCA) is performed to assess the anatomical significance of the stenosis (Kristensen et al., 2010; van Werkhoven et al., 2009). The assessment of severity in QCA takes into account various parameters such as percent Area stenosis (AS), lesion length and percent diameter.

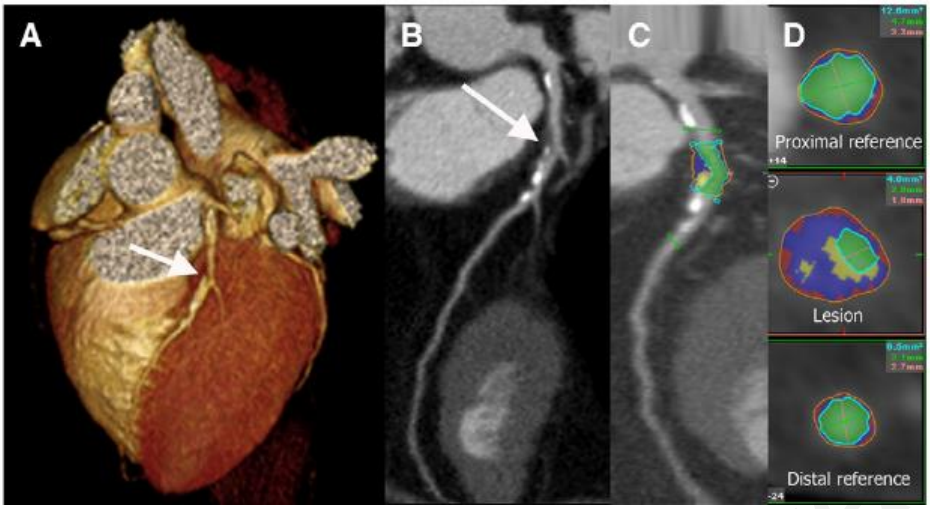

Figure 2.5: Three dimensional and curved multi-planar reconstruction of the left anterior descending artery (A, B). Vessel analysis using the plaque tool in a longitudinal plane (C) and transverse sections (Kristensen et al., 2010)

Intravascular ultrasound (IVUS)

Intravascular ultrasound (IVUS) is another important tool used to diagnose the coronary disease. Intravascular ultrasound (IVUS) is a medical imaging methodology that exploits the principal of sound for viewing the inner walls of the artery. It uses a specially designed catheter having a small ultrasound probe attached to the end of the catheter. Another end of the catheter is attached to computerized ultrasound equipment. It makes use of the piezoelectric transducer or CMUT to produce ultrasound that travels to the area of interest and reflects back depending upon the material it encounters. The reflected sound is used to construct the image. This technique has enhanced the understanding atherosclerotic (a disease of the arteries characterized by the deposition of fatty material on their inner walls) process to great extent. It allows the cross-sectional anatomical imaging to be obtained. Since the IVUS offers greater sensitivity in terms of diagnosing the disease, it is widely used as a standard method for identifying anatomical atherosclerosis in vivo (Nissen & Gurley, 1991; Nissen & Yock, 2001). Even though these techniques have helped to view and understand the atherosclerotic process to large extent but still they poses few limitations such

- Inability to insert the catheter into the regions of excessively lengthy and complex vessels, calcified, non-calcified, fibrous stenosis, and in remarkably small arteries.
- Non-uniform rotational distortion (NURD) with mechanical IVUS transducers and the distortion of the cross-sectional image if the IVUS catheter image plane is not perpendicular to the long axis of the vessel (Tobis et al., 2007).

2.2.2 Flow across Stenosis

Coronary artery disease (CAD) is the end result of the accumulation of non-obstructive vulnerable coronary atherosclerotic plaques in the walls of the coronary arteries. CAD is the leading cause of death in the world. CAD presents as a myocardial infarction (MI) or sudden cardiac death in ~50% of individuals with the pathology (branch of medicine that deals with the laboratory examination of samples of body tissue for diagnostic or forensic purposes). The stenosis formation is caused by deposition of fat or calcified material on the inner lining on the artery. These deposition leads to narrowing of artery which is termed as stenosis. The stenosis formed out of this process can generally have elliptic shape but it can have some other shapes as well. It is reported by Mustapha et al. that the pressure drop across the cosine stenosis was more than that of the irregular ones

(Mustapha et al., 2010). Lorenzini & Casalena (Lorenzini & Casalena, 2008) investigated the effect of plaque shape, dimension and locations of stenosis on the blood flow in cylindrical artery. It was established through 35 different cases that the shape and height of stenosis affects the disturbance lengths and peak velocities, whereas re-circulations are strongly influenced by the stenotic slope. The pressure drop is one of the vital parameter that can indicate the health of artery or severity of stenosis. Generally, the pressure drops due to blockage formed because of resistance offered to

blood flow due to stenosis. This is true for all types of vessels whether coronary or any other artery such as renel artery etc. (Kagadis et al., 2008).

The pressure drop of eccentric stenosis could be higher than that of concentric stenosis (Melih Guleren, 2013). According to Melih Guleren, the pressure drop for eccentric was found to be 17% as opposed to 9% of concentric 75% occlusion (the blockage or closing of a blood vessel). An asymmetric shape and surface could produce different effect as compared to symmetric stenosis. It is seen that for stenosis in artery of 40% area occlusion, at low Reynolds number the flow resistance is practically unaffected by surface irregularities. Whereas an increase in pressure drop of 10% was observed for smooth stenosis for higher Reynolds number (Andersson et al., 2000). The shape of stenosis plays a vital role in determining the pressure and flow characteristics. The disturbance in length and peak velocities is mainly affected by shape and height of stenosis (Lorenzini & Casalena, 2008). It is also reported that the trapezium plaques shape geometries are the most sever pathologies as they favour higher stain and further more chances of depositions on the walls of artery.

Zhang et al. (Zhang et al., 2012) investigated the 3D sinusoidal pulsatile blood flow through the models of internal carotid artery with different geometries by computational simulation. They found low and high oscillatory wall shear stress in three preferred areas in carotid artery. They concluded that the curvature and planarity of blood vessel plays a significant role in the flow pattern in internal carotid artery siphon. The rheological properties of blood also affect the flow pattern significantly (Tu & Deville, 1996). It is believed that the pulsatile and harmonic flow produces similar flow behaviour which was demonstrated by considering these two flow types for same volume stroke (Zendehbudi & Moayeri, 1999) for stenosed artery of 61% area reduction. The pulsatile blood flow in coronary arteries is reported by few other authors as well using the non-Newtonian and Newtonian model (Johnston, et al., 2006). Their

study showed that the non-Newtonian model is more appropriate than the Newtonian model to study the blood flow in detail. The non-Newtonian flow model is quite popular in studying the blood flow behaviour. The effect of non-Newtonian property of blood flow through stenosed artery (Ishikawa, et al., 1998) revealed that at high Stokes and Reynolds numbers, strength of vortex at downstream of stenosis was reduced by the property of non-Newtonian blood provided that the flow is stagnant. Ikbal (Ikbal, 2012) defined a mathematical model of Non-Newtonian blood flow through stenotic artery under unsteady conditions. A numerical study of Newtonian and six non-Newtonian viscosity models for 30% and 60% stenosis carotid artery (Razavi, et al., 2011) under transient condition showed some variations in results. It was reported that the velocity and wall shear stress for power-law model has more deviation than the other models. The area reduction of stenosis is quite difficult to judge thus different authors have considered even irregular area reduction. One such example is observed in the study of Manimaran (Manimaran, 2011) who studied Non-Newtonian blood flow in arterial stenosis of 48% area occlusion to investigate the surface irregularities of stenosis. It was noticed that at low Reynolds number the pressure drop across the stenosis was unaffected by surface irregularities. There have been efforts to develop an analytical expression for skin-friction and flow resistance using a non-Newtonian blood flow model through a stenosed artery (Misra & Shit, 2006). It is found that the maximum value of skin friction and flow resistance was observed at the throat of the stenosis and minimum at the end of the stenosis. It was also noticed that increase in the stenosis height increases the skin friction and flow resistance. The heat and mass transfer along with Sherwood number is also a function stenosis shape as suggested in a non-Newtonian blood flow through different shapes of stenotic arteries (Chakravarty & Mandal, 2009). It is found that the flow pattern, heat and mass transfer, wall shear stress and Sherwood number strongly depends on the shape of stenosis. Maximum Sherwood

number and the high shear stress was observed at the throat of the stenosis, and the formation of several recirculation zones are observed that may further develop the disease in the downstream vicinity from the stenosis. There are few other parameters such as bifurcations in the artery, the curvature, magnetic field etc. which have profound effect on flow characteristics. Across bifurcations in regions opposite the flow dividers, a low wall shear stress was observed (Soulis et al., 2006). These sites are anatomically predisposed for atherosclerotic development. A rang of 0.75 to 2.25 N/m^2 low wall shear stress was found on the left main coronary artery bifurcation opposite to the flow divider. Three dimensional diseased and normal left anterior descending (LAD) arterial tree of porcine was modelled by Su et al. (Su et al., 2014) to investigate the effect of stenosis on the blood flow and haemodynamic parameters. The anatomical model was extracted from computed topography of heart of the porcine. The results show that more than 75% area reduction stenosis affect the pressure drop and total flow rate in bifurcation and branched arteries.

The flow pattern gets modified by the presence of magnetic field and increases the heat transfer rate as seen in a mathematical model of multi stenosis subjected to static magnetic field (Tashtoush & Magableh, 2008). It's further revealed that thermal boundary layer thickness and temperature gradient was increased by magnetic field torque. The secondary flow pattern gets significantly affected by the presence of non-uniform magnetic field (Kenjereš, 2008). The flow separation zone occurs mostly towards the downstream of the irregular shape multi-stenosis subjected to magnetic field (Mustapha, et al., 2009).

The spiral flows too have influence on flow characteristics. The effect of spiral blood flow in a 3 dimensional stenosed artery model with 75% area reduction was

investigated by Paul & Larman (Paul & Larman, 2009). They found that an increase in both the total pressure and velocity of the blood due to spiral flow for Re=500. A significant difference was also observed between the wall shear stress of spiral and non-spiral flows downstream of stenosis. The most effect of spiral flow was on the tangential component of the velocity which increases with the increase in spiral flow speed.

A numerical study was conducted to study the effect of rotation on blood flow with different angular velocities by Sung et al. (Sung, Ro, & Ryou, 2009). The Non-Newtonian Carreau model was used to represent the flow of blood, and pulsatile velocity profile was employed at the inlet. The results show that flow recirculation zone contracts and its duration was decreased as compared to the no rotation case. And also wall shear stress of no rotation case was twice smaller for the than that of rotation case.

2.3 Blood flow analysis in tapered arteries

Some of the arteries could be considered as tapered in geometry that further complicates the blood flow behaviour. It is observed that the velocities through the converging tapered artery are less than those in the non-tapered artery under stenotic conditions and the diverging tapered artery (Nadeem, et al., 2011). It is further noticed that with an increase in the height and shape of stenosis velocity decreases while increases with increases in tapering. A mathematical model of non-Newtonian blood flow in tapered artery was developed by Ismail et al. (Ismail, et al., 2008) The effect of tapering due to pulsatile nature of blood was studied by using the generalised power law model. The governing equation of motion was solved by the finite difference scheme. They found a lower values for the axial velocity profile, flow rate and wall shear stress for tapering of artery while higher value for resistive impedances than Newtonian

model. Similarly, Chakravarty & Mandal (Chakravarty & Mandal, 2000) developed a two dimensional mathematical model of blood flow in presence of overlapping stenosis in tapered arteries. The nonlinear term such as tapering angle was accounted in the Navier-Stokes governing equation of blood flow. Their analytical model calculated the axial and radial velocity profile with a low computational complexity. The irregular stenosis of arterial segment was analytically studied by Chakravarty & Mandal (Chakravarty & Mandal, 2005) and Kumar Mandal (Kumar et al., 2007) in other studies. The results obtained for smooth shape stenosis and cosine shape stenosis models shows well agreement with the existing literature. The Non-Newtonian blood flow through tapered arteries with stenosis was numerically studied by Mandal (Mandal, 2005). The flow of blood was characterised by generalised power law model. The Unsteady non-linear governing Navier-Stokes equation for flow was solved by finite difference scheme. The analytical model evaluated the rate of flow, resistance impedance and wall shear stress. The model is also employed to investigate the effect of tapering and wall deformation, severity of stenosis with fixed length.

2.4 Blood flow analysis in curved arteries

It is well known that the flow through curve sections offers more resistance to flow than the straight flow sections. The artery wall curvature substantiates the flow resistance in that complicates the flow behaviour already affected by stenotic blockage. The radius of curvature at a given point defines the degree to which the vessel deviates from being straight. Thus, vessels with smaller radius of curvature (or larger curvature) bend more sharply. It is noted that the blood while flowing across curved section forms low velocity zones due to obstructions offered by curvature. Thus these areas are more prone to formation of additional thrombus, stenosis and aneurysm, atherosclerosis as well as other vascular diseases in curved arteries such as aortic arch, coronary artery and

cerebral artery, though, from a macroscopic perspective, these vessels differ from each other in dimension and shape (Calfon, et al., 2010; Huang, et al., 2010; Jou, et al., 2010; Naruse & Tanishita, 1996; Shipkowitz, et al., 2000; Stroud, et al., 2000).The curvature further decreases the pressure at the site of stenosis for a given stenosis severity. Hence it is highly desirable to study the influence of artery wall curvature on the coronary diagnostic parameter FFR, and CDP and LFC for a given stenosis severity from straight artery to curved artery and identify a region of misdiagnosis when assessing the anatomical significance of stenosis severity using FFR as a standard parameter. There is some notable work in the area of artery curve such as Liu (Liu, 2007) who studied the pulsatile blood flow pattern in the curved artery with stenosis by computational simulation. The effect of stenosis on the haemodynamic parameters, such as flow separation, wall shear stress and pressure drop was calculated. He found drastic changes in the flow pattern of downstream region as the severity of stenosis reaches to a certain level. He also reported the flow separation area and also observed area of low and oscillating wall shear stress and blood pressure at the outer wall in downstream of the artery. Leguy et al. (Leguy, et al., 2009) investigated the influence of curvature on the velocity profile by computational fluid dynamics. Poiseuille, Womersley and cosine θ model was used to compare and calculate the blood volume flow. They found that for radius of curvature of 50 and 100mm the time average blood volume flow was under estimated by maximally 10.4% and 7.8% respectively for Poisuille and Womersley. They concluded that velocity wave form at the position of the maximum rather than the centre stream velocity wave form combined with the Womersley method should be chosen.

The presence of catheter in curved artery seems to introduce additional errors in the estimation of functional severity of stenosis. Krams et al. (Krams et al., 1999) carried

out computational fluid dynamic study in a curved tube resembling coronary artery to analyse the influence of the catheter placement inside a tube on the 3D velocity profile by. They observed a redistribution of 3D axial velocity field away from the catheter and also found increase in peak axial velocity, shear stress, and axial pressure drop, decrease in peak secondary velocities. They concluded the presence of catheter in curved tube significantly changes the velocity field and reduces the secondary patterns.

Keshavarz-Motamed & Kadem (Keshavarz-Motamed & Kadem, 2011) developed a simplified model of aortic stenosis with coexisting coarctation of the aorta to investigate the pulsatile blood flow. The model consisted of three severities of aortic stenosis. The results demonstrated that a significant impact on the flow in curved pipe in terms of secondary flow pattern, wall shear stress and pressure drop due to the coexistence of both the pathological conditions and also appeared that presence of aortic stenosis can lead to the overestimation of the severity of coarctation of the aorta. Wang & Li (Wang & Li, 2011) presented a biomechanical behaviour of curved artery with flexible wall was subjected to physiological conditions. They studied the effect of artery curvature, flexibility on peak wall Von Mises stress, and distribution pattern in detailed. They concluded from the findings that may provide the important individualized treatment for patient with cardiovascular disease. Qiao et al. (Qiao, et al., 2004) numerical studied the pulsatile blood flow in a S-shaped curved arteries with different diameter. The finite element method was used to analyse the haemodynamic parameters such as secondary flow, wall shear stress and pressure in the arteries. The results represented more complex secondary flow in the large S-shaped curved artery than that of the small diameter artery. They also observed the haemodynamic variables causes most important effects on the arterial endothelium in the region, which leads to the development of the cardiovascular diseases such as atherosclerosis.

2.5 Blood flow analysis in bifurcation arteries

The arteries are designed so elegantly that they make branches at various locations to move into various sections of the body in order to supply the blood. The bifurcation of artery is other important geometrical parameter that has influence on the blood flow behavior. A bifurcation lesion is a coronary artery narrowing that may occur adjacent to, and/or involving the origin of a significant side branch. There are studies that have established a correlation between plaque formation and the angulation of coronary bifurcation (Sun & Cao, 2011). There are many procedures that are followed to treat bifurcation lesions (Lefèvre et al., 2000; Yamashita et al., 2000), however no clear information about which side branch lesion to be treated first after stenting the main branch lesion. It is believed that the angiographic evaluation of the functional significance of the stenosis severity in side branch lesions overestimate the functional significance of the lesion and FFR may be useful in treating bifurcation lesions and it is both safe and feasible (Koo et al., 2005). Different aspects of blood using various models have been reported. For instance, a 3 dimensional rigid wall and deformable-wall models are developed to simulate the arterial rigidity on wall shear stress by Toloui et al. (Toloui et al., 2012). They studied the influence of blood on two different rheological models (Newtonian and Carreau–Yasuda). They concluded that wall shear stress distribution was greatly affected by the blood rheological model. Chen & Lu (Chen & Lu, 2004) demonstrated the influence of Non- Newtonian property and plane curvature in non-planar daughter vessel on the wall shear stress and flow phenomena. The finite element method was used to solve the Navier-Stokes flow equations in three dimensions. They observed the skewing of velocity profile towards outer wall creating the low wall shear stress at the inner wall and found that the velocity profile shifts

towards the flow divider in the downstream of bifurcation. In a further study by Chen & Lu (Chen & Lu, 2006), the pulsatile nature of blood was accounted to investigate the effect of Non- Newtonian property and plane curvature in non-planar daughter vessel in bifurcating model. Their result shows a flattened velocity profile due to shear thinning behaviour because of the Non Newtonian property of the fluid. Also found significant differences between Newtonian and Non-Newtonian flow during the cycle.

Chaichana et al. (Chaichana et al., 2011) investigated the influence of angulation of left coronary artery on the hemodynamic based on the simulated and realistic arteries models. They developed twelve models consisting eight simulated and four realistic models of coronary having left anterior descending and left circumflex branches. They evaluated wall shear stress, velocity and wall pressure in simulated and realistic models. Their results show the disturbed flow pattern in the models with the wider angulation during the cardiac cycle. In the left bifurcation with wide angle low wall shear stress gradient was observed. Similarly, the influence of blood viscosity in a small calibre bifurcated artery on the hemodynamic parameters was numerically investigated by Kanaris et al. (Kanaris, et al., 2012). The Casson model was used to calculate the viscosity of blood. Their results demonstrated that as the viscosity increases the heart also must increase the pumping power to keep output unchanged. The lower value of wall shear stress was observed at the outer wall of the bifurcation.

The numerical investigation of blood flow dynamics through stenosed of subject specified carotid bifurcation model was studied by Lee et al. (Lee, et al., 2008). The spectral element method was used to simulate under the pulsatile inlet based on in-vivo condition. Their results demonstrated the rapid fluctuation in the velocity and pressure pattern in the transitional state in the post stenotic region of carotid artery. They also

observed a high instantaneous wall shear stress within the stenosis during the systolic compared to health carotid artery. They suggested that complex flow, turbulence and biomechanical stresses could be predicted by this study. Alishahi et al. (Alishahi, M. et al., 2011) developed a real model of stenosed abdominal aorta and iliac arteries to evaluate the pulsatile flow and arterial wall behaviour. The models were developed by extracting the data from CT scan images and simulated the flow and tissue interactions are performed. Their results show maximum wall shear stress across the bifurcation where the risk of particle deposition is more, also observed that pressure drop was lower by 15% for the flexible model, as compared to rigid and complaint model.

2.6 Experimental studies on blood flow in arteries

There have been efforts to evaluate the blood flow behaviour using experimental means to judge the functional significance of various flow characteristics. Some of the studies that relied on experimental setup are those of (Ahmed, 1998; Ha & Lee, 2014; & Schröder, et al. 2012) etc. An experimental study to investigate the blood flow disturbance in downstream region of modelled stenosed rigid artery was conducted by Ahmed (Ahmed, 1998). The velocity data for 25% 50% and 70% area reduction were obtained from ensemble averaging techniques (phase-locked waveform). The results indicated that the flow disturbances could be used as a powerful diagnosing tool in early identify the cardio vascular diseases. Ha & Lee (Ha & Lee, 2014) investigated the effect of spiral blood flow in axisymmetric stenosis model using particle image velocimetry velocity field measurement technique and streak line flow visualization. The swirling effect was achieved through two different helical pitches (10D and 10/3D) which have been mounted before the stenosis. Their result shows that the length of recirculation flow was reduced by spiral flow and also provokes the early break out of turbulent intensity. They suggested that the effect of spiral flow would contribute to better

understanding of the haemodynamic and diagnosis procedures for clinical treatments. The effect of vessel elasticity on the flow was experimentally studied by Pielhop et al. (Pielhop et al., 2012) using time-resolved image velocimetry combined with the simultaneous evaluation of static pressure in elastic transparent vessel with the pulsatile flow. They found an oscillation wall shear stress distribution in the region of plaque-prone which induces the phenotype endothelial cells that supports the progression of atherothrombotic lesion in downstream of the throat region.

The influence of downstream collaterals on the different diagnostic parameters was experimentally studied by Peelukhana et al. (Peelukhana, Back, & Banerjee, 2009). The FFR, CDP and LFC were evaluated for the different degree of stenosis and tested for possible misinterpretation in the severity of stenosis for variable collateral flow. Their result shows FFR and LFC increased from 0.74 to 0.77 and 0.58 to 0.62 respectively for the case of intermediate stenosis. CDP decreased from 47 to 42 for no collateral to fully collateral flow. They suggested the variability in the diagnostic parameters leads to the underestimation of stenosis severity.

2.7 Diagnostic parameters and their effects on hemodynamic

2.7.1 Fractional flow reserve (FFR)

The fractional flow reserve (FFR) is defined as the ratio of maximum blood flow in a stenotic artery to maximum blood flow if the same artery was normal (Park et al., 2012; N. H. Pijls et al., 1995).

$$FFR = \frac{\tilde{p}_d - \tilde{p}_v}{\tilde{p}_a - \tilde{p}_v} \tag{2.1}$$

where $\tilde{p}_a$ is the time averaged aortic pressure (mmHg), $\tilde{p}_d$ is the time averaged distal

stenotic pressure (mmHg) measured at the end of pressure recovery (Konala, Das, & Banerjee, 2011) and $\tilde{p}_v$ is the venous pressure which is assumed to be 0 mmHg.

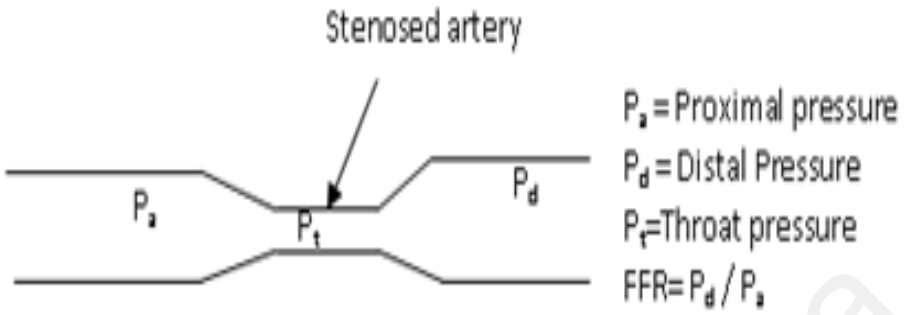

Figure 2.6: Simplified schematic representation of stenosis geometry. P_a and P_d are measured by guiding the catheter attached with a pressure sensor

2.7.2 Pressure drop coefficient (CDP)

At hyperemia, CDP is a dimensionless functional parameter derived from fluid dynamics principles by considering time averaged pressure drop ($\Delta\tilde{p}$) and the velocity proximal to the stenosis (Peelukhana et al., 2009; Siebes, Chamuleau, Meuwissen, Piek, & Spaan, 2002).

$$\text{CDP} = \frac{\Delta\tilde{p}}{0.5\rho U_a^2} \tag{2.2}$$

Where $\Delta\tilde{p} = (\tilde{p}_a - \tilde{p}_d)$ (N/m^2) and Ua is the proximal velocity (m/s). CDP associates both viscous loss and loss due to momentum change in the flow across the stenosis.

2.7.3 Lesion flow coefficient (LFC)

Konala et al. (Konala et al., 2011) developed normalized and dimensionless functional diagnostic parameter lesion flow coefficient (LFC) by considering the functional endpoints and the geometric parameters. The LFC ranges from 0 to 1 and it is

the ratio of percentage AS and the square root of CDP evaluated at the site of the stenosis.

$$\text{LFC} = \frac{percentage\ AS}{\sqrt{\Delta\tilde{p}/0.5\rho U_{(a-h)}^2}} \tag{2.3}$$

Where $U_{(a-h)}$ is the velocity at the site of the stenosis (m/s)

Many of the clinical studies show that a FFR value of ≤ 0.75 identifies ischemia-causing coronary stenosis with an accuracy of 90% FFR is clinically well proven diagnostic parameter (Pijls et al., 1995; Pijls & Sels, 2012). In the presence of stenosis, a cut-off value of FFR <0.75 is almost able to induce myocardial ischemia, whereas FFR > 0.8 never associated with exercise-induced ischemia in a single vessel coronary artery disease (CAD) as evident from the numerous clinical trials (De Bruyne et al., 2012; Pijls et al., 1995; Pijls et al., 2010; Tonino et al., 2009) which indicates that the grey zone for FFR is between 0.75 and 0.80 (Park et al., 2012) that falls under the intermediate area stenosis.

The coronary diagnostic parameters FFR, CFR, and CDP were experimentally investigated by Goswami et al. (Goswami, et al., 2013) for the variation with diameters and vascular conditions with guide wire inserted into the coronary artery. The diagnostic parameters calculated for mild (64% area reduction), intermediate (80% area reduction) and sever (90% area reduction) for 2.5 mm and 3mm diameter arteries. They observed that for the case of mild and intermediate stenosis arterial diameter does not effect on FFR but varies for sever condition. And also found a variation in the CDP for the various diameters of arteries. They suggested CDP holds good for functional assessment of stenosis severity in clinical setting. The effect of lesion length on the hemodynamics and the diagnostic parameters was presented by brosh et al. (Brosh, et

al., 2005) for a given percentage area stenosis severity. They performed quantitative coronary angiography in 63 patients having intermediate lesions by pressure guidewire. The results demonstrated that the lesion length has significant impact on the physiological significance of intermediate coronary lesions.

The influence of arterial wall –stenosis compliance had been studied in detail by konala et al. (Konala et al., 2011). The blood was modelled as non-Newtonian fluid using Carreau model. Their result showed that for a given stenosis geometry, the hyperemic pressure drop across the stenosis decreases as the wall compliance increases and hence the current clinical diagnostic parameter FFR increases. This increment in FFR leads the clinician to misdiagnose the severity of the stenosis and postponement of the coronary interventional procedure, especially for the intermediate stenosis severity. The misdiagnose region was found between 78.7%- 82.7% AS. Further, the CDP and LFC also affected which confirms that the arterial wall-stenosis compliance might lead to misinterpretation of stenosis severity.

2.8 Effect of guidewire on haemodynamic

The investigation of effect of catheters of various diameters on the blood flow in 180^0C curved artery was numerically simulated by Torri et al. (Torii et al., 2007). The commercially available software CFX10 was used to simulate the blood flow. They observed an increase in pressure by 1.3-4.3mmHg depending on the diameter of the guide wire and causes reduced pressure-velocity phase lag. The under estimation of 15-21% of velocity measurement was also observed due to the catheter depending on its diameters. The investigation of effect of guide wire size and stenosis dimensions are analytically presented by Rajabi-Jaghargh et al. (Rajabi-Jaghargh, et al., 2011). The three percentage of area reduction corresponding to moderate (64%), intermediate

(80%) and severe (90%) was considered to analyse the pressure drop. They observed that increase in the throat length increases only the viscous loss for a given percentage of area reduction. The increase in both loss momentum change and viscous loss was found due to the increase in severity of stenosis and guide wire insertion.

A mathematical analysis was performed to investigate the effect of catheterized curved artery with stenosis on the various physiological flow characteristics by Dash et al. (Dash, et al., 1999) using double series of perturbation in small arteries with stenosis. The results show that flow characteristics vary a markedly, and a considerable increase in the magnitude of pressure drop, impedance and wall shear stress was observed due to the increase in the catheter size. The combined effect of stenosis and curvature on the flow characteristics are also performed and found that effect of stenosis is more severe than that of the curvature of artery. The study of hemodynamic conditions due to insertion of guide wire was investigated by Sinha Roy et al. (Sinha Roy et al., 2006) to determine the mean pressure drop and distal mean coronary pressure which was used to estimate the uncertainty in diagnosis of moderate lesion. They found mean pressure drop 72mmHg as compared to 75mmHg under patho-physiological conditions without guide wire during hyperemia. The guide wire surface shear stress was 35-50% as compared to the value of wall shear stress for the transient and steady flow.

2.9 Effect of stenosis in realistic coronary arteries

The effect of plaques on hemodynamics in left coronary artery model is simulated by Chaichana et al. (Chaichana et al., 2012). The simulation was carried out to compare wall shear stress for Newtonian and non Newtonian fluid models. The pressure gradient and flow velocity was calculated and compared in models with and without stenosis. They found that high pressure gradient exists at the stenosis and low

velocity at the post stenosis. They also observed that wall shear stress at the stenosis is similar for the Newtonian and non Newtonian fluid models. In another study the authors studied the hemodynamic effect of various types of plaque configuration in left coronary artery (Chaichana et al., 2013a). They calculated velocity, wall shear stress and pressure gradient for the plaque configurations. They found a highest velocity and pressure gradient in a type of plaque configuration which involves the plaque position in all the three left coronary branches. The authors further investigated the effect of stenosis in four suspected coronary artery disease patients (Chaichana, Sun, & Jewkes, 2013b). They observed recirculation regions at post stenosis location and an increase in wall shear stress at the stenosis for all the four patients. The investigation of plaque located in left coronary artery and effect on wall shear stress (WSS) and wall pressure stress gradient (WPSG) was simulated by computational fluid dynamics (Chaichana et al., 2014). Their result demonstrates that the WSS decreases while the WPSG increases due to presence of plaque in left coronary side branches.

2.10 Critical literature review

It is understood clearly from the literature that there is a substantial amount of research work been carried out on hemodynamic by various researcher across the world. The researchers have considered the idealistic models of coronary artery, as well as geometrical models which have been extracted from the real image data. Many researchers have considered the multi-physics fluid as well as wall deformation to simulate the fluid structure interaction in different arterial models. It is noted that there is not much of work particularly focusing on the shapes of stenosis in arteries since the stenosis formed does not have particular shapes. Hence it is highly desirable to investigate the effects of shapes of stenosis on hemodynamics and hence the diagnostic parameters. There is not much investigation on the effect of angle of downstream

curvatures in arteries which also influences the flow pattern, wall shear stress and pressure drop in presence of stenosis. It is also observed that a limited amount of work has been carried out on the realistic left coronary arties with the various degree of stenosis in different position. Since it is imported to know the flow behaviour when the stenosis present at different location. Hence it is highly desirable to investigate the effect of different degree of stenosis on the hemodynamic, present at various locations. It is noted that there is scarcity of literature on flow behaviour when multiple stenosis exists on various locations across the coronary arteries. This particular issue need to be addressed since it has been seen that multiple stenosis occurs in many patients. Thus, current study is focussed on all those above mentioned areas to get to know the blood flow behaviour to assist in diagnosis of patients suffering from coronary diseases.

CHAPTER 3: METHODOLOGY

3.1 Introduction

This chapter has been divided into two sections. The first section describes with the governing equation of fluid flow in computational fluid dynamics (CFD) domain. Moreover, the assumptions made in CFD analysis of simple ideal as well as patient specific models of coronary artery are discussed. In the second section methodology adopted is presented for modeling the 3D real coronary artery such as normal and disease coronary artery. The meshing and numerical setup for CFD is also given for the ideal and patients specific coronary artery models.

3.2 Governing equations

In this section, the governing equations for computational fluid dynamics analysis is provided with detailed information. Commercially available finite volume software ANSYS CFX 14.5 is used in the current study for the computational fluid dynamics (CFD) simulation. The computational domain is subdivided into large number of control volumes to be applicable for finite volume method. The conservation equation applicable in the form of control volume integration as a starting point is given as in equation 3.1.

$$\int_{CV} \frac{\partial(\rho\phi)}{\partial t} dv + \int_{CV} div(\rho\phi u) dv = \int_{CV} div(\Gamma grad\phi) dv + \int_{CV} S_{\phi} dv \tag{3.1}$$

This equation consists of various transport process such as the rate of change and convective term on the left side of the equation and diffusion term and source terms on

the right side of the equation. By applying Gauss's divergence theorem, volume integral of the convective and diffusive terms are rewritten as

$$\int_{CV} div(a)dv = \int_{A} n.a\, dA \tag{3.2}$$

$n.a$ is the component of vector *a* in the direction of the vector ***n*** normal to surface element d*A*. The equation (3.1) can be written as

$$\frac{\partial}{\partial t}\left(\int_{CV} \rho\phi dV \right) + \int_{A} n.(\rho\phi u)\, dA = \int_{A} n.(\Gamma grad\ \phi)\, dA + \int_{CV} S_{\phi} dv \tag{3.3}$$

It is common practice to set up control volumes near the edge of the domain in such a way that the physical boundaries coincide with the control volume boundaries (Versteeg & Malalasekera, 2007).

3.3 Equation for computational blood flow model

The basic equations of computational fluid dynamics are based on the fluid dynamics equations. The conservation laws of physics represents in the form of mathematical equations. The flow of blood governs by the Navier-Stokes equations with the assumptions of incompressible and homogenous and non-Newtonian fluid. The blood density (ρ) is assumed as 1050 Kg/m^3.

$$\rho\left(\frac{\partial v}{\partial t} + v.\nabla v \right) = -\nabla.\tau - \nabla p \tag{3.4}$$

and the continuity equation for incompressible flow is

$$\nabla . v = 0 \tag{3.5}$$

Here v is the three dimensional velocity vector, t the time, ρ the blood density, p the pressure and τ the stress tensor. The Bird-Carreau model is used to represent non-Newtonian fluid in this work, and the blood viscosity μ given in poise (P) as a function of shear rate $\dot{\gamma}$ given in s^{-1} is given by

$$\mu = \mu_{\infty} + (\mu_0 - \mu_{\infty})[1 + (\lambda\dot{\gamma})^2]^{(n-1)/2} \tag{3.6}$$

Where, λ (Time constant) = 3.313s, n (Power law index) = 0.3568, μ_0 (Low shear viscosity) = 0.56 P and μ_{∞} (High shear viscosity) = 0.0345 P. since the above both equation can be used for incompressible laminar and turbulence flow. Analytical solutions of the Navier-Stokes equations exist for only a few laminar flow cases, such as pipe and annulus flows or boundary layers. Turbulent flows are modeled by using various turbulence modeling schemes.

3.4 Turbulence modelling

Two equation turbulence models such as $k-\varepsilon$ and $k-\omega$ models are widely used. In the $k-\varepsilon$ model k is the turbulence kinetic energy and ε is the turbulence eddy dissipation (the rate at which fluctuation in velocity dissipates). In the $k-\omega$ turbulence model, k is the turbulent kinetic energy and ω is the turbulent frequency (Wilcox, 1994). The k-ω model has a capability to solve the near wall treatment for low Reynolds computation. Since the flow through stenosed artery during hyperemia condition

becomes turbulent. In this work the standard *k-ω* model and *k-ω* based Shear Stress Transport (SST) have been discussed in detail.

3.4.1 Standard (k-ω) model

$$\frac{\partial \rho}{\partial t} + \frac{\partial}{\partial x_i}(\rho u_i) = 0 \tag{3.7}$$

$$\frac{\partial}{\partial t}(\rho u_i) + \frac{\partial}{\partial x_j}(\rho u_j u_i) = \frac{\partial}{\partial x_j}(-\rho \delta_{ji} + \tilde{\tau}_{ji}) \tag{3.8}$$

$$\frac{\partial}{\partial t}(\rho k) + \frac{\partial}{\partial x_j}(\rho u_j k) = \tau_{ij}\frac{\partial u_i}{\partial x_j} - \beta^* \rho \omega k + \frac{\partial u}{\partial x_j}\left[(\mu + \sigma^* \mu_T)\frac{\partial k}{\partial x_j}\right] \tag{3.9}$$

(Kaye et al.2010)

$$\frac{\partial}{\partial t}(\rho \omega) + \frac{\partial}{\partial x_j}(\rho u_j \omega) = \alpha \frac{\omega}{k}\tau_{ij}\frac{\partial u_i}{\partial x_j} - \beta \rho \omega^2 + \frac{\partial}{\partial x_j}\left[(\mu + \sigma \mu_T)\frac{\partial \omega}{\partial x_j}\right] \tag{3.10}$$

$$\hat{\tau}_{ij} = 2\mu\left(S_{ij} - \frac{1}{3}\frac{\partial u_k}{\partial x_k}\delta_{ij}\right) + \tau_{ij} \tag{3.11}$$

$$\tau_{ij} = 2\mu_T\left(S_{ij} - \frac{1}{3}\frac{\partial u_k}{\partial x_k}\delta_{ij}\right) + -\frac{2}{3}\rho k \tau_{ij} \tag{3.12}$$

$$\mu_T = \alpha^* \rho k / \omega \tag{3.13}$$

$$S_{ij} = \frac{1}{2}\left(\frac{\partial u_i}{\partial x_j} + \frac{\partial u_j}{\partial x_i}\right) \tag{3.14}$$

In Eqs. (3.7 - 3.14), t is the time, x_i is position vector, u_i is velocity, ρ is density, *p* is pressure, μ is molecular viscosity, and $\hat{\tau}_{ij}$ is the sum of molecular and Reynolds stress tensors. Also, δ_{ij} Kronecker delta, *k* is the turbulence kinetic energy, ω is the turbulent

frequency τ_{ij} is Reynolds stress tensor, and μ_T is eddy viscosity. The six parameters $\alpha^*, \alpha, \beta^*, \beta, \sigma^*$ and σ are closure coefficients whose values are given as:

$$\alpha^* = \frac{\alpha_0^* + \mathrm{Re}_T / R_k}{1 + \mathrm{Re}_T / R_k} \tag{3.15}$$

$$\alpha = \frac{5}{9} \frac{\alpha_0 + \mathrm{Re}_T / R_\omega}{1 + \mathrm{Re}_T / R_\omega} \left(\alpha^*\right)^{-1} \tag{3.16}$$

$$\beta^* = \frac{9}{100} \frac{5/18 + \left(\mathrm{Re}_T / R_\beta\right)^4}{1 + \left(\mathrm{Re}_T / R_\beta\right)^4} \tag{3.17}$$

$$\beta = \frac{3}{40}, \ \sigma^* = \sigma = 1/2 \tag{3.18}$$

$$\alpha_0^* = \beta/3, \ \alpha_0 = 1/10 \tag{3.19}$$

$$R_\beta = 8, \ R_k = 6, \ R_\omega = 2.7 \tag{3.20}$$

Where Re_T is the turbulence Reynolds number defined by

$$\mathrm{Re}_T = \frac{\rho k}{\omega \mu} \tag{3.21}$$

3.4.2 Shear-Stress Transport (SST) k-ω (or k-ω-SST) model

The $k-\omega$ based SST model accounts for the transport of the turbulent shear stress and gives highly accurate predictions of the onset and the amount of flow separation under adverse pressure gradient (F. Menter, Kuntz, & Langtry, 2003; F. R. Menter, 2009) .

$$\frac{\partial(\rho k)}{\partial t}+\frac{\partial(\rho U_i k)}{\partial x_i}=\tilde{P}_k-\beta^*\rho k\omega+\frac{\partial}{\partial x_i}\left[(\mu+\sigma_k\mu_t)\frac{\partial k}{\partial x_i}\right] \tag{3.22}$$

$$\frac{\partial(\rho\omega)}{\partial t}+\frac{\partial(\rho U_i \omega)}{\partial x_i}=\alpha\frac{1}{v_t}\tilde{P}_k-\beta\rho\omega^2+\frac{\partial}{\partial x_i}\left[(\mu+\sigma_\omega\mu_t)\frac{\partial\omega}{\partial x_i}\right]+$$

$$2(1-F_1)\rho\sigma_{\omega 2}\frac{1}{\omega}\frac{\partial k}{\partial x_i}\frac{\partial\omega}{\partial x_i} \tag{3.23}$$

The turbulent eddy viscosity is defined as

$$v_t=\frac{a_1 k}{\max(a_1\omega, SF_2)};\ S=\sqrt{2S_{ij}S_{ij}} \tag{3.24}$$

$$P_k=\mu_t\frac{\partial U_i}{\partial x_j}\left(\frac{\partial U_i}{\partial x_j}+\frac{\partial U_j}{\partial x_i}\right) \tag{3.25}$$

$$\tilde{P}_k=\min\left(P_k, 10\cdot\beta^*\rho k\omega\right) \tag{3.26}$$

Where F_1 and F_2 are blending function which are equal to zero away from the surface and are defined by

$$F_1=\tanh\left\{\left\{\min\left[\max\left(\frac{\sqrt{k}}{\beta^*\omega y},\frac{500v}{y^2\omega}\right),\frac{4\rho\sigma_{\omega 2}k}{CD_{k\omega}y^2}\right]\right\}\right\}^4 \tag{3.27}$$

$$F_2=\tanh\left[\left[\max\left(\frac{2\sqrt{k}}{\beta^*\omega y},\frac{500v}{y^2\omega}\right)\right]^2\right] \tag{3.28}$$

$$CD_{k\omega}=\max\left(2\rho\sigma_{\omega 2}\frac{1}{\omega}\frac{\partial k}{\partial x_i}\frac{\partial\omega}{\partial x_i},10^{-10}\right) \tag{3.29}$$

Where, k is the turbulence kinetic energy, ω is the turbulence frequency, y is the distance to the nearest wall, S is the strain rate, ρ is the density and U_i is the flow velocity. Constants are computed from the $k-\varepsilon$ and the $k-\omega$ model through

$\alpha = \alpha_1 F_1 + \alpha_2 (1 - F_1)$ The model constants are $\beta^* = 0.09, \alpha_1 = 5/9, \beta_1 = 3/40$, $\sigma_{k1} = 0.85, \sigma_{\omega 1} = 0.5, \alpha_2 = 0.44, \beta_2 = 0.0828, \sigma_{k2} = 1, \sigma_{\omega 2} = 0.856$.

3.5 3-Dimensional Computational models of ideal coronary artery

The present section describes the 3-dimensional model generated using computer aided design for an ideal coronary artery of human.

3.5.1 Modeling of different shapes of stenosis in coronary artery

First in the current study, an idealized coronary artery model with different shapes of stenosis were created in ANSYS workbench. The model has 70% (moderate), 80% (intermediate) and 90% (severe) Area Stenosis (AS) with various shapes. Since according to the clinical data stenosis does not have any particular shapes so in the current study an attempt is made to create the different geometrical shapes of stenosis (elliptical, trapezoidal and triangular) as shown in figure 3.1. The trapezium model has converging (of length l_c), throat (of radius r_m and length l_m), and diverging (of length l_r) sections, whereas triangular shape stenosis consists of converging (of length l_c), and diverging (of length l_r) sections. Moreover, proximal and distal radius is assumed to be identical (of length r_d). The diameter of the artery is 3mm and the stenosis length has been fixed to 10mm in all the model. Table 3.1 shows the dimensions used for the triangle and trapezium to develop the models of stenosis considered in the current study. The elliptical shape stenosis model was developed by using the following equation (Dash, et al., 1999)

$$\frac{\tilde{\eta}(\tilde{z})}{a} = 1 - \frac{h}{a} \sin \pi \left(\frac{\tilde{z} - d}{L} \right), \; d \le \tilde{z} \le d + L, \tag{3.30}$$

Where, $\tilde{\eta}(\tilde{z})$ is the radius of stenosis, a, is the radius of an artery, $\tilde{z}$ is along the axis of the artery and h is the maximum projection of the stenosis into the lumen.

$$\text{Area stenosis (AS)\%} = \frac{(\pi \times a^2) - [\pi \times (a-h)^2]}{\pi \times a^2} \quad (3.31)$$

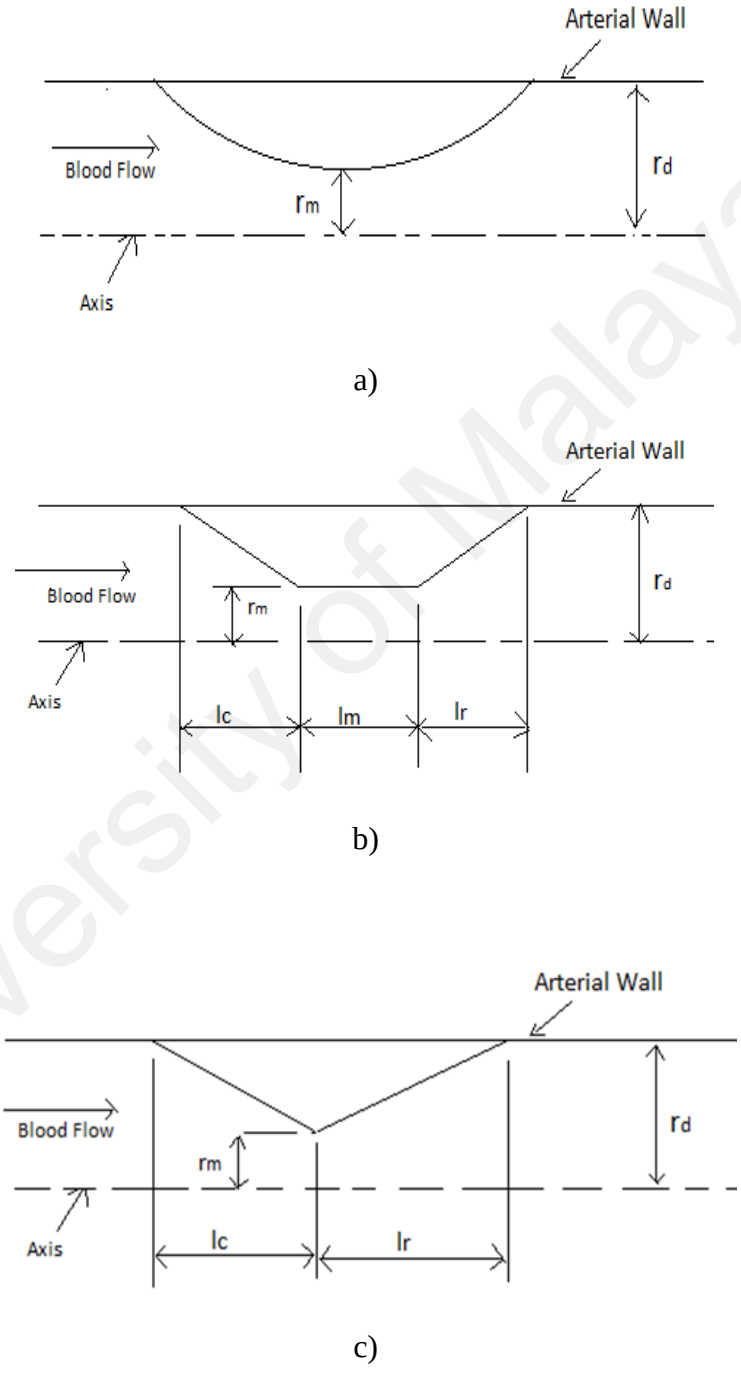

Figure 3.1: Schematic diagram for a) elliptical, b) trapezium and c) triangular stenosis geometry

Table 3.1: Dimensions of different stenosis shapes (All the dimension are in mm)

Area stenosis (AS)			Triangle			Elliptical			Trapezium		
	r_d	r_m	l_c	l_m	l_r	l_c	l_m	l_r	l_c	l_m	l_r
70%	1.5	0.82	5	-	5	-	-	-	3.5	3	3.5
80%	1.5	0.67	5	-	5	-	-	-	3.5	3	3.5
90%	1.5	0.47	5	-	5	-	-	-	3.5	3	3.5

3.5.2 Modeling of coronary artery with varying angle of curvature

In order to investigate the influence of angle of curvature, four solid models representing 30^0, 60^0, 90^0 and 120^0 curvature angle of coronary artery were developed in ANSYS workbench. L1 and L3 represent the length prior to the stenosis and immediate after the curvature which is 30 mm and 40 mm respectively. The curvature length L2 for all the four models under investigation is kept at constant value of 10mm. Figure 3.2 shows the geometric representation of 30^0 curved artery model. The various size of stenosis was introduced prior to the beginning of curvature in the coronary artery models. The percentage area stenosis was calculated by using equation (1). Table 3.2 shows the length and dimension of stenosis as given by (Govindaraju et al., 2014; Konala et al., 2011; Rajabi-Jaghargh et al., 2011).

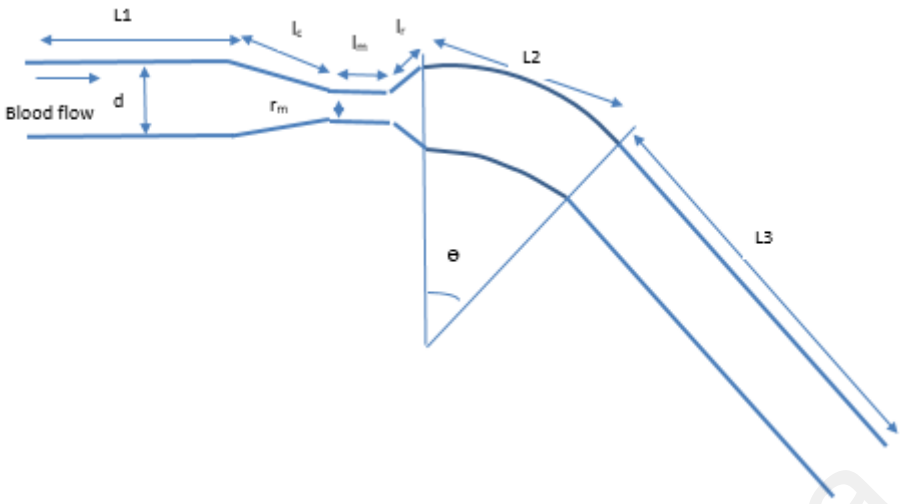

Figure 3.2: Geometric representation of curved artery for 30^0 degree

Table 3.2: Dimensions of different degree of stenosis in the models (All dimension are in mm) (Konala et al., 2011)

Area stenosis (AS)	d	r_m	l_c	l_m	l_r
70%	3	0.82	6	3	1.5
80%	3	0.67	6	1.5	1.5
90%	3	0.47	6	0.75	1.5

3.5.3 Mesh generation for ideal coronary artery models

The coronary artery models developed in ANSYS workbench is exported into Step file format. In order to create a high quality mesh ANSYS ICEM CFD 14.5, a mesh generator has been used. The model were imported into ANSYS ICEM CFD 14.5, where mesh with hexahedral elements is generated. Figure 3.3 and figure 3.4 shows the grid structure generated for Elliptical model for 80%AS and 30^0 degree curved artery model (70% AS) respectively.

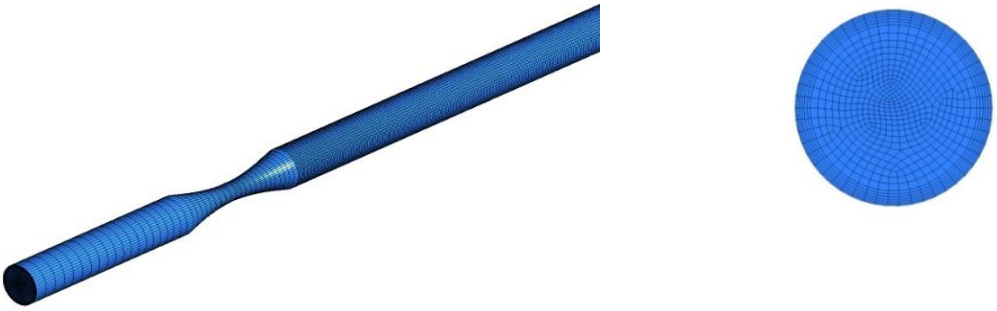

a) b)

Figure 3.3: Computational mesh used for numerical study in the elliptical model for 80%AS (a) front view b) side view

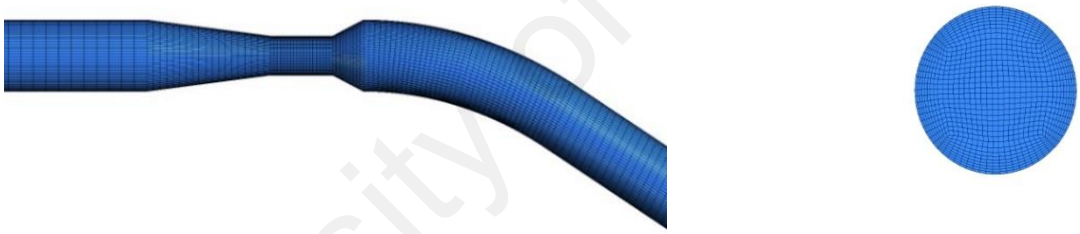

a) b)

Figure 3.4: Grid structure for the curved stenosis artery of 30 degree (a) front view b) side view

3.6 Mesh independent study

The accuracy of computational simulations depends on the quality of the mesh used. A mesh independent study was carried out before selecting the number of elements based on the results obtained. A simulation of three sets of large numbers of

elements has been performed and the results were plotted as shown in figure 3.5 and figure 3.6 and table 3.3. The velocity at appoint mid of the stenosis during the cardiac cycle and pressure drop along the axial length for the peak systole shows identical results for the three different sets of mesh elements. It is evident from table 3.3 that the mesh size of elements 258894 gives mesh independent study within reasonable amount of CPU time. Thus mesh elements in this range is chosen for simulation.

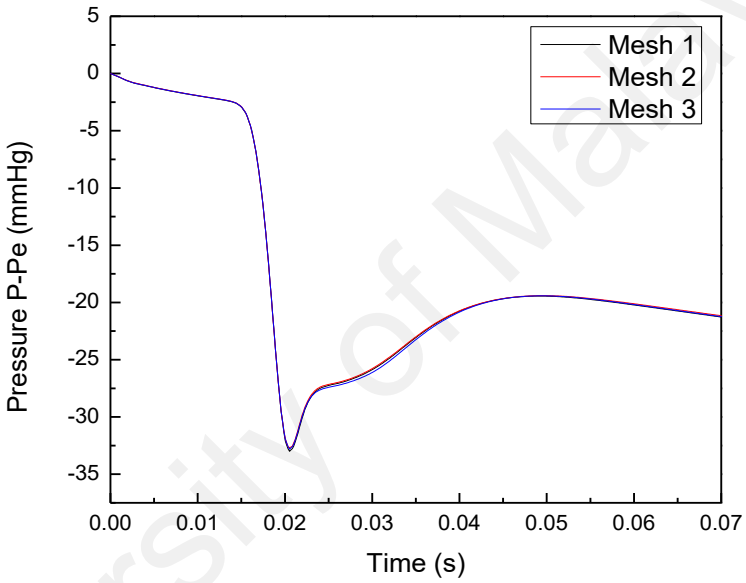

Figure 3.5: Axial pressure drop along the length of the artery for elliptical model in 70% AS

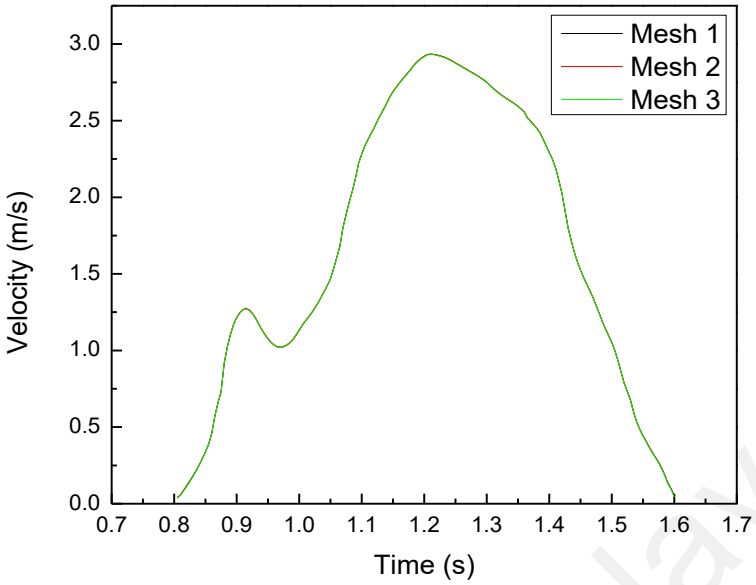

Figure 3.6: Velocity profiles at a point mid of the stenosis for elliptical model in 70% AS

Table 3.3: Mesh independent study

Elliptical model with 70%AS	Number of Elements	Peak velocity (m/s)	Maximum Pressure drop P-Pe (mmHg)	Time (s)
Mesh 1	258894	2.93494	-32.9981	5:25:33
Mesh 2	360360	2.93484	-32.6757	6:9:12
Mesh 3	447755	2.93221	-32.8087	7:43:45

3.7 Modeling of 3D realistic left coronary artery by using 2D CT scan images

The realistic coronary artery model can be constructed from CT scan image data of suspected patients of coronary artery diseases. The 2D DICOM (Digital Imaging and Communications in Medicine) images data of patients is converted into the 3D CAD

model using the image processing software, such as MIMICS and Analyzer etc. later a surface model is imported into a suitable CAD software to develop a solid realistic coronary artery model. In the current study, the realistic coronary artery models were developed from the CT image were obtained from Hubli Scan Center with professional radiologist in India. In the current study CT scan data of five patients of suspected coronary artery disease is considered to develop the 3D coronary artery models. The patients detail and stenosis location in the models is as shown in table 3.4. The MIMICS software has been used for generating the 3D realistic coronary artery models throughout this study. The scan interval should be as low as possible in order to avoid the stair-step which is found across the curved surfaces on the models and less than 2mm thickness is recommended for the accurate segmentation of models. In the current study all the models were developed with slices more than 300 in the coronal, sagital and axial plans.

Table 3.4: Patient's details of suspect's coronary artery disease

Patient	Gender	Age	Stenosis Location
1	M	37	RAMUS
2	M	39	LAD
3	M	46	LCX
4	M	49	LAD
5	M	49	LAD

A MIMIC is a medical image processing software, which creates 3D model. The 2D cross section medical images obtained from computed tomography (CT) and magnetic resonance imaging (MRI) scan are used to generate the 3D models. These images acquired during scanning in the direction XY plane (axial), XZ plane (coronal) and YZ plane (sagittal) can be loaded in to the Mimics software. The process of

converting these anatomical data from images into 3D model with measurement and accuracy is called segmentation. Once the 3D model is segmented, it can be exported into a different formats and engineering applications, such as FEA, surgical simulation, design and additive manufacturing and more.

In this study the reconstruction of realistic left coronary arteries is performed by importing the 2D CT scan images of suspected coronary artery disease patients in DICOM (*.dcm) file format in to the MIMICS. The images were acquired in the 128 slicer scanner with the following specification: the Beam collimation 0.6, pitch, 1.4, reconstruction interval of 0.6mm with the tube voltage of 100kVp current ranging from 300 to 650mAs. The slice thickness in the axial direction was 0.6mm with the 0.75mm increment. These scan images in all the three direction (axial, sagittal and coronary) is imported into MIMICS to create model. The images consist of grayscale information, based on these gray values (Hounsfield Units) user generates models. These gray values is associated with each image pixel which defines the shade (white, gray) of the pixel. The density of the material and gray values assigned to each pixel is directly related. Density of bones is higher than the soft tissues, which helps to differentiate the soft tissues and bones. All the images is compressed and merges in MIMICS software to generate a single volume file format MIMICS (*.mcs) according to the same pixel size value. Later on the segmentation of left coronary artery is carried out by selecting an appropriate thresholding values. A range of threshold values is defined to create the segmented mask of left coronary artery. The value of thresholding for arteries is within the range of soft tissue and it differs from patients to patients ranging from -150 to 450 HU (Hounsfield Units). Further an automatic region growing function is used to create the left coronary artery model after the segmentation process. The 2D CT scan images (coronal, sagittal and axial), 3D volume rendering of left and right coronary artery along

with ascending aorta, heart after the segmented procedure as shown in figure 3.5. Later the manual segmentation was performed to edit the mask in order to remove the floating pixel and unconnected regions which do not constitutes the left coronary artery. The 3D model of left coronary artery is visualized through the 3D rendering tool in MIMICS, as shown in figure 3.7. To examine and ensuring the accuracy of anatomical model, 3D rendering tool helps. Once the modeling of left coronary is confirmed as per the clinical observation, it is converted into stereo-lithography (*.stl) file format and exported to 3-matic for mesh generation.

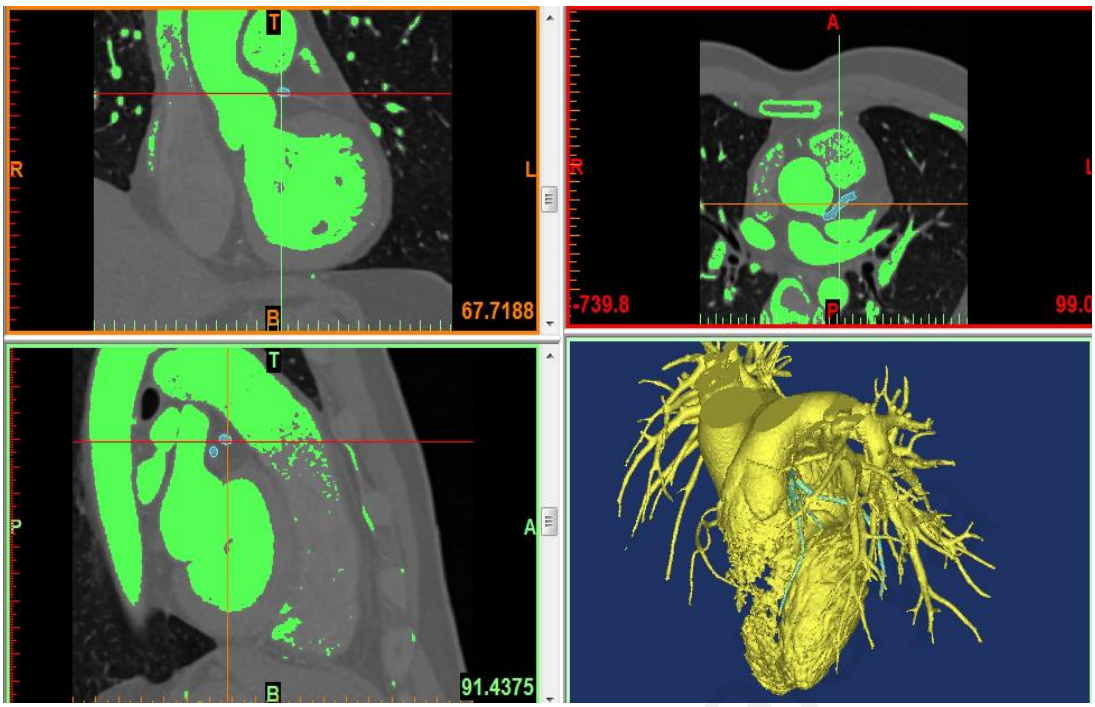

Figure 3.7: 2D CT scan images with 3D volume rendering image of normal left coronary artery

3.8 Generating 3D left coronary artery models and meshing using 3-matic software

The 3D anatomical models of left coronary artery is imported using the stereo-lithography (*.stl) file format from MIMICS in to the 3-matic. The 3D surface models of left coronary artery is further edited until a smooth and refined surface is obtained by using smoothing function in order to remove the sharp edges and corners in 3-matic. The ends of all the branches of left coronary artery model are trimmed to obtained flat surfaces, for applying boundary conditions.

The left coronary artery surface model is initially meshed with the triangular elements by using re-mesh function, later the quality of surface mesh is analyzed by using inspection tool. The mesh quality in 3-matic can be controlled by various parameters, such skewness, orthogonal angle, element quality, edge length etc. A skewness of 0.4 is set to control the quality of elements in the current study. Once

optimize surface mesh is generated then volume mesh was performed by using the volume mesh tool in 3-matic. The coronary artery model is then meshed with tetrahedral elements further the quality of elements was inspected in order to have an optimized mesh models as shown in figure 3.8.

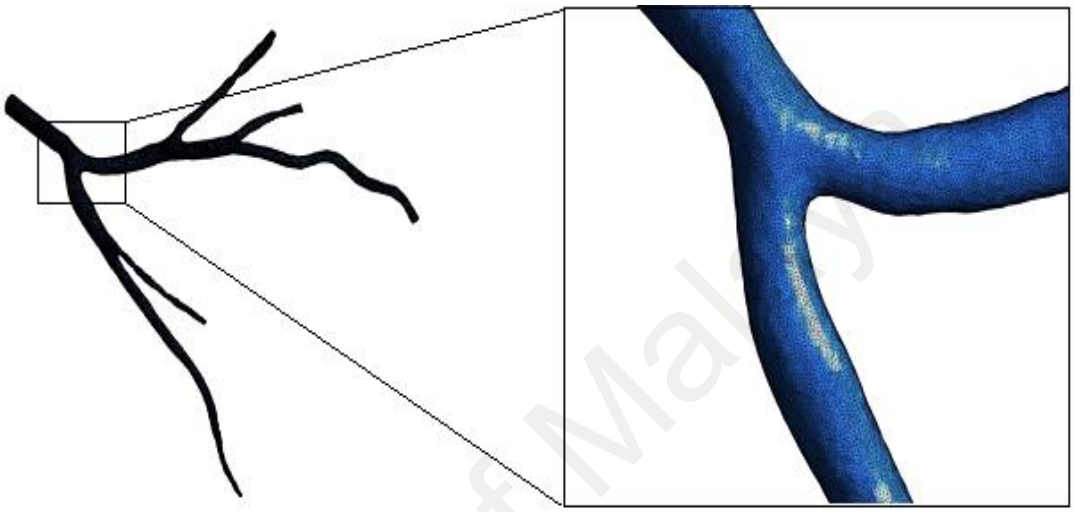

Figure 3.8: Normal left coronary artery with fine mesh using tetrahedral elements

In order to ensure the realistic physiological conditions, the 3D numerical simulation for the idealized coronary models with different shapes of stenosis is performed with a transient Pulsatile pressure p(t) (figure 3.9) at the inlet, and transient parabolic velocity u(t) (figure 3.9) at the outlet. The pulsatile pressure and parabolic velocity is obtained from the literature konala et al. (Konala et al., 2011; Tang et al., 2009) and Banerjee et al. (Cho, Back, Crawford, & Cuffel, 1983; Sinha Roy et al., 2006) respectively. A no-slip condition is applied at the wall. The mean hyperemic flow rate $(\tilde{Q})$ 175ml/min, 165ml/min and 115ml/min is used to acquire the velocity profile for 70%, 80% and 90% AS respectively. The shear stress transport (SST) turbulence model belonging to k-ω model was used for modelling the flow which gives the

accurate and robust results for high Reynolds number as noted by Jozwik et al. (Jozwik & Obidowski, 2010) and Kagadis et al. (George C. Kagadis et al., 2008).

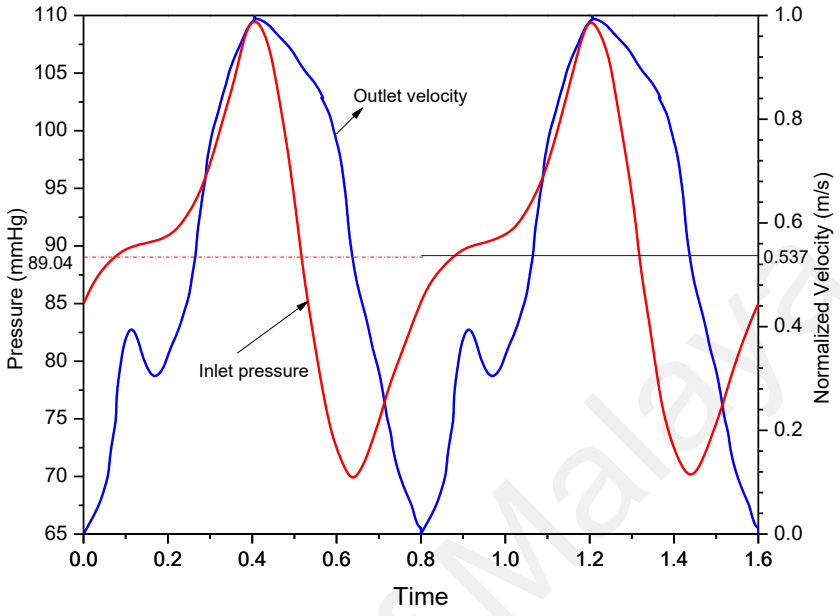

Figure 3.9: Physiological pressure (Konala et al., 2011; Tang et al., 2009) and velocity applied at the inlet and outlet (Cho et al., 1983; Sinha Roy et al., 2006) respectively. The peak velocity corresponds to a normalized velocity of 1.0, so that the ratio of mean to peak velocity is 0.537

3.9 Validation of simulation results with published results

In recent years Computational Fluid Dynamics (CFD) simulations are extensively used as replacement to experimental studies due to the reason that CFD can give high accuracy in predicting the various kind of flow behaviour in many engineering and scientific fields. The second important point that has attracted researchers to use CFD is that it can answer many what if scenarios which otherwise becomes extremely difficult to answer for any experimental study. In some cases it is impossible to get the experimental results due to value of human life involved and moreover CFD can predict the secondary variables quite easily which is extremely difficult to get through experimental means. Another reason to opt CFD can be

attributed to the fact that, it gives results in very short time as compared to that of experimental studies thus compressing the huge amount of time which helps researchers to devote extra time on interpreting various kinds of scenarios. However, in order to obtain accurate numerical simulation and results, it is necessary to validate the results obtained from numerical simulations against the experimental data. For this reason, the bench mark validation case has been done for guide wire flow obstruction effect on pressure drop across the stenosis and hence the coronary diagnostic parameters in-vitro experimental setup

3.10 Simulation of guide wire measurement of stenosis severity in vitro experimental setup

In order to compare the present methodology, our model was reduced to the base model for which the results are available in open literature. A 3-D model replicate of coronary artery model with stenosis employed experimentally by Banerjee et al (R. K. Banerjee, Peelukhana, & Goswami, 2014) to study the pressure drop across the stenosis and hence the diagnostic parameter was considered for the benchmark validation. In this experimental work, the coronary test section consists of converging, throat and diverging part. The various geometrical dimensions involved for the coronary artery for 80% AS are given in Table 3.1. This geometry was well validated with clinical data in several occasions (Ashtekar, Back, Khoury, & Banerjee, 2007; R. Banerjee et al., 2008). In this benchmark validation, the CFD analysis was carried out with the coronary artery model used by Banerjee et al (Banerjee et al., 2014) by assuming blood as non-Newtonian fluid which follow Carreau model. Experiments of Banerjee et al. (Banerjee et al., 2014) consists of a guide wire of diameter 0.014” to measure the pressure drop across the stenosis having the pulsatile flow. The hyperemic flow rate was found from the clinical data (Wilson et al., 1988) which was used in their experiment to evaluate FFR and CDP. The experimental mean hyperemic flow rate was 135 ml/min in the case

of intermediate stenosis severity (80% AS). These results could be used as a benchmark case for validation of the CFX simulations. In addition to achieve the goal of validation of CFX simulation solver for computing pressure drop across the stenosis to find the functional significance of the stenosis severity, this study focuses on the effect of mesh density, laminar and $k-\omega$ SST model on the accuracy of results.

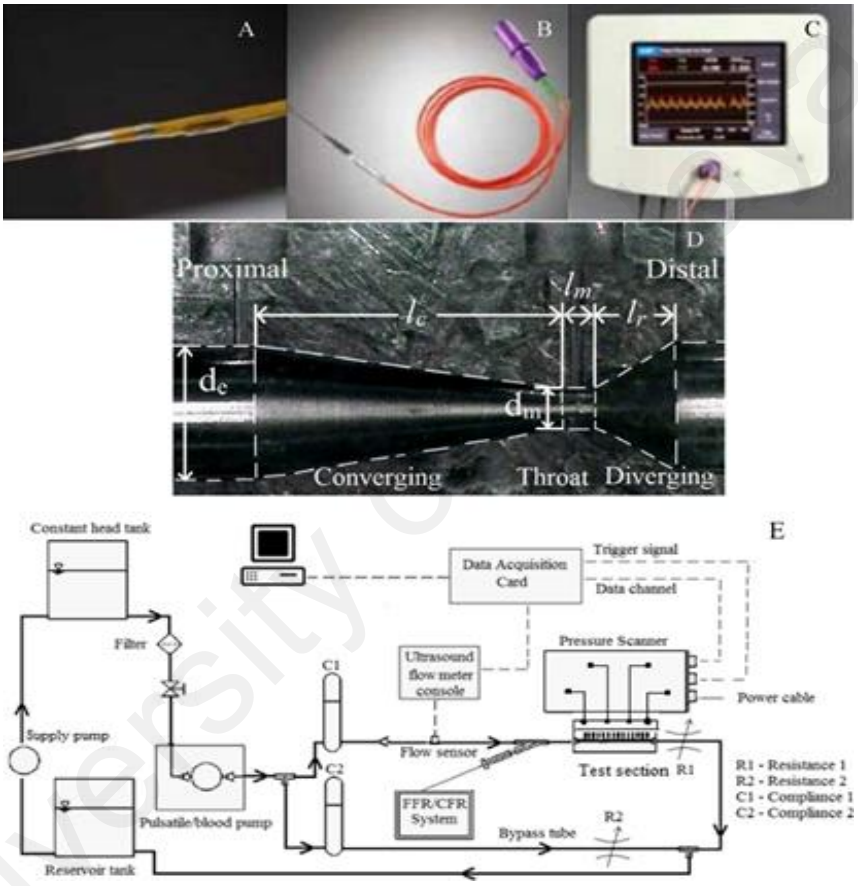

Figure 3.10: Experimental setup of coronary artery model, Reprinted from (Banerjee et al., 2014), Copyright (2015) with permission from Elsevier

3.11 Pressure drop comparison

Figure 3.5 shows the pressure drop comparison of present results using $k-\omega$ SST models with the experimental results of Banerjee et al (Banerjee et al., 2014) . It is obvious from this figure that the present methodology is quite accurate enough in predicting the various flow characteristics.

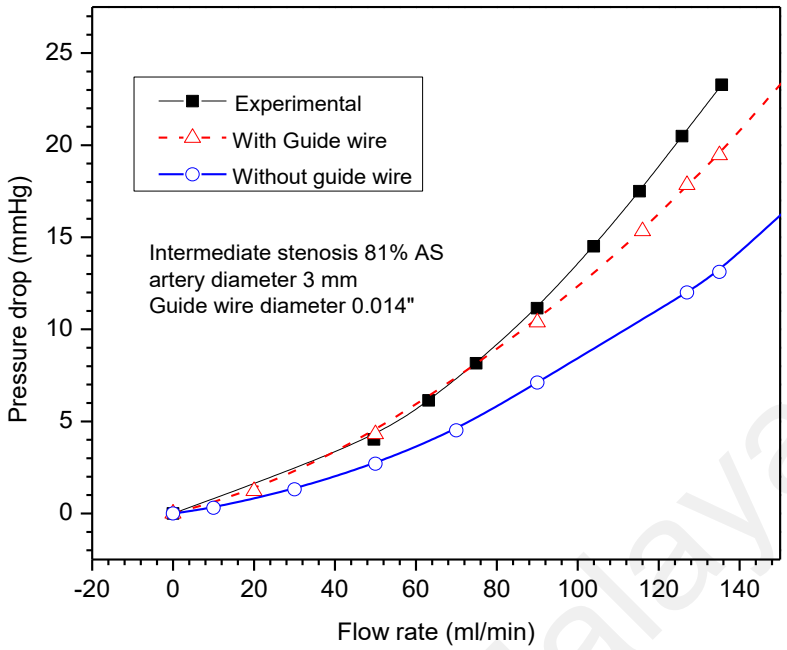

Figure 3.11: Results of Experimental data (Banerjee et al., 2014) and computational data of with and without guide wire

3.12 FFR and CDP comparison

The values of FFR, and CDP obtained from the simulation study under hyperemic flow condition, were compared with the previous work done by Konala et al. and it can be seen from figures clearly that there is a good agreement of our numerical results with the results of Konala et al. (Konala et al., 2011), thus validating the present methodology

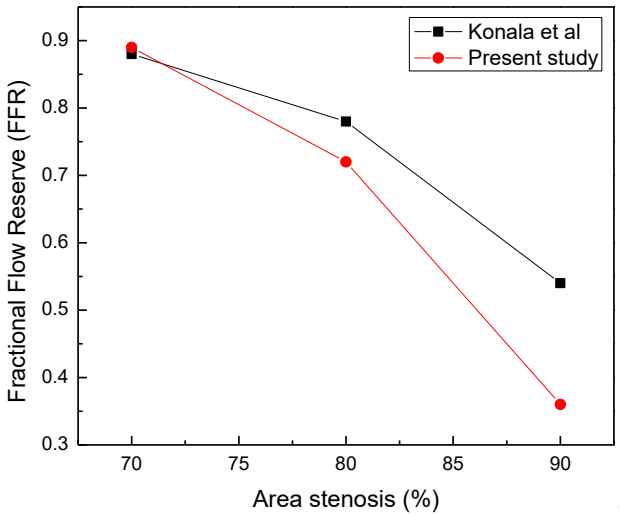

Figure 3.12: Compression of FFR for rigid plaque wall model reported by Konala et al. (Konala et al., 2011)

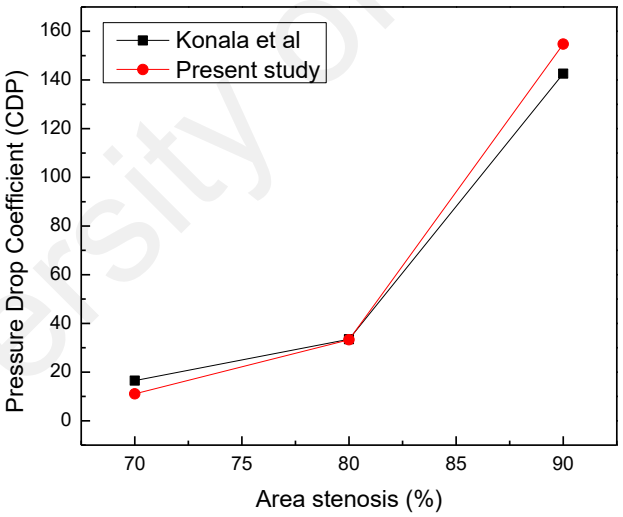

Figure 3.13: Compression of CDP for rigid plaque wall model reported by Konala et al.(Konala et al., 2011)

CHAPTER 4: RESULTS AND DISCUSSION

4.1 Introduction

In this chapter, the detailed analysis has been carried out to investigate the blood flow in a stenosed left coronary artery. The results obtained from the simulation of ideal and realistic left coronary artery models were presented. The effect of different shapes of stenosis, variation of angle of curvature, and influence of deferent degree of stenosis in left coronary artery on the hemodynamic parameters such as, pressure, velocity and wall shear stress were reported in detail, along with the diagnostic parameters FFR, CDP and LFC.

4.2 Effect of shapes of stenosis on pressure and diagnostic parameters

Figure 4.1 Shows time average pressure drop in the triangular, elliptical and trapezium models. The $\Delta\widetilde{p}$ for trapezium shape stenosis was higher than the other two models and is followed by the elliptical and triangular shapes of models for a fixed stenosis severity. The $\Delta\widetilde{p}$ increases in non-linear manner as percentage AS increases for all the models. This could be characterized by the non-linear nature of momentum changes on account of area constriction and vary with a second power of flow rate (Konala et al., 2011). For triangular shape stenosis model, the pressure drop for 70% AS was 4.89 mmHg, however as the percentage AS increased from 70% to 80%, the pressure drop increased to 7.71 mmHg whereas from 80% to 90% AS, increased to 15.53 mmHg. In case of elliptical model, for 70% AS the drop in pressure was 6.17mmHg, but for 80% AS, it increased to 9.58mmHg whereas for 90% it further increased to 16.78mmHg. Similarly for trapezium models pressure drop for 70%AS was 7.43mmHg, increased to 12.45mmHg as stenosis severity increased from 70% to 80% AS and further increased to 24.85 mmHg as stenosis severity increased to 90%. The

comparison of axial pressure drop in the models (Triangular, Elliptical and Trapezium) for a given percentage AS revealed that the trapezium shape stenosis models has higher pressure drop than in the other two models (Triangular, Elliptical) during a cardiac cycle. This is due to the effect of the stenotic shape (‘‘shape-effect’’), for triangular model after the convergent, stenosis starts diverging to maximum so that the flow would be maximum which results in less drop in pressure. In case of elliptical stenosis, the rounded surface affects the flow to lesser extent in terms of localized losses of pressure and recirculation. Consequently, both triangular and semi ellipse represents a less-severe pathology than a trapezium, reducing the risks of deposit, setting and enhancement of a stenosis. The trapezium shape consists of throat section after the convergent which significantly affect the pressure drop as compared to the other two models. This shows that the shape of the stenosis plays a very important role.

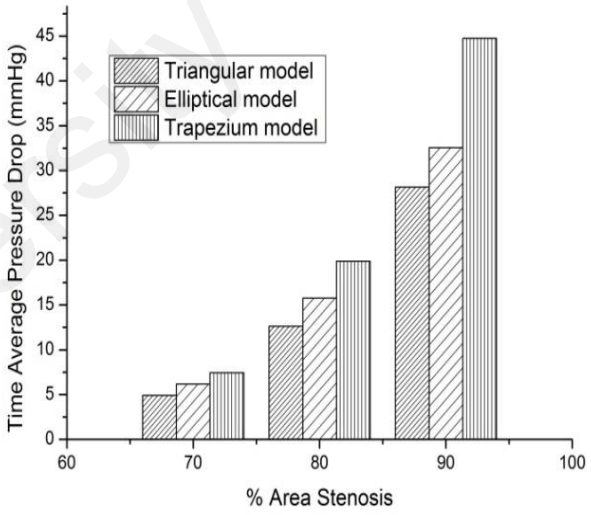

Figure 4.1: Bar graph showing variation of time averaged pressure drop across a given area stenosis with different shape stenosis (triangular, elliptical and trapezium)

figure 4.2 shows that the value of Fractional Flow Reserve (FFR) for all the models decreases with the increase in the percentage AS. The FFR for the different shapes of models, obtained is in close agreement with available literature reported by Konala et al.

(Konala et al., 2011). Konala et al. have considered only trapezium model with a little change in geometry of stenosis. The computed values of FFR was plotted for the best fit approximation with linear correlation R^2=0.97. A horizontal line was drawn at FFR=0.75 which represents the cut-off value, to determine a range of AS with possible misdiagnosis as shown in the figure. 4.2. This horizontal line intercepted the FFR–AS lines intersect at 76.5%, 79.5% and 82.7% AS in trapezium, elliptical and triangular model, respectively. For AS < 76.5%, the FFR value for all the models (triangular, elliptical, trapezium) were well above the cut-off value of 0.75, and in the range of 76.5%- 79.5% the value of FFR for triangular and elliptical model was observed to be greater than 0.75, whereas the FFR value for trapezium model was lower than the cut-off value of 0.75, which could lead the misdiagnosis of stenosis severity. Similarly in the range of 79.5%- 82.5% AS, the elliptical model and trapezium models were below the cut of value of 0.75 whereas the triangular model shows FFR of 0.75, raising the potential of misdiagnosis. At 82.7%, the triangular model shows FFR of 0.75 whereas trapezium and elliptical models show the FFR value of less than 0.75. For AS≥ 82.7 the coronary interventional procedure could be carried out irrespective of the stenosis shape. Thus the variation in FFR in the region of 76.5-82.7% AS could lead to the misdiagnosis of intermediate stenosis to decide upon coronary intervention around the clinically used cut-off value of 0.75 if the decision is based only on angiography instead of the actual measurement of FFR. From the above discussion it is obvious that the shape of stenosis plays important role in evaluating functional significance of the stenosis severity.

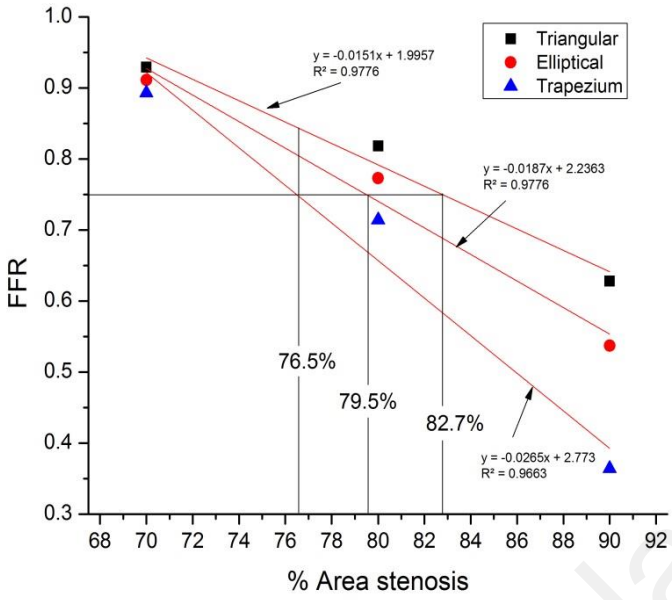

Figure 4.2: Variation of FFR values with different shapes of stenosis (triangular, elliptical and trapezium)

The non-linear increase in the value of Pressure drop coefficient (CDP) was observed for all the three different shapes of stenosis models as shown in figure. 4.3. For triangular model 3 fold increases in the value of CDP from 7.29 to 21.17 was observed in stenosis severity from 70% to 80% AS, whereas an increase in stenosis severity further to 90% AS elevated the CDP value by 4.6 times to 97.34. An elliptical model also shows a similar nonlinear trend, such as 1.9-fold increase in CDP value from 9.19 to 26.45 was observed as the stenosis severity changed from 70% to 80 AS; this value further increased to 112.5 (4.3 fold)with an increase in the stenosis severity to 90% AS. For the case of trapezium model a 3 fold increase in the CDP value from 11.0 to 33.2 was observed in the stenosis severity from 70% to 80% AS, further increase in stenosis severity to 90% AS elevated the CDP value by 154.7.

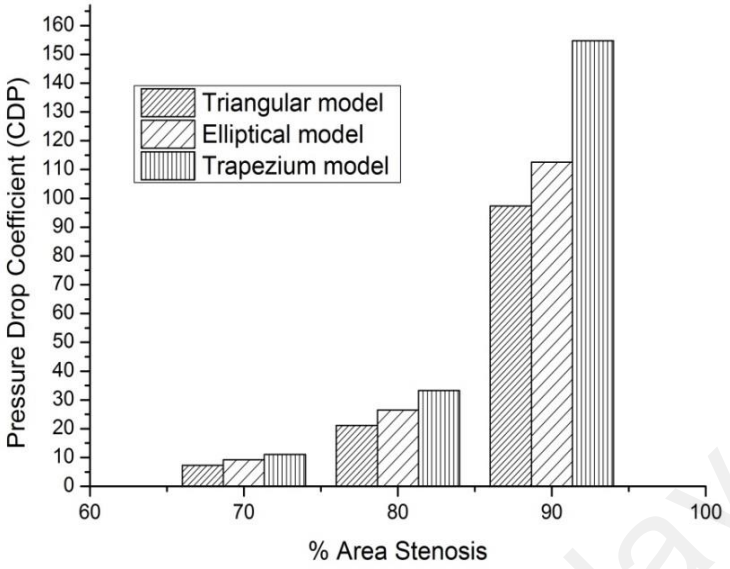

Figure 4.3: Variation of CDP with %AS in various shapes of models (triangular, elliptical and trapezium)

Figure 4.4 depicts the variation of LFC (Lesion Flow Coefficient) for the different shapes of stenosis in different percentage AS. The value of LFC was found to be higher for the trapezium model than that of the other two models (triangular and elliptical). For the triangular shape stenosis, the increase in severity from 70% to 80% AS shows 1.1% increase in the LFC value. A further increase in 5.7% was observed for an increase in stenosis severity to 90%AS. However the elliptical model does not exhibit variation in the value of LFC (0.77) with corresponding increase in severity from 70% to 80% AS. For 90% AS the LFC increased to 11.6% (0.86). For the case of trapezium model the LFC was found to be same (0.70) for both 70% and 80% and is increased to 4.2% (0.73) for 90% AS.

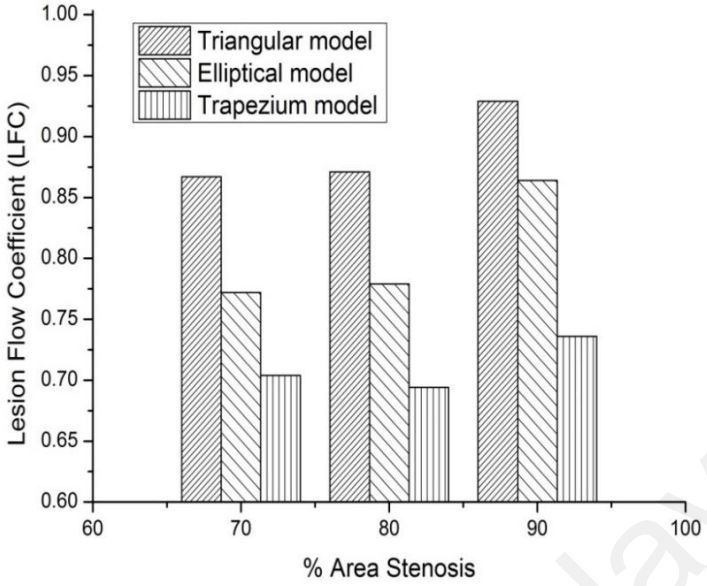

Figure 4.4: Variation of LFC with %AS in different shapes of models (triangular, elliptical and trapezium)

4.3 Influence of shapes of stenosis on velocity parameters

Figure 4.5 shows the variation of radial velocity along the stenosis for the 70%AS elliptical model in different time steps. The velocity profile for the time step 1.05s. 1.2s, 1.38s and 1.51s represents the near beginning of the systole, peak systole, early diastole and later diastole respectively. As expected, the velocity profile at peak systole (1.2 sec) is maximum as compared to the other time steps due to maximum inlet velocity at 1.2 sec. It is observed that the blood velocity at proximal (Z=1) is lower as compared to the mid of throat (Z=II), just after stenosis distal (Z=III) and at the distal (Z=IV) location for all the times step. The maximum velocity was noted at the midpoint of the throat (Z=II) segment for the time step 1.05s, 1.2s, 1.38s and 1.51s is 1.46m/s, 2.92m/s, 2.45m/s and 0.93m/s respectively as compared to other locations with respect to their time steps during the cardiac cycle.

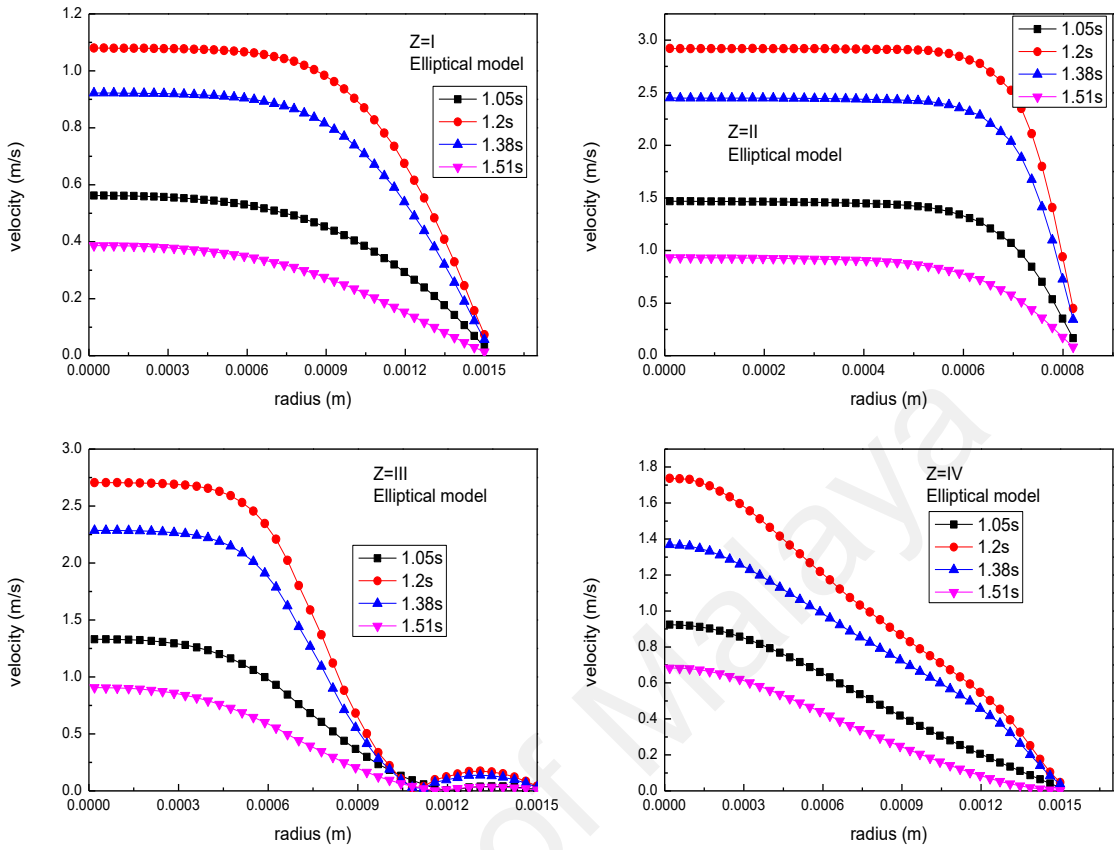

Figure 4.5: Velocity profile at some locations along the stenosis at various times for 70%AS in elliptical model

Figure 4.6 illustrates the velocity variation in the radial direction along the stenosis for the 80%AS elliptical model in for time steps during the cardiac cycle. It is observed that the velocity profile shows no significant difference for the proximal (Z=1) location as compared with the 70%AS elliptical model. The increase in velocity was noted at the throat (Z=II) from 1.46m/s, 2.92m/s, 2.45m/s and 0.93m/s to 2.17s, 4.43s, 3.69s and 1.36s for the time step 1.05s, 1.2s, 1.38s and 1.51s respectively. Similarly at the distal just after the stenosis (Z=III) the increase in velocity pattern is observed for the respective time steps, whereas decrease in the velocity pattern is also observed for the location (Z=IV) distal from stenosis expect for the time step 1.05s which shown increase in velocity from 0.9s to 1.24s.

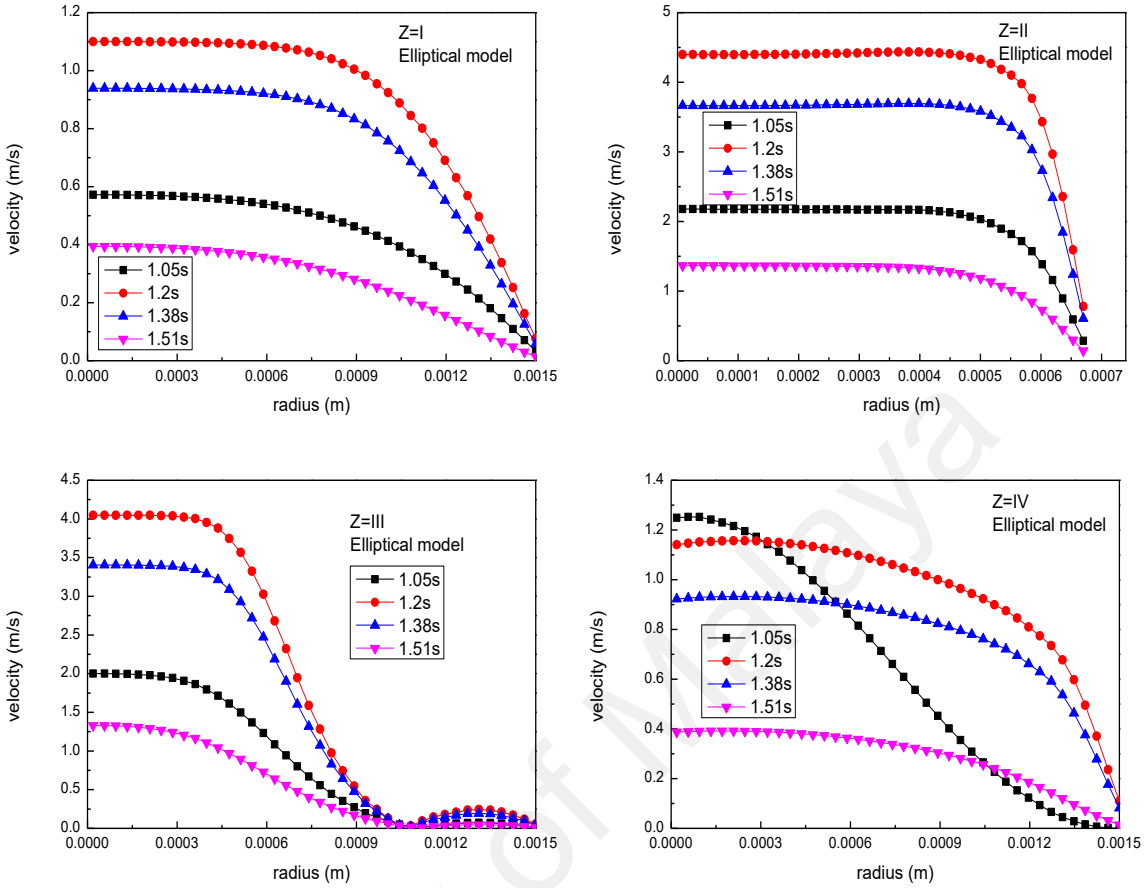

Figure 4.6: Velocity profile at some locations along the stenosis at various times for 80%AS in elliptical model

Figure 4.7 depicts the velocity variation in the radial direction along the stenosis for the 90%AS elliptical model during the cardiac cycle. For the case of 90%AS elliptical model, the proximal velocity (Z=I) is also affected as shown in figure 4.7, unlike the 70%AS and 80%AS. The further increase in the velocity was found at the throat (Z=II) as compared to the 70%AS and 80%AS. This velocity profile increases inside the stenosis throat region due to venturi effect. For the location just after the stenosis (Z=III), higher velocity was noted as compared with the same location for 70%AS and 80%AS during the cardiac cycle. The decrease in flow velocity was noted at position far from the stenosis (Z=IV) in 90%AS elliptical model as compared with the 70%AS and 80%AS elliptical model during the cardiac cycle.

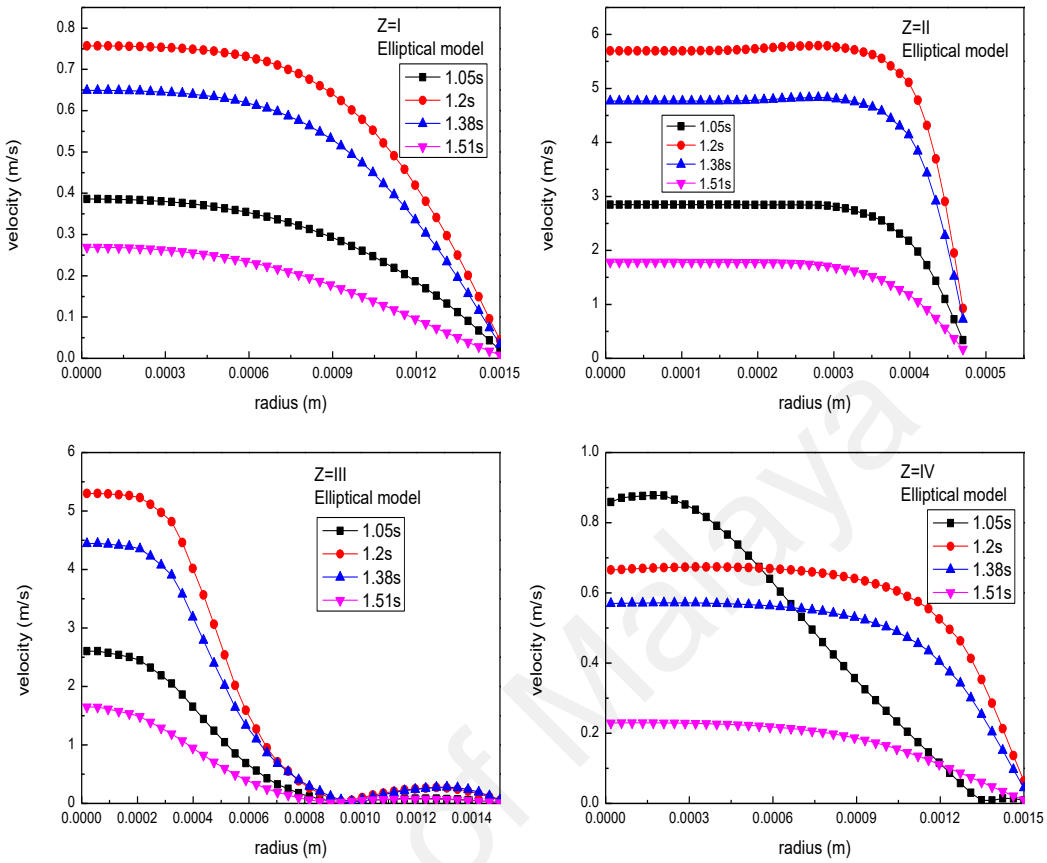

Figure 4.7: Velocity profile at some locations along the stenosis at various times for 90% AS in elliptical model

The velocity variation in the radial direction along the stenosis for the trapezoidal model in 70%AS is shown in figure 4.8 for various time steps during the cardiac cycle. The maximum velocity observed at the proximal (Z=I) location is 0.56m/s, 1.07m/s, 0.92m/s and 0.38m/s for 1.05s, 1.2s, 1.38s and 1.51s times step during the cycle respectively. The further increase in the velocity was found at the throat (Z=II) and just after the stenosis region (Z=III) for the trapezoidal model in 70%AS. However, the decrease in the velocity pattern was found in the region far from the stenosis (Z=IV) as compared to the throat and just after the stenosis region. The maximum velocity at far from the stenosis (Z=IV) is 0.98m/s, 1.67m/s, 1.3m/s and

0.68m/s for the time step 1.05s, 1.2s, 1.38s and 1.51s respectively.

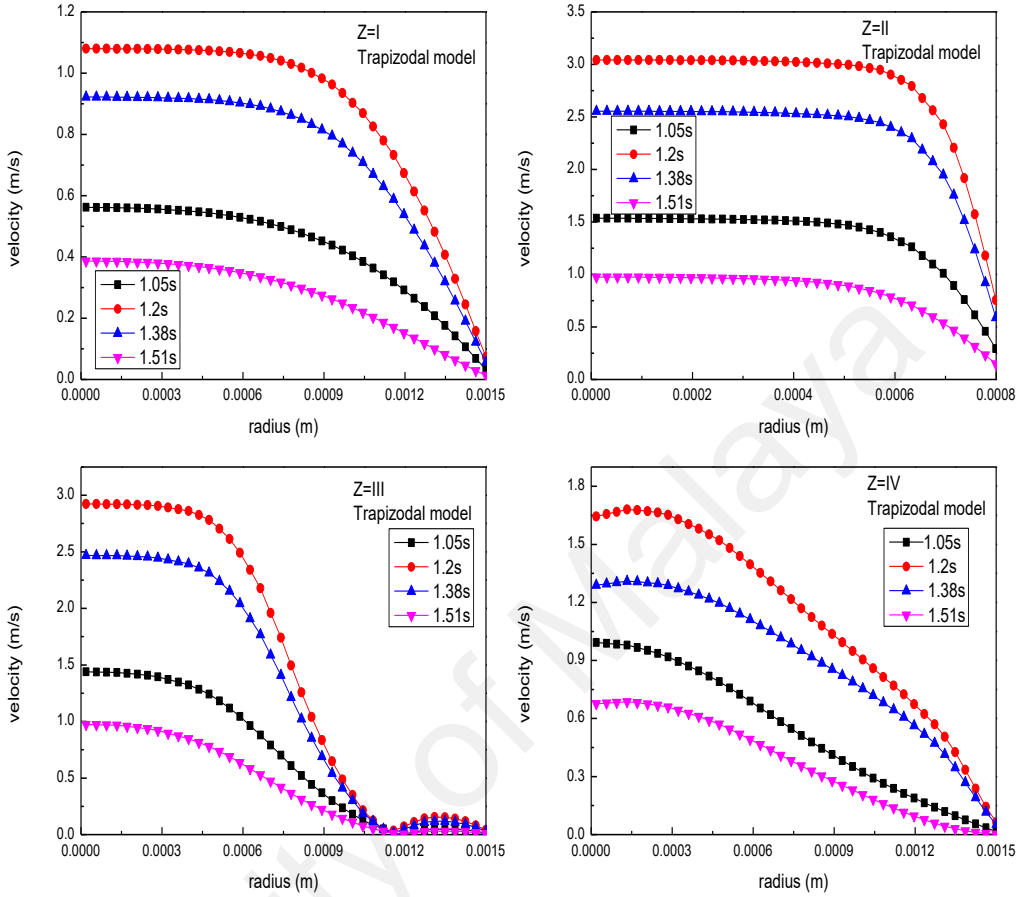

Figure 4.8: Velocity profile at some locations along the stenosis at various times for 70%AS in trapezoidal model

Figure 4.9 represents the variation of velocity in the radial direction along the stenosis for trapezoidal model in 80%AS for different time steps during the cardiac cycle. The velocity pattern shows no significant difference in the proximal (Z=I) position as compared with the 70%AS trapezoidal model. The increase in the maximum velocity was noted at the throat (Z=II) location as compared with the 70%AS trapezoidal model (figure 4.6). Similarly increase in the maximum velocity was observed for the region just after the stenosis (Z=III) as compared with the 70%AS trapezoidal model. The highest velocity at the position far from the stenosis (Z=IV) is

1.45m/s, 1.11m/s, 0.9m/s and 0.37m/s for the time step 1.05s, 1.2s, 1.38s and 1.51s respectively.

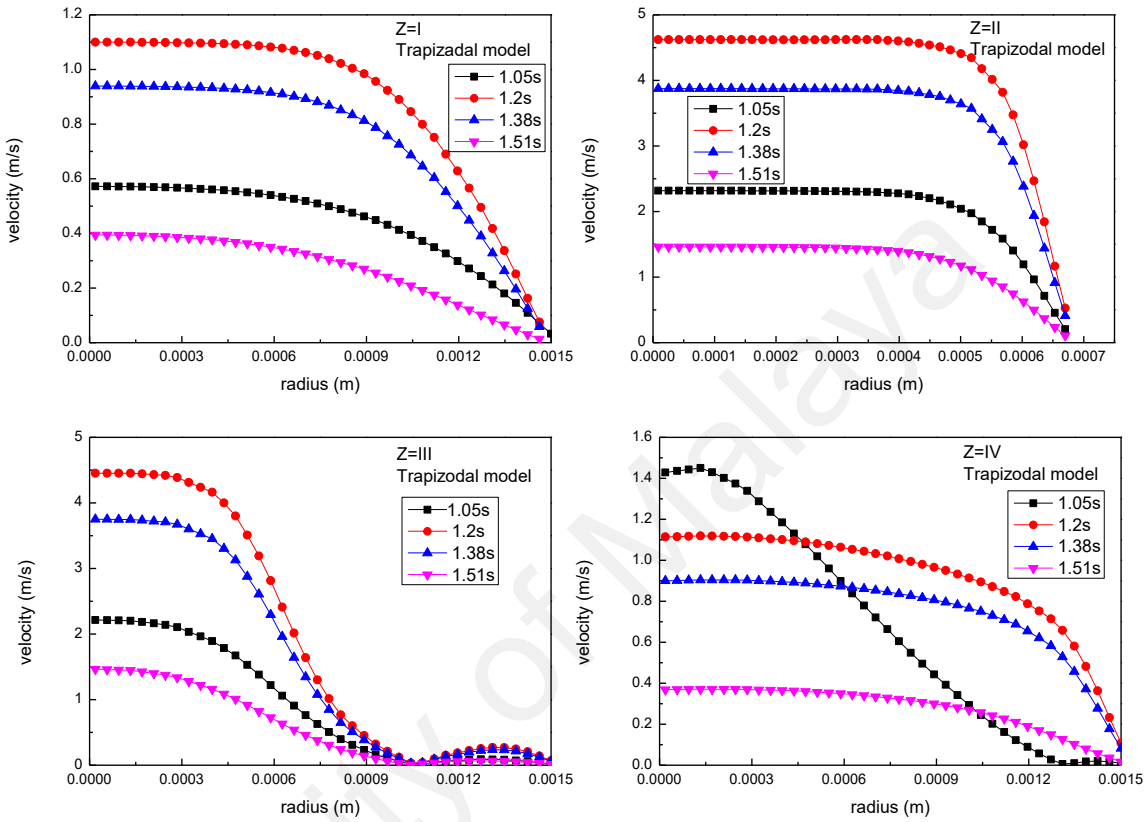

Figure 4.9: Velocity profile at some locations along the stenosis at various times for 80%AS in trapezoidal model

Figure 4.10 depicts the velocity variation in the radial direction along the stenosis for the 90%AS trapezoidal model during the cardiac cycle. It is noted that there is not much variation in the proximal velocity (Z=I) for 90%AS trapezoidal model as compared to 70%AS and 80%AS trapezoidal model as shown in figure 4.10. Whereas significant increase in the velocity at the mid of throat (Z=II) position is found when compared with the 70%AS and 80%AS trapezoidal model. Similarly higher velocity flow pattern was noted at the position just after the stenosis (Z=III) in 90%AS trapezoidal model. The decrease in the maximum velocity was recorded as 0.58m/s,

0.65m/s, 0.56m/s and 0.22m/s for the time step 1.05s, 1.2s, 1.38s and 1.51s respectively as compared with 70%AS and 80%AS trapezoidal models.

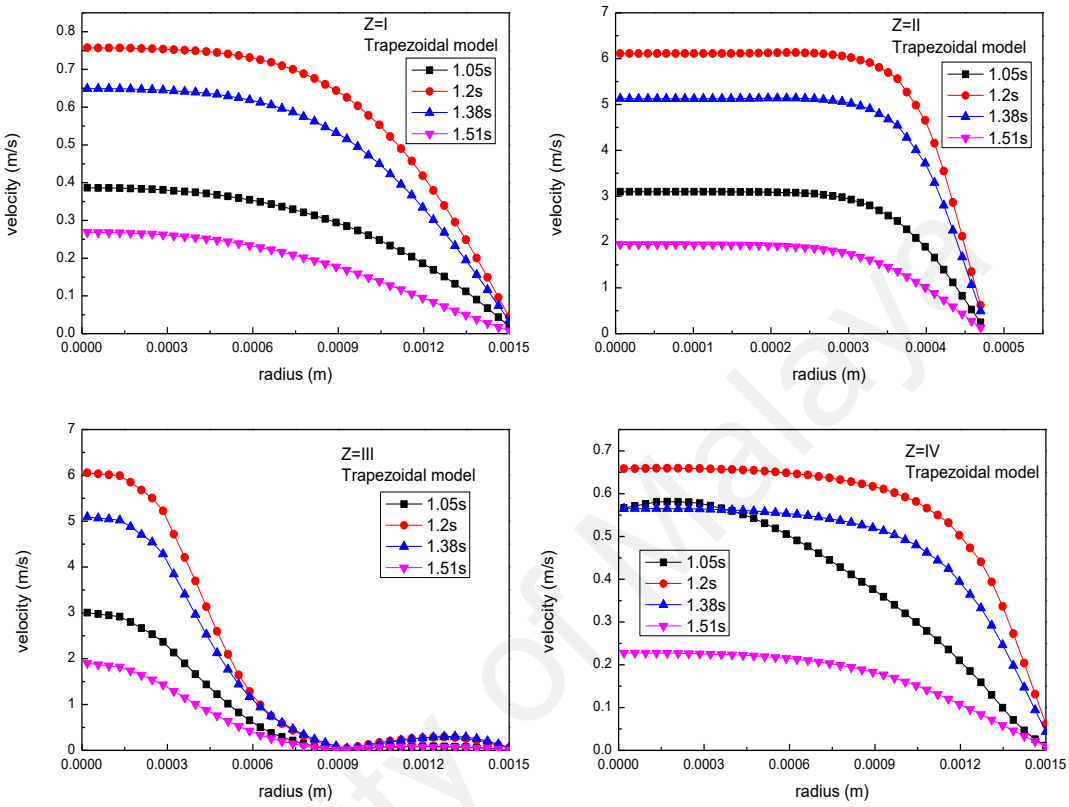

Figure 4.10: Velocity profile at some locations along the stenosis at various times for 90%AS in trapezoidal model

Figure 4.11 shows the velocity variation in the radial direction along the stenosis for the 70%AS triangular model during the cardiac cycle. The maximum velocity observed at the proximal (Z=I) shows no significant difference for the various times step during the cycle respectively. It is also noted the maximum velocity at different time step is lower than that of the 70%AS elliptical and trapezoidal models for the region at throat (Z=II) and just after the stenosis region (Z=III). The highest velocity at the region (Z= IV) for the times step 1.05s, 1.2s, 1.38s and 1.51s is 0.8m/s, 1.83m/s, 1.47m/s and 0.62m/s noted respectively. It is found that the velocity profile for triangular geometry is smallest of the three models being investigated.

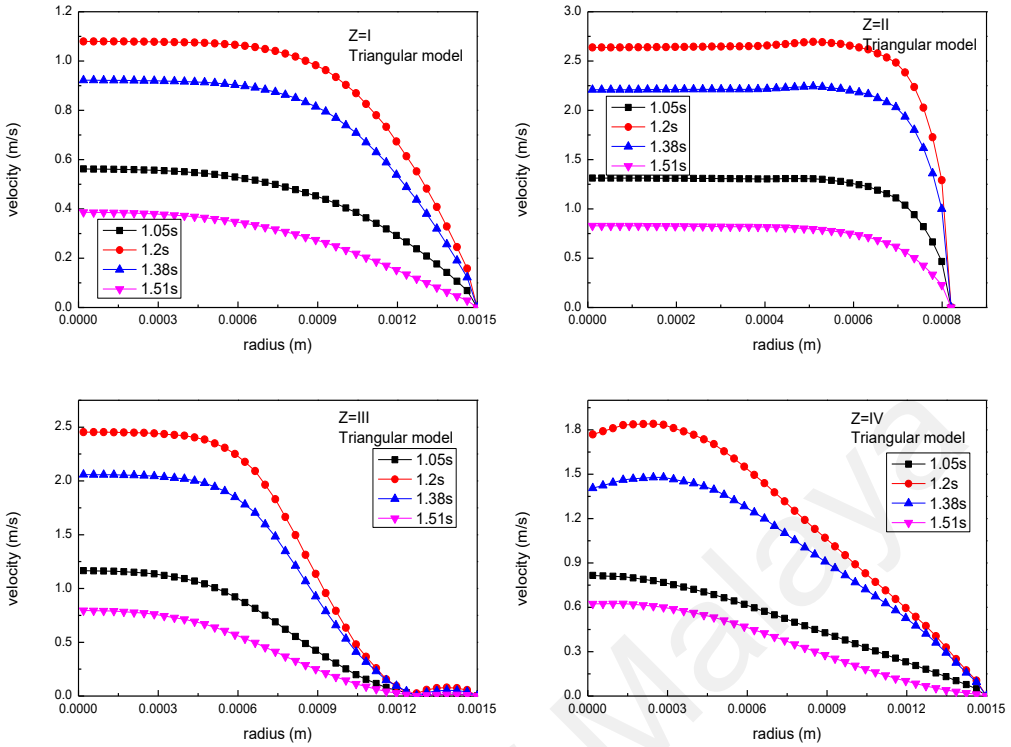

Figure 4.11: Velocity profile at some locations along the stenosis at various times for 70%AS in triangular model

Figure 4.12 represents the variation of velocity in the radial direction along the stenosis for triangular model in 80%AS for different time steps during the cardiac cycle. From figure 4.12 it is observed that there is no variation in maximum velocity pattern in the proximal (Z=I) region as compared to the other two models (elliptical and trapezoidal). The increase in the maximum velocity at the mid of throat (Z=II) and just after the stenosis (Z=III) position was noted unlike the other models observed at that positions. The higher velocity at the region (Z=IV) is 1.2m/s, 1.19m/s,0.95m/s and 0.44m/s for the time step1.05s, 1.2s, 1.38s and 1.51s recorded respectively.

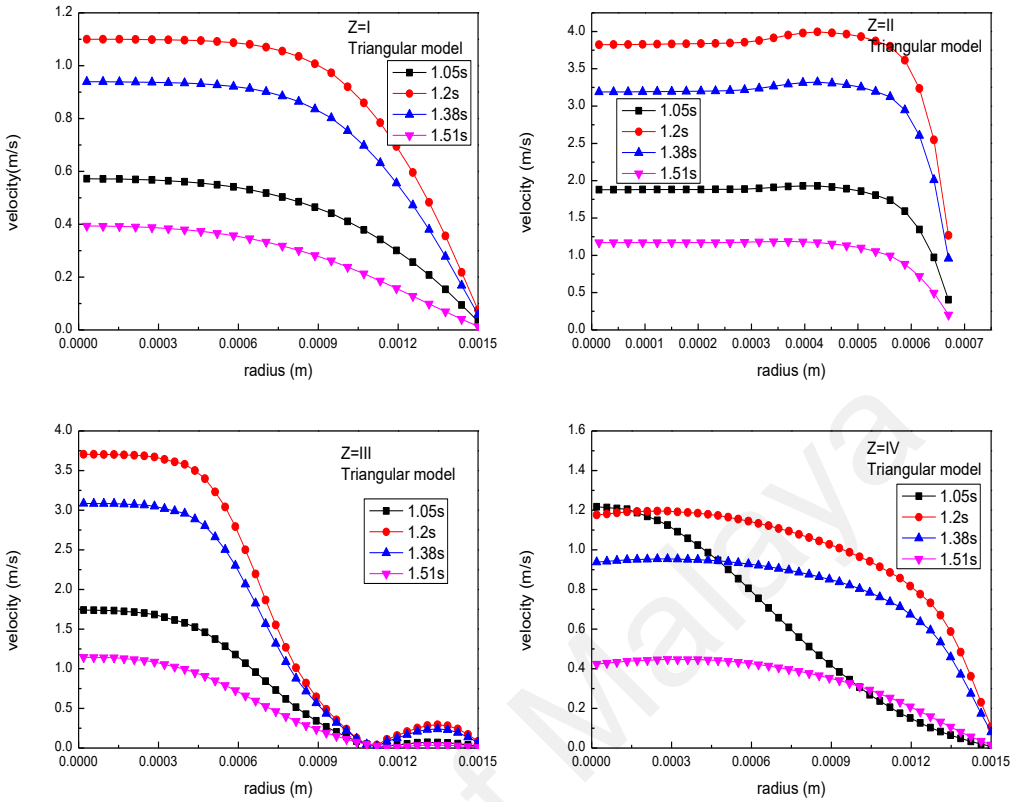

Figure 4.12: Velocity profile at some locations along the stenosis at various times for 80%AS in triangular model

Figure 4.13 depicts the velocity variation in the radial direction along the stenosis for the 90%AS trapezoidal model during the cardiac cycle. The effect of increase in %AS in triangular stenosis is similar to that of other two cases (elliptical and trapezoidal) considered. The velocity at Z=III increased by 0.93 times due to increase in AS from 70% to 90%. Similarly higher velocity flow pattern was noted at the position just after the stenosis (Z=III) in 90%AS triangular model. The higher velocity at the region (Z=IV) is 1.05m/s, 1.2m/s,1.38m/s and 1.51m/s for the time step 1.05s, 1.2s, 1.38s and 1.51s recorded respectively.

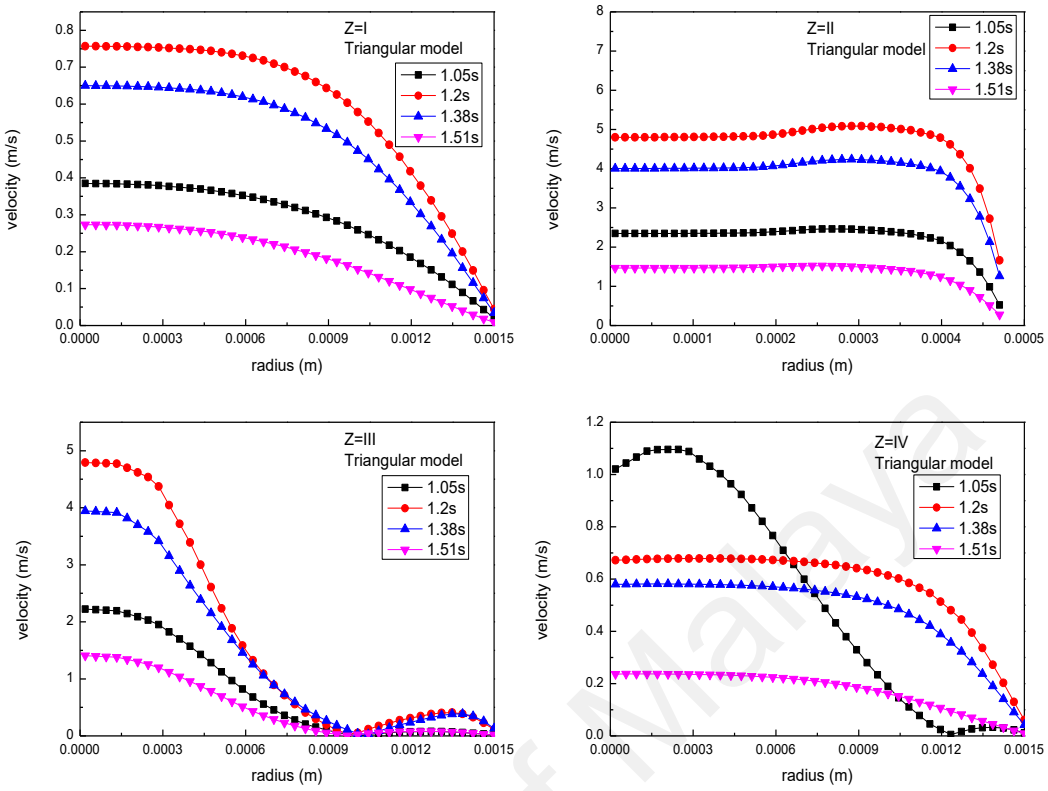

Figure 4.13: Velocity profile at some locations along the stenosis at various times for 90%AS in triangular model

4.4 Influence of shapes of stenosis on pressure

The pressure drop developed due to the presence of stenosis is very important parameter to understand the severity of blockage that may lead to fatal situation if not diagnosed and measured accurately. It is well known that the doctors in under developed countries rely heavily on angiographic images to make decision about severity of stenosis where % AS is considered as deciding parameter without giving much attention to the geometry of stenosis. The pressure drop across the length of artery at various pulse time and different geometry of stenosis is shown in figure 4.14, 4.15 and 4.16. The pressure drops suddenly when blood flow encounters stenosis and then starts recovering after having passed through the blockage area. As expected, the preserve drop across stenosis increases substantially when %AS increases.

Figure 4.14 depicts the pressure drop across the length of artery at various pulse time for elliptical model in 70%AS, 80%AS and 90%AS models. The T_1 T_2 T_3 and T_4 represents the pulse time near beginning of systole (1.05s), peak systole (1.2s), early distal (1.38s) and later distal (1.51s) respectively. The maximum pressure drop along the stenosis for the peak systole is -32.7mmHg, -76.4mmHg and -134.1mmHg for 70%AS (figure 4.14a) 80%AS (figure 4.14b) and 90%AS (figure 4.14c) respectively. The minimum pressure drop was observed for later distal is -2.6mmHg, -6.76Hgmm, -12.7mmHg for 70%AS 80%AS and 90%AS respectively. It is evident from figure 4.14 that the pressure drops around 3 times for elliptical stenosis when %AS increases from 70% to 90%, which represents a severe condition. As expected, the pressure drop across stenosis increases substantially when %Area Stenosis increases.

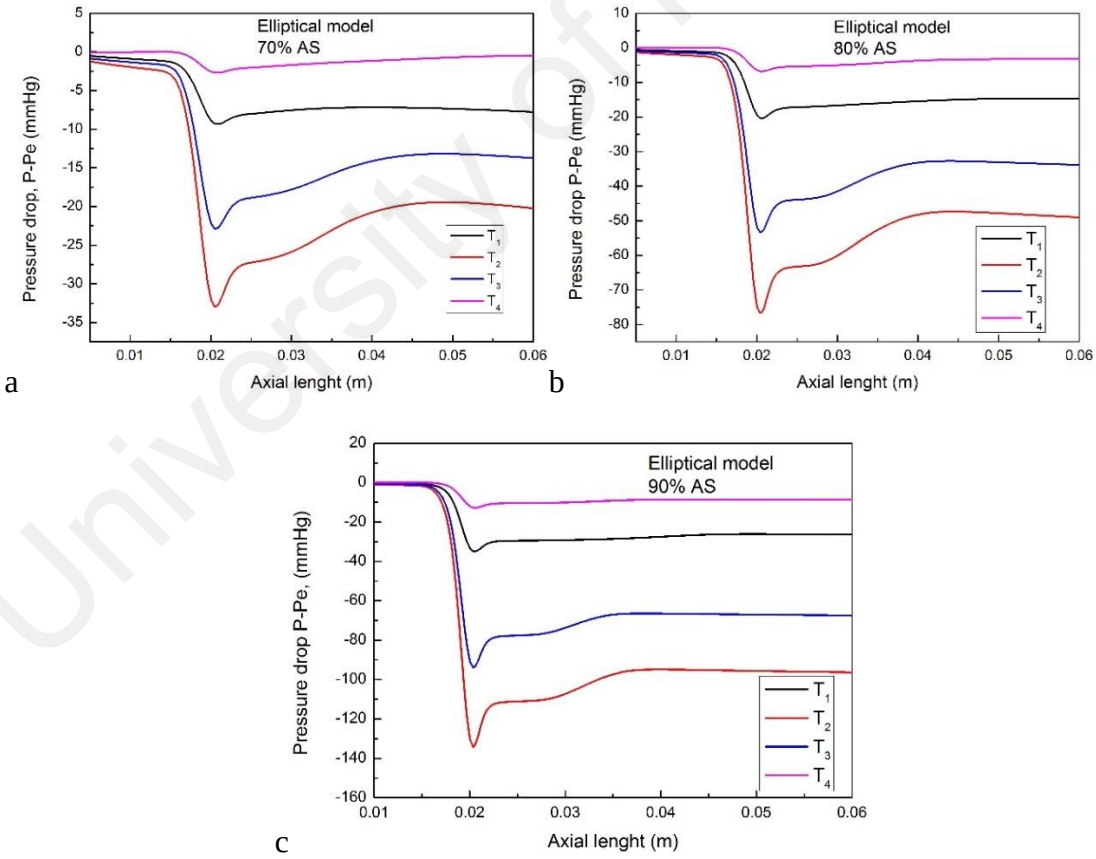

Figure 4.14: Axial pressure drop (P-Pe), along the stenosis at various time step for Elliptical model a) 70%AS b) 80%AS c) 90%AS

Figure 4.15 illustrates the pressure drop across the length of artery at various pulse time for trapezoidal model in 70%AS, 80%AS and 90%AS. It is observed that the maximum pressure drop during the peak systole are -36.5mmHg, -86.3mmHg and -162.3mmHg for 70%AS (figure 4.15a), 80%AS (figure 4.15b) and 90%AS (figure 4.15c) respectively. Whereas the minimum pressure drop -3.03mmHg, -7.87mmHg and -16.4mmHg for 70%AS, 80%AS and 90%AS was noted during the later distal respectively. It is found from the figure 14.5 that the pressure drop is higher as compared to that of the elliptical model during the entire cardiac cycle.

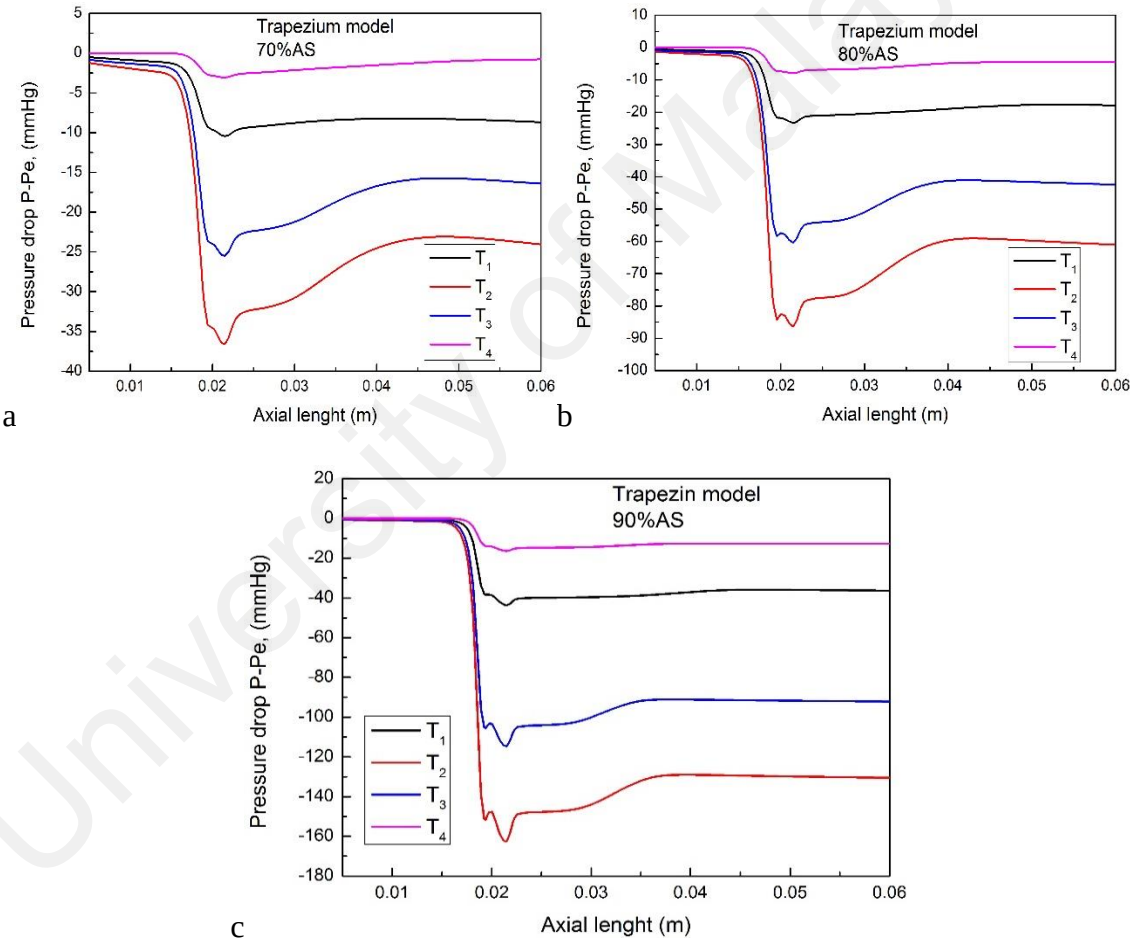

Figure 4.15: Axial pressure drop (P-Pe), along the stenosis at various time step for trapezoidal model a) 70%AS b) 80%AS c) 90%AS

The pressure drop across the length of artery at various pulse time for triangular model in 70%AS, 80%AS and 90%AS was demonstrated in figure 4.16. It is found that

the maximum pressure drop during the peak systole were -28.3mmHg, -65.3mmHg and -111.0mmHg for 70%AS, (figure 4.16a) 80%AS (figure 4.16b) and 90%AS (figure 4.16c) respectively. Whereas the minimum pressure drop -2.0mmHg, -5.3mmHg and -9.8mmHg for 70%AS, 80%AS and 90%AS was noted during the later distal respectively. It is obvious from figures 4.14, 4.15 and 4.16 that the shape of stenosis has significant effect on pressure drop since trapezoidal stenosis (figure 4.15) produces substantial higher drop in pressure as compared to elliptical stenosis (figure 4.14) which in turn is higher than that of triangular shape stenosis (figure 4.16). For instance, the pressure drop across elliptical stenosis for 90% AS is 23 mmHg greater than triangular stenosis and trapezoidal shape gives 28 mmHg higher pressure drop than that of elliptical shape for same %AS.

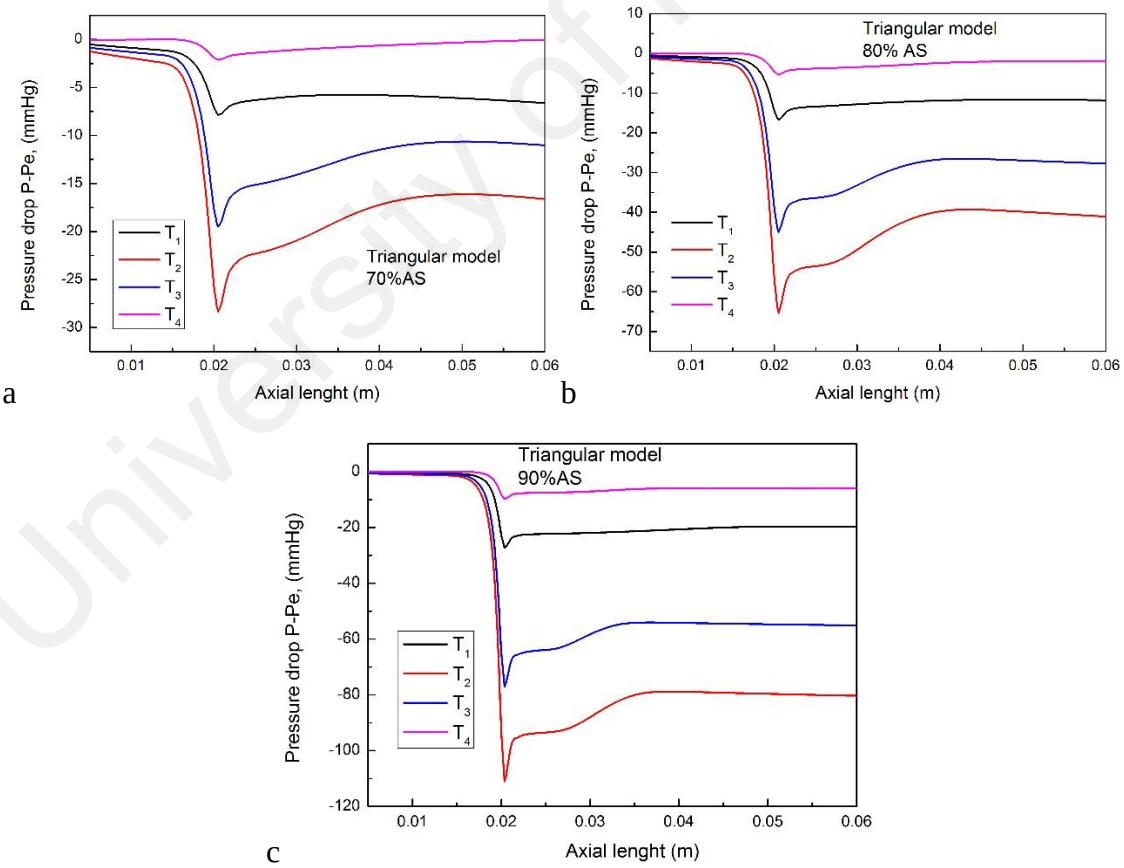

Figure 4.16: Axial pressure drop (P-Pe), along the stenosis at various time step for triangular model a) 70%AS b) 80%AS c) 90%AS

4.5 Effect of shapes of stenosis on wall shear stress

The shear stress at the arterial wall is the indication of health of arterial wall in the long run. Figure 4.17 shows the wall shear stress along the artery for various time step for elliptical model during the cardiac cycle. The shear stress at the wall around stenosis area is much higher than the other areas and the stress increases from 107Pa to 382Pa with increase in the blockage stenosis area from 70% to 90% during the peak systole as shown in figure 4.17. The maximum wall shear stress during the peak systole of 107Pa, 220Pa and 382Pa for 70%AS (figure 4.17a), 80%AS (figure 4.17b), and 90%AS (figure 4.17c), noted respectively. Whereas minimum wall shear stress of 19Pa, 40Pa and 69Pa for 70%AS, 80%AS and 90%AS is observed during the later distal period.

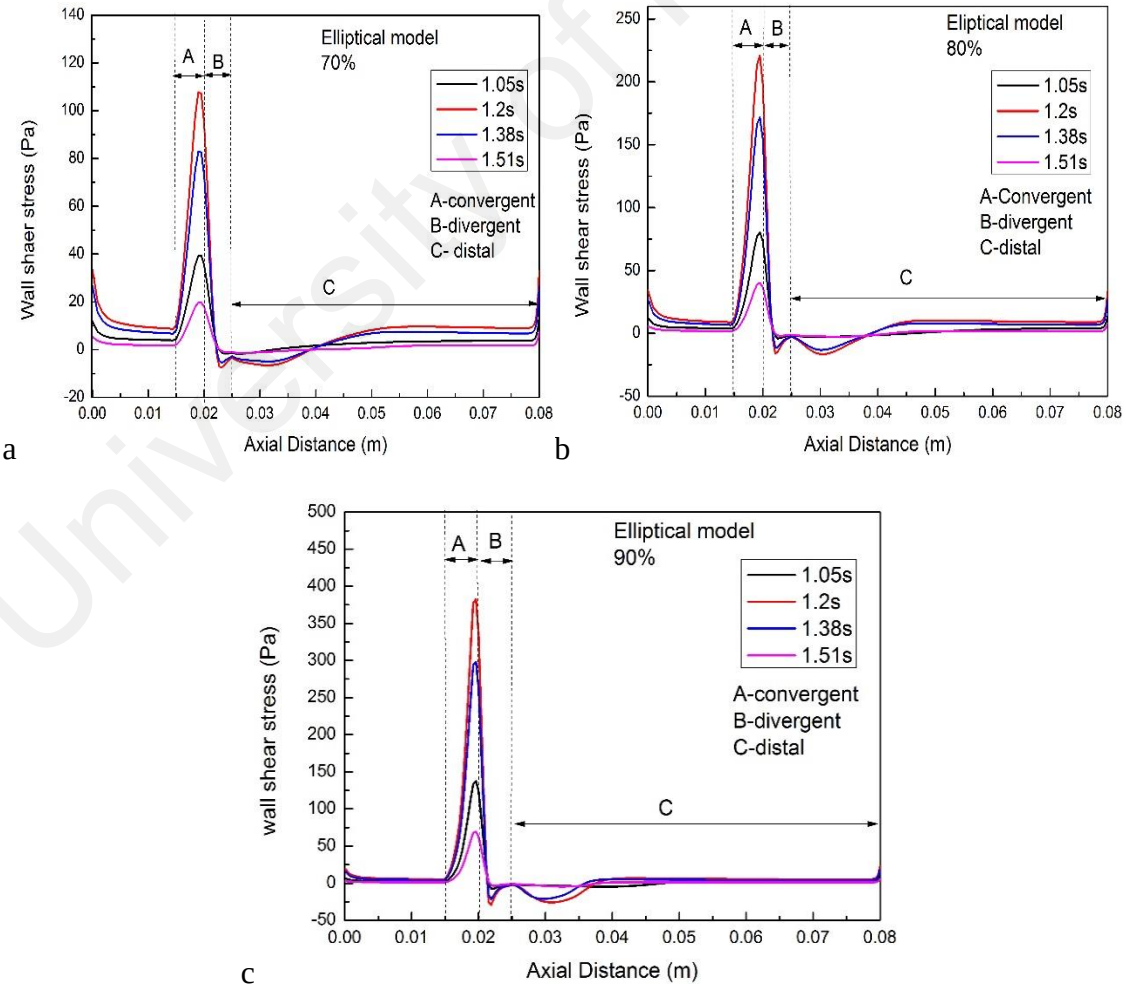

Figure 4.17: Wall shear stress along the artery at various time steps for elliptical model during the cardiac cycle a) 70%AS b) 80%AS c) 90%AS

Figure 4.18 shows the wall shear stress along the artery for various time step for trapezoidal model during the cardiac cycle. The wall shear stress increase as the %area stenosis increased from 165Pa to 646Pa for 70% to 90% during the peak systole respectively as shown in figure 4.18. The maximum wall shear stress during the peak systole of 165Pa, 355Pa and 646Pa for 70%AS, 80%AS, and 90%AS, noted respectively. The minimum wall shear stress recorded during the later distal is 27Pa, 59Pa and 107Pa for 70%AS (figure 4.18a), 80%AS, (figure 4.18b) and 90%AS (figure 4.18c) respectively. It is found that the wall shear stress is much higher in trapezoidal stenosis model as compared to that of elliptical model (figure 4.17) during the entire cardiac cycle.

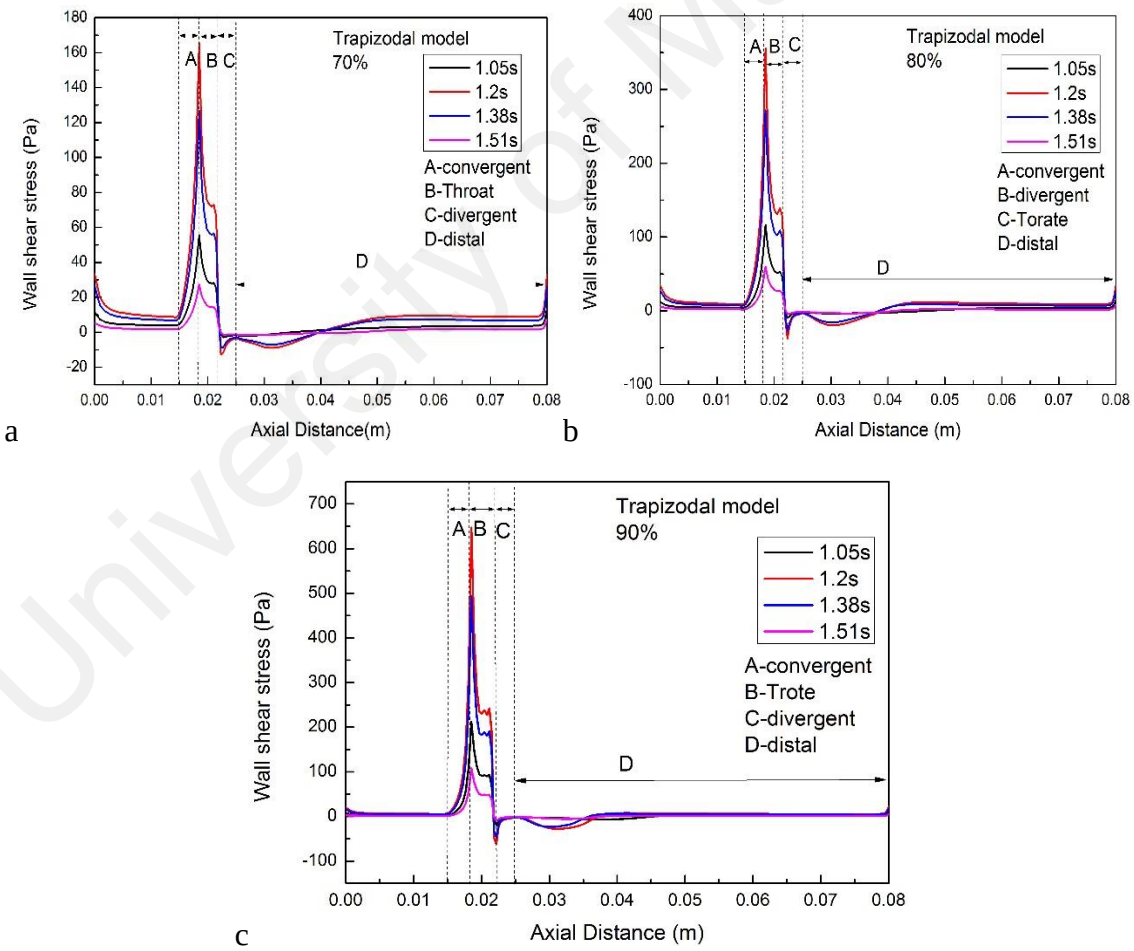

Figure 4.18: Wall shear stress along the artery at various time steps for trapezoidal model during the cardiac cycle a) 70%AS b) 80%AS c) 90%AS

Figure 4.19 shows the wall shear stress along the artery for various time step for triangular model during the cardiac cycle. The increase in the wall shear stress was observed when blockage percentage area stenosis increased from 70% to 90% during the cardiac cycle. The maximum wall shear stress found during the peak systole is 144Pa, 308Pa and 558Pa for 70%AS (figure 4.19a), 80%AS (figure 4.19b), and 90%AS (figure 4.19c), respectively. Whereas the minimum wall shear stress for 70%AS, 80%AS and 90%AS is 23Pa, 49Pa and 92Pa during the later distal respectively. It is also found that the wall shear stress is greater as compared to the the elliptical model stenosis, whereas it is lower than the trapezoidal model stenosis.

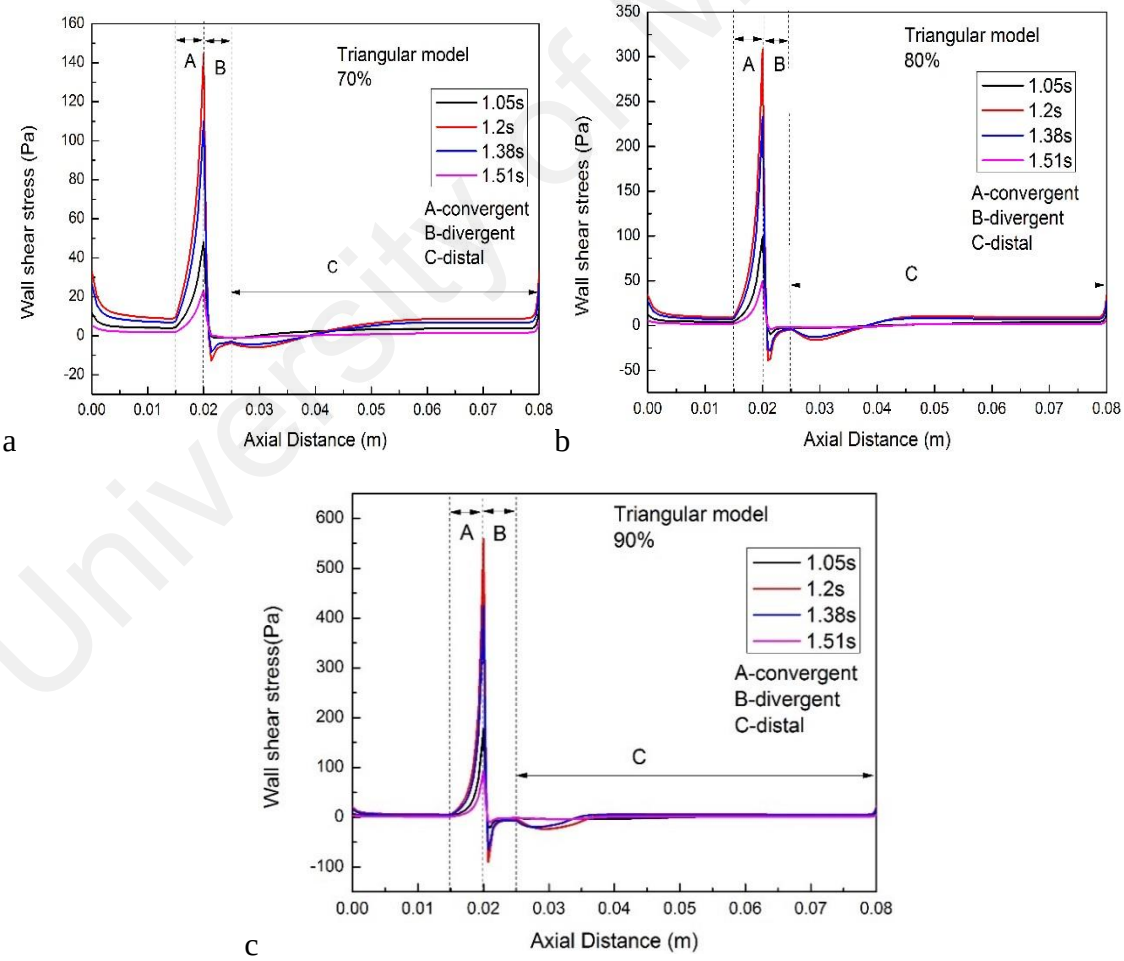

Figure 4.19: Wall shear stress along the artery at various time steps for triangular model during the cardiac cycle a) 70%AS b) 80%AS c) 90%AS

figure 4.20 Shows the overall transient pressure drop $\Delta\tilde{p}$ = P_a-P_r (where P_a is the pressure measured at 3mm proximal to the start of converging portion and P_r is the distal recovery pressure) which was taken during the third and fourth cardiac cycles for the stenosis. The mean pressure drop by integrating over the cardiac cycle shown by the horizontal dash line in figure 4.20, were -12.6mmHg, -15.7mmHg and -19.8mmHg for the triangular, elliptical and trapezoidal shapes of stenosis respectively. The above mentioned mean pressure drop values further emphasis that the trapezoidal shaped stenosis poses a significant higher risk to the patient as compared to the other two stenosis geometries (elliptical and triangular).

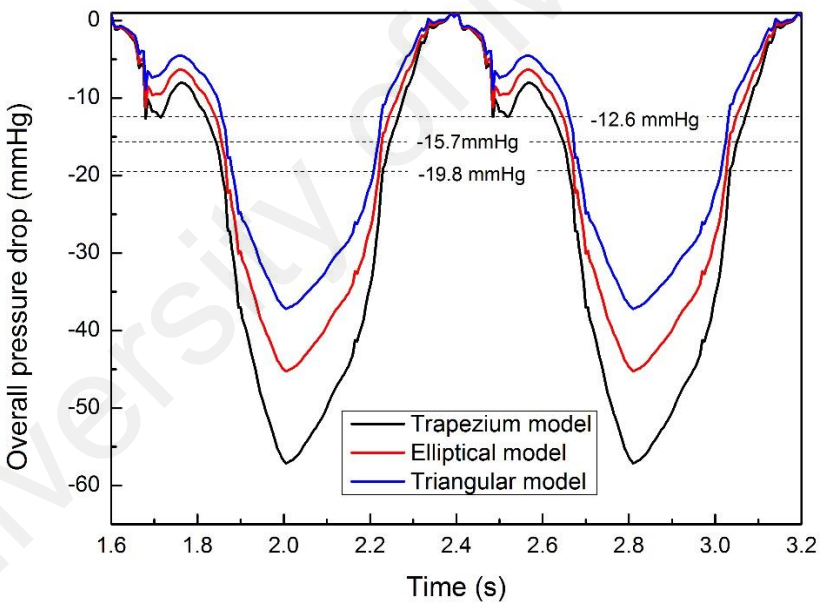

Figure 4.20: Overall pressure drop across the different shapes of stenosis (Trapezium, Elliptical and Triangular) during the cardiac cycle at hyperemic flow in 80%AS

4.6 Influence of angle of curvature on pressure

Figure 4.21 represents the pressure drop profile along the axial length of 70%AS with various angle of curvature. It is observed that the pressure drop is lowest across the throat area and the recovery of pressure at the downstream is slower as the angle of

curvature increased. The drop in pressure was increased as the percentage area of stenosis increased. The maximum drop in pressure until 73.4mmHg, 74.2mmHg, 74.7mmHg and 75.8mmHg is found for 30^0, 60^0, 90^0, and 120^0 angle of curvature models respectively. Whereas the recovery of pressure at the curvature region in case of 120^0 is slower as compared to the other curvature models.

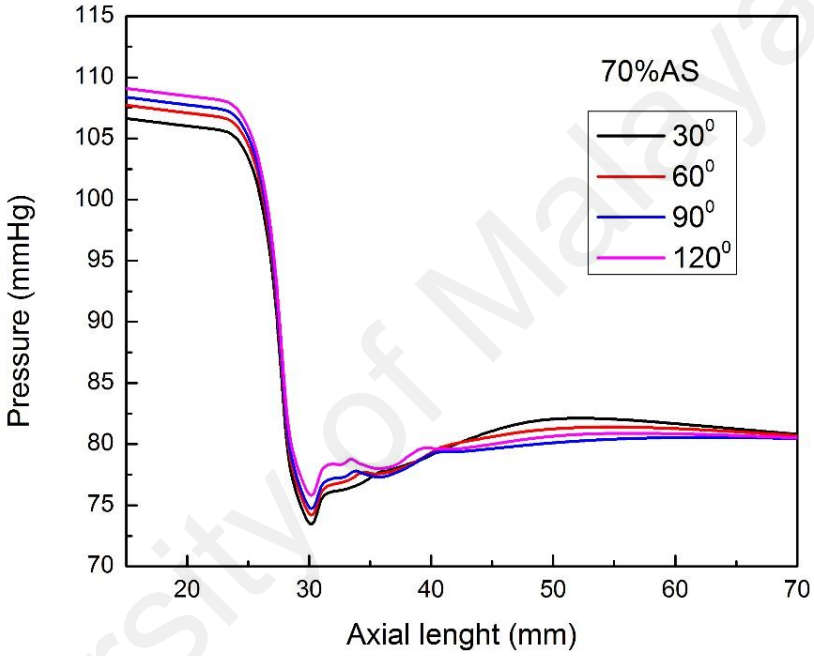

Figure 4.21: Pressure drop along the axial length for various curvature of artery of 70%AS

The pressure drop along the axial length of artery models with various angle of curvature for 80%AS is shown in figure 4.22. The highest pressure drop across the throat region is noted as similar to the 70%AS model with different angle of curvatures (figure 4.21). The maximum drop in pressure until 51.3mmHg, 52.15mmHg, 52.18mmHg and 53.6mmHg is observed for 30^0, 60^0, 90^0, and 120^0 angle of curvature models respectively. The pressure recovery at the curvature location is slower in case of 120^0 as compared to the 30^0 curvature model.

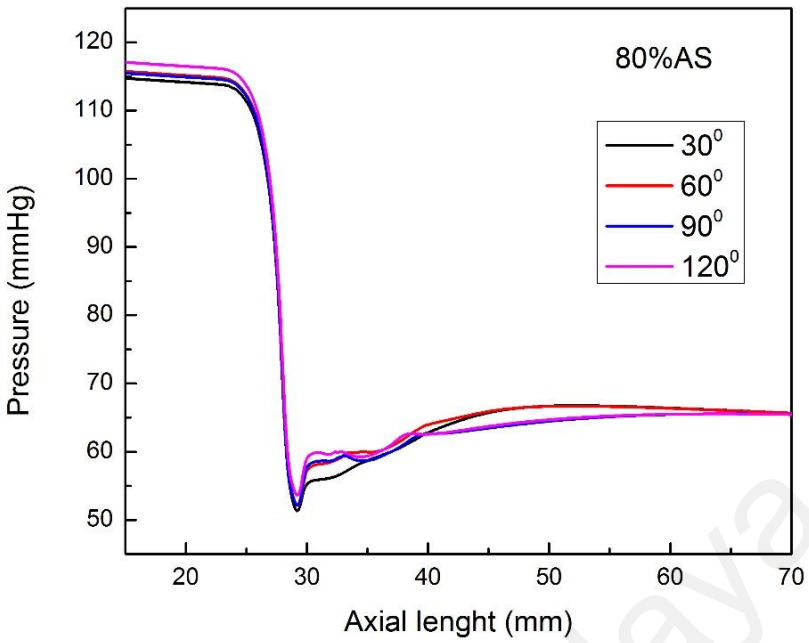

Figure 4.22: Pressure drop along the axial length for various curvature of artery of 80%AS

Figure 4.23 represents the pressure drop profile along the axial length of 90%AS with different angle of curvature. The highest pressure drop across the throat region is observed as similar to the other percentage area stenosis models. The pressure drop increases as the percentage area stenosis increases as compared to the other two model (70%AS and 80%AS) with the different angle of curvatures. There is no significant difference was observed in pressure for 90%AS with various angle of curvature, whereas the recovery of pressure for 30^0 is higher as compared to the other models as shown in figure 4.23. This clearly shows that the presence of curvature augments the increased flow resistance due to stenotic lesions. The effect of angle of curvature could not be neglected even though the stenosis plays an important role in the pressure drop. Therefor the angle of curvature and stenosis both plays a significant role thus both of them should be considered in the diagnosis of coronary angiogram.

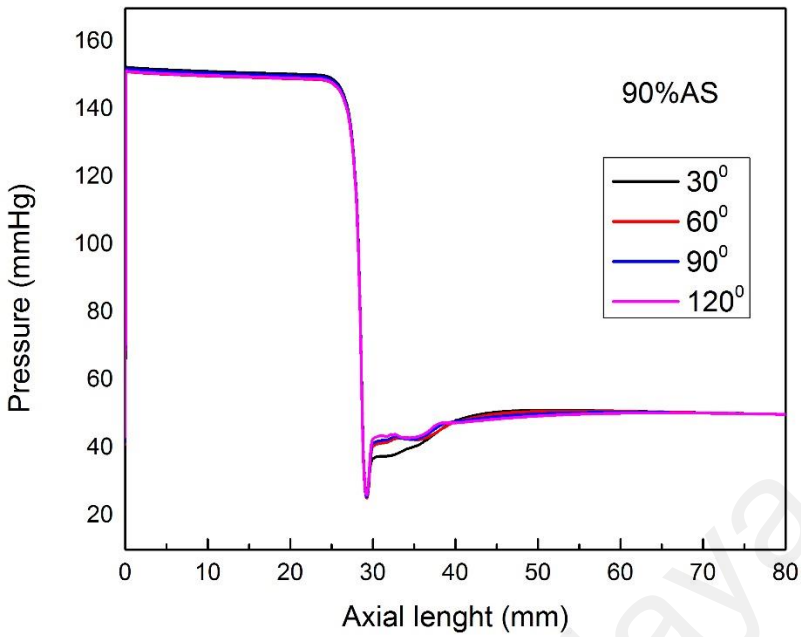

Figure 4.23: Pressure drop along the axial length for various curvature of artery of 90%AS

4.7 Influence of angle of curvature on velocity

Figure 4.24 shows the velocity vector in the curvature region for various angle of curvature in 70%AS models during the peak systole. It can be clearly observed that the blood flow characteristics were strongly influenced by the curvature of artery wall. The maximum velocity is noted across the throat region is in the range from 2.3m/s to 3.1m/s. The velocity field in the curvature plane skewed towards the outer side of the curvature and also shows that this skewing becomes more noticeable as the angle of curvature increases. This could pose the danger of another stenosis formation at inside wall of curvature if blood contains stenotic material since there is lesser flow at inner wall of curvature, creating an opportunity for stenotic material deposition. On the other hand, the upper wall of artery is subjected to severe pressure due to high blood flow rate.

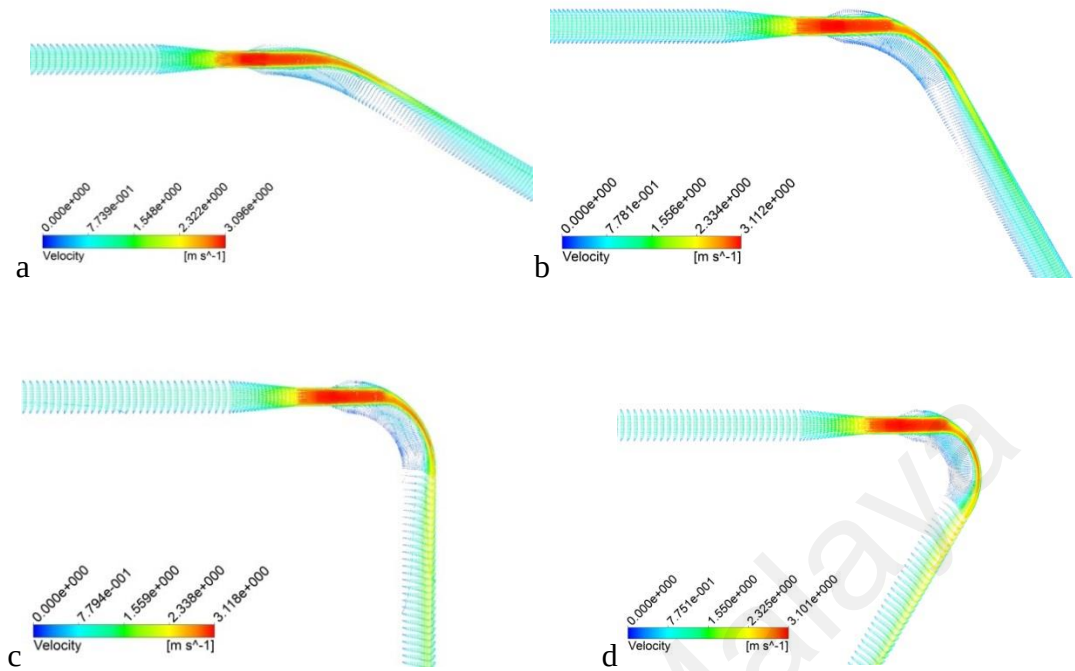

Figure 4.24: Velocity contours for various curvature of artery with 70% area stenosis during the peak systole of cardiac cycle a) 30^0 b) 60^0 c) 90^0 d) 120^0

Figure 4.25 depicts the velocity vector in the curvature region for various angle of curvature in 80%AS models during the peak systole. It can be clearly seen that the velocity increased across the throat region in the range from 3.1m/s to 4.1m/s as compared to the 70% AS models with different angle of curvatures. A similar pattern of velocity skewed towards the outer wall with the creation low flow region across the inner wall as compared to the 70%AS model with various angle of curvature (figure 4.24). Figure 2.25 also shows that the skewing becomes more noticeable as the angle of curvature increases.

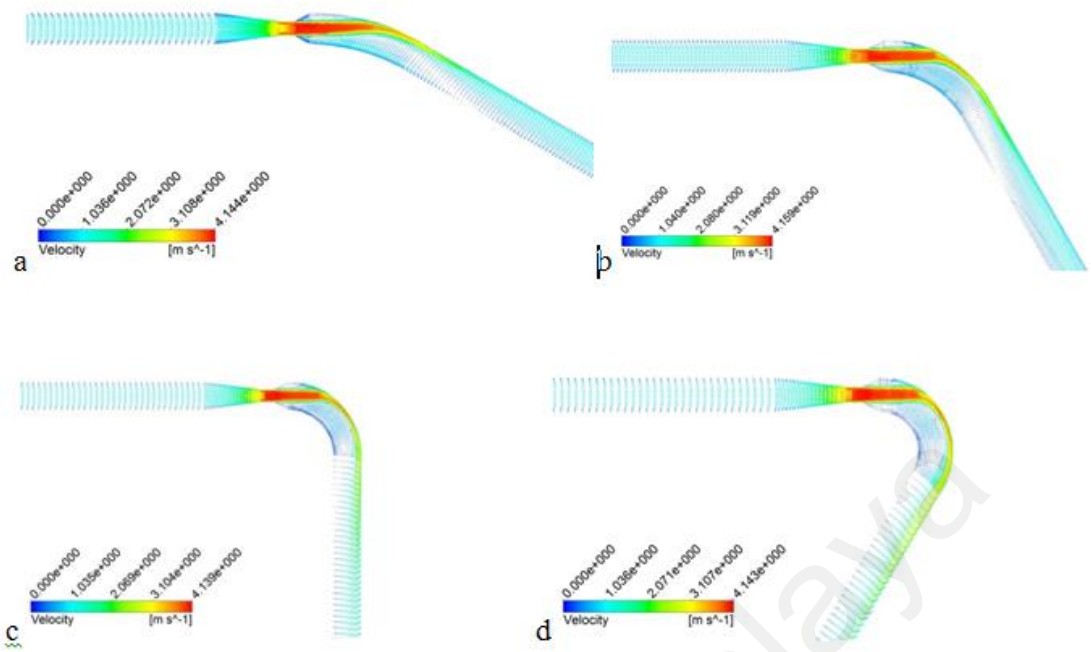

Figure 4.25: Velocity contours for various curvature of artery with 80% area stenosis during the peak systole of cardiac cycle a) 30^0 b) 60^0 c) 90^0 d) 120^0

Figure 4.26 represents the velocity vector in the curvature region for various angle of curvature in 90%AS models during the peak systole. It is found that the velocity at the stenosis increased sharply in the range from 4.2m/s to 5.6m/s across as compared to the 70%AS and 80%AS models of various angle of curvatures. Figure 4.26 also showed a similar pattern of velocity skewed toward the outer wall with the low flow region across the inner wall. It is found that the direction of the flow is from the inner wall towards the outer wall and comes back to the inner wall again when moving towards the downstream as angle of curvature increased from all the models (figures 4.24, figures 4.25 and figures 4.26) with different degree of stenosis.

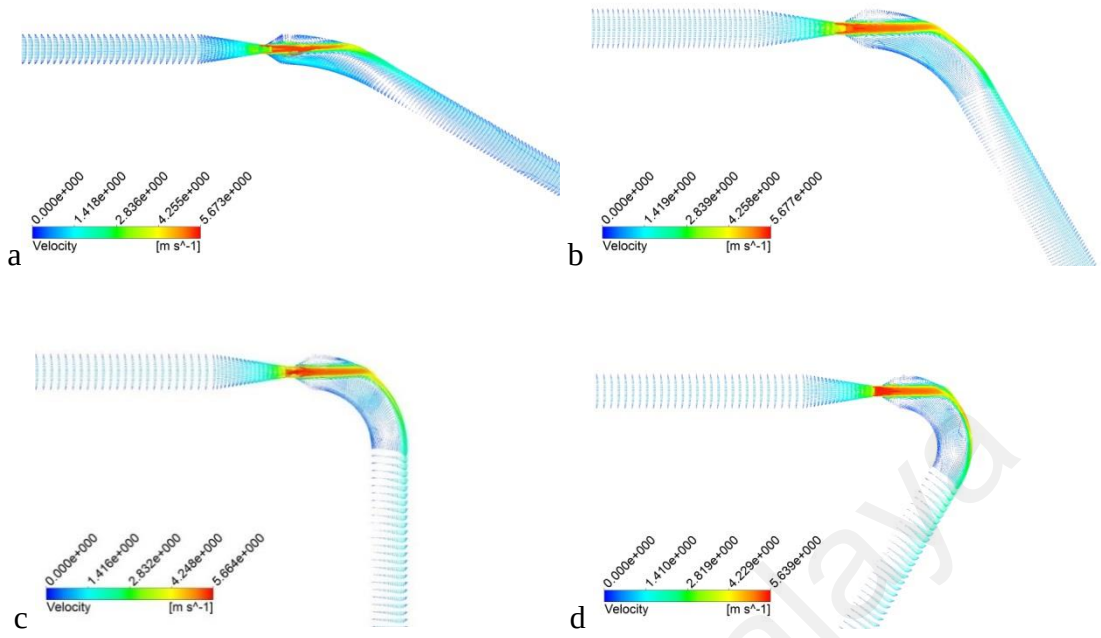

Figure 4.26: Velocity contours for various curvature of artery with 90% area stenosis during the peak systole of cardiac cycle a) 30^0 b) 60^0 c) 90^0 d) 120^0

Figure 4.27 illustrates the velocity profile along the axial length of the artery in different angle curvature with 80%AS. It is clearly seen that the velocity increased sharply across the stenosis region until 4.1m/s. Among the four angles of curvature, the 30^0 curvature has least recovery of velocity when the blood passes through stenosis as shown in figure 4.26. It is also observed that the lower curvature angle produces lowest minimum velocity in the curve region of artery and the point of occurrence of minimum velocity moves further away with decrease in angle of curvature.

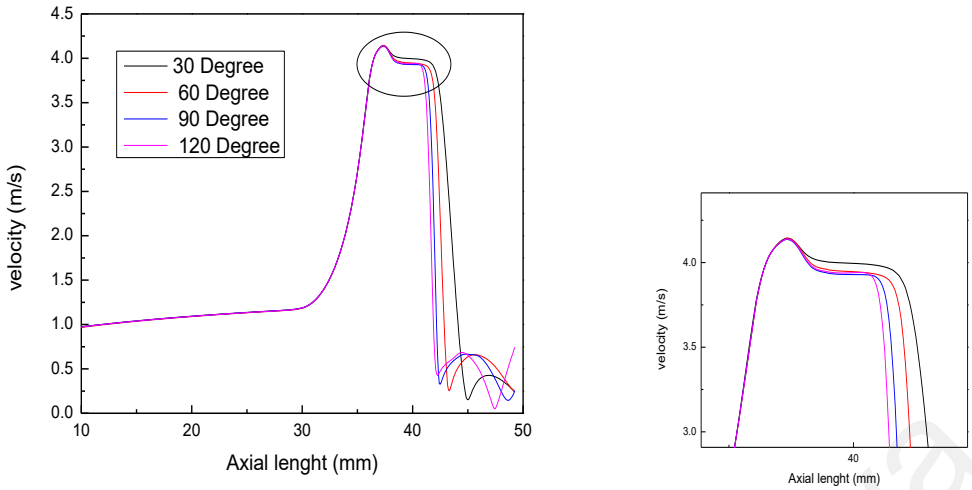

Figure 4.27: Axial velocity profile along the artery with different angle of curvature for 80%AS, a) main figure b) enlarged maximum velocity

Figure 4.28 illustrates the velocity profile along the axial length of the artery in different angle curvature with 90%AS. It is found that the velocity increased as the percentage area stenosis increase from 80% to 90%. The maximum velocity noted across the stenosis is 5.6m/s. there is not much variation observed for 60^0, 90^0 and 120^0 curvatures models.

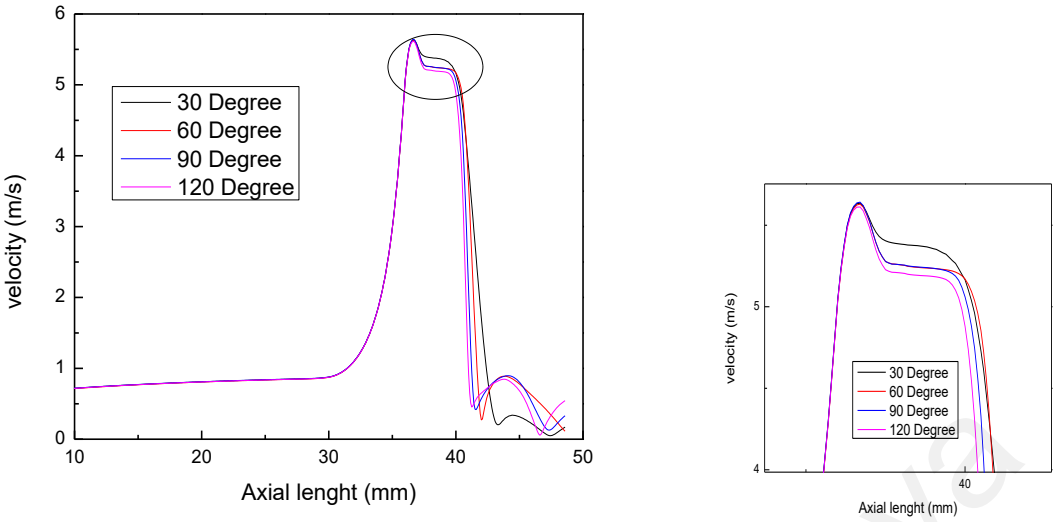

Figure 4.28: Axial velocity profile along the artery with different angle of curvature for 90%AS , a) main figure b) enlarged maximum velocity

4.8 Influence of angle of curvature on wall shear stress

Figure 4.29 depicts the variation in wall shear stress in different angle of curvature models for the 70%AS during the peak systole. The wall shear stress across the throat of stenosis increases as the angle of curvature increases except for 120^0 curvatures model. The wall shear stress is found to be higher at the outer wall as compared to the inner wall in all the four models. The wall shear stress increases as the angle of curvature increase. The highest shear stress at the throat is in the range from 112Pa to 124Pa, 116Pa to 129Pa, 118Pa to 131Pa and 112PA to 125Pa, for 30^0, 60^0, 90^0 and 120^0 noted respectively.

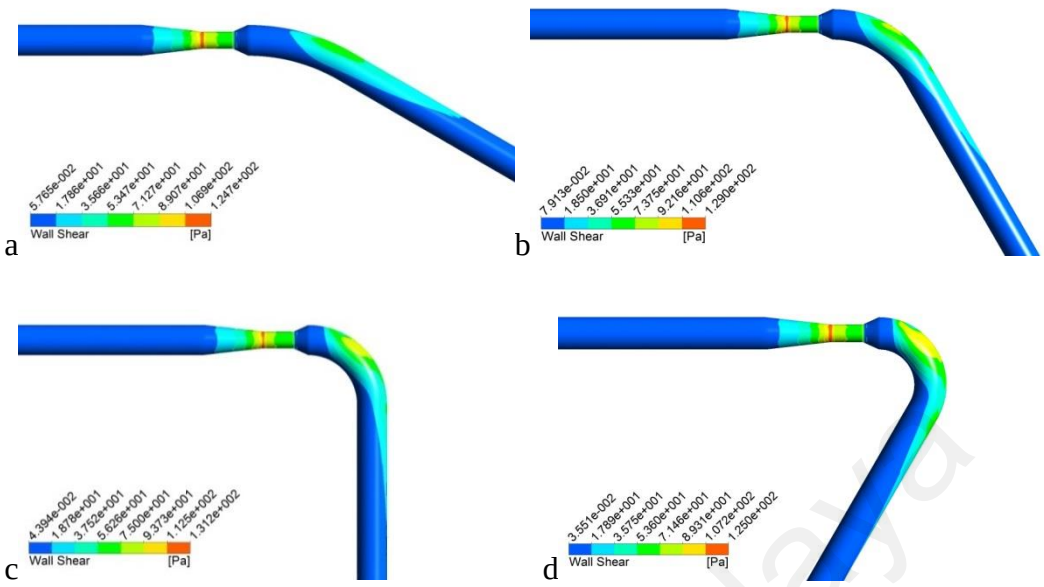

Figure 4.29: Wall shear stress contour for various angle of curvature during peak systole in 70%AS

The distribution of wall shear stress in different angle of curvature with 80%AS during the peak systole is shown in figure 4.30. The wall shear stress at the beginning of throat of stenosis is found to be higher for 80%AS as compared to that of 70%AS model with various curvature angles (figure 4.29). The wall shear stress is found to increase with increase in curvature increases. The maximum stress across the beginning of throat is in the range from 232Pa to 258Pa, 232Pa to 258Pa, 223Pa to 248Pa and 226Pa to 252Pa for 30^0, 60^0, 90^0 and 120^0 respectively.

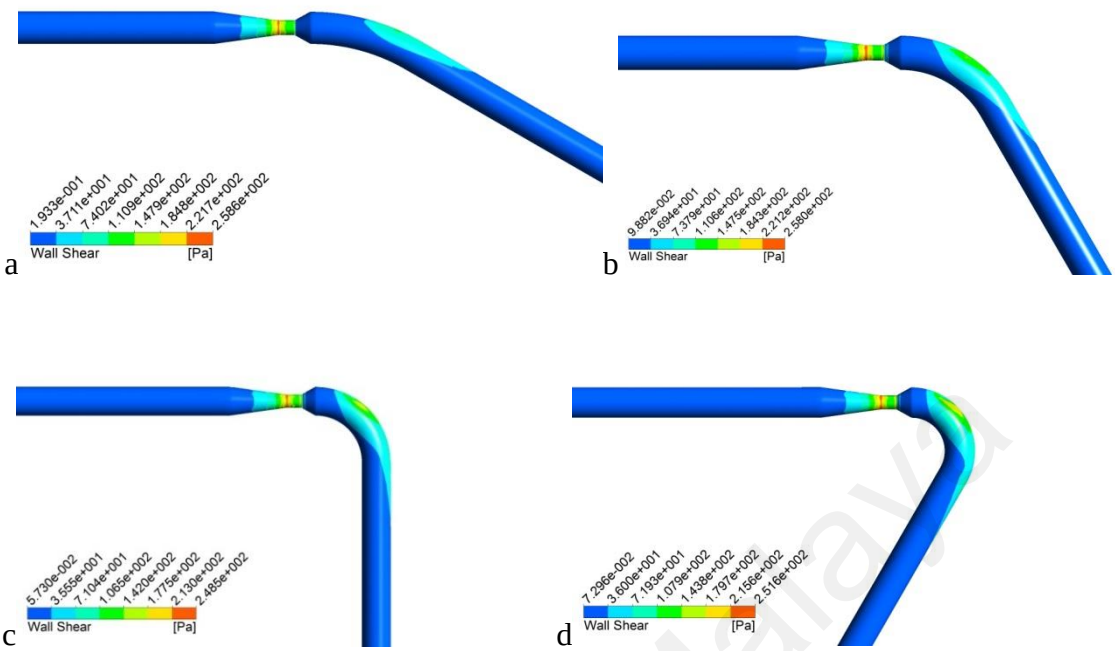

Figure 4.30: Wall shear stress contour for various angle of curvature during peak systole in 80%AS

Figure 4.31 represents the variation in wall shear stress in different angle of curvature models for the 90%AS during the peak systole. The wall shear stress at the throat of stenosis for 90%AS is found to further increase as compared to the 70%AS and 80%AS models with different angle of curvature. The stressed area at the outer wall increases as the angle of curvature increases. The highest wall shear stress across the beginning of stenosis is in the range from 481Pa to 534Pa, 485Pa to 539Pa, 482Pa to 535Pa and 460Pa 511Pa for 30^0, 60^0, 90^0 and 120^0 respectively.

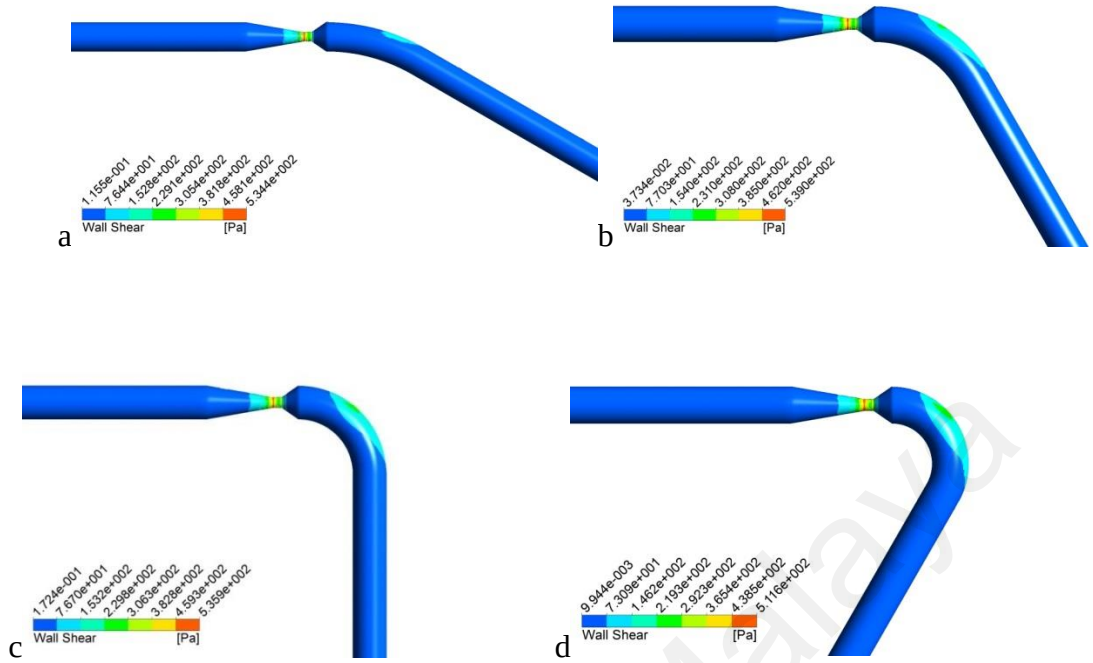

Figure 4.31: Wall shear stress contour for various angle of curvature during peak systole in 90%AS

4.9 Effect of angle of downstream curvature on average pressure drop and diagnostic parameters

Figure 4.32 shows the time average pressure drop for various downstream curvature angles. For a given percentage area stenosis, the time average pressure drop increases with increase in downstream angle of curvature. The significant increase in pressure drop was found as the downstream curvature increases for a given percentage area stenosis. The increase in time average pressure drop from 6.34 mmHg to 9.71 mmHg, 12.13 mmHg to 17.8 mmHg, and 25.99 mmHg to 34.62 mmHg, was found as the curvature increased from 0^0 to 120^0 for 70%, 80% and 90% AS models. These results indicate that the downstream curvature raises the flow resistance in addition to the resistance caused by the presence of area stenosis. Therefore, the highest pressure

drop was observed for minimal area of cross section (90%AS) and the downstream curvature contributes to the additional pressure drop in the curved coronary artery.

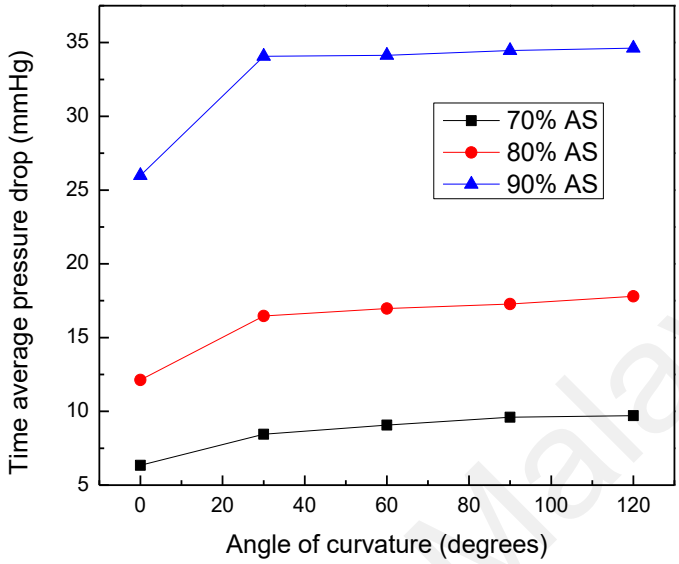

Figure 4.32: Variation of time averaged pressure drop across the stenosis in 70%, 80% and 90% AS for various angle of curvature

4.10 Effect of angle of downstream curvature on fractional flow reserve (FFR)

The figure 4.33 shows the significant decreases in FFR as the percentage areas stenosis increases. It is also found that as the downstream curvature increases the FFR decreases for a given percentage area stenosis in stenosed curve artery. As the angle of downstream curvature changes from 0 to 120 degree, the FFR decreased from 0.91 to 0.86 (5%), 0.81 to 0.74 (8%) and 0.61 to 0.53 (13%) in 70% 80% and 90%AS, coronary models respectively. These results show that the downstream curvature in stenosed artery contributes to the additional decrease in FFR. The highest decrease in FFR was observed for severe stenosis (90%AS) as compared to intermediate stenosis (70%AS, and 80%AS). The computed values of FFR were plotted for the best fit approximation with linear correlation $R2$= 0.97. A horizontal line was drawn at FFR = 0.75 which

represents the cut-off value to determine a range of AS with possible misdiagnosis as shown in figure 4.34 This horizontal line intercepted the FFR—AS lines intersect at 77.43% and 81.63% in straight and 120-degree curve artery. As the percentage area stenosis increases the pressure drop increases across the stenosis and this is owing to the momentum changes caused by the increase in flow velocity across the stenosis configuration. The significant difference by statistical analysis was observed in pressure drop for a fixed percentage area stenosis and pressure derived FFR between straight and downstream curved arteries. The current results show that the value of FFR calculated across the stenosis is significantly higher in 0-degree downstream curvature as compared with the 120-degree downstream curvature stenotic model for a fixed percentage area stenosis. The FFR derived from pressure drop across the stenosis decreases with the increase in percentage area stenosis. Figure 4.35 shows a comparison of FFR for straight stenosed artery models obtained in the present study with the numerical results presented previously by Konala et al.(Konala et al., 2011) for 70%, 80% and 90% AS with rigid wall and rigid plaque models. The FFR value reflects the functional severity of stenosis. It is noted that a FFR of less than 0.8 is functionally significant. If FFR drops less than 0.75 then clinicians recommend an angioplasty or coronary artery bypass graft (CABG). For the cases of FFR values mora than 0.8, surgical procedure may not be required and the patient is advised to undergo a medical therapy. Thus, FFR can guide the clinicians as what type of medical treatment to be adopted. The FFR gray zone comprises a mere 5% difference (i.e., 0.75 to 0.80), which falls under intermediate stenosis severity. The variation in downstream curvature of the artery strongly affect the pressure drop across the stenosis and hence the FFR, for a given percentage area stenosis as confirmed by the current study. For AS <77.43%, the FFR values for both the models (0 and 120 degree) were well above the cut-off value of 0.75 and for AS < 81.63%, the FFR value for 120 degree curved model was observed

below the cut-off value whereas the other models (0 degree) show above the cut-off value of 0.75. This clearly indicates that stenosis severity would be misdiagnosed when the curvature effect is neglected that generally happens if judgement is just based on image of the artery. From the well-established cut-off value of FFR = 0.75 for single vessel CAD, we found a region of uncertainty in evaluating the anatomical significance of stenosis severity between 77.43 and 81.63% AS by plotting a linear approximate correlation between FFR and per cent AS. Our numerical analysis is to demonstrate proof of concept of influence of artery wall curvature on the anatomical assessment of stenosis severity that needs to be tested in human arteries.

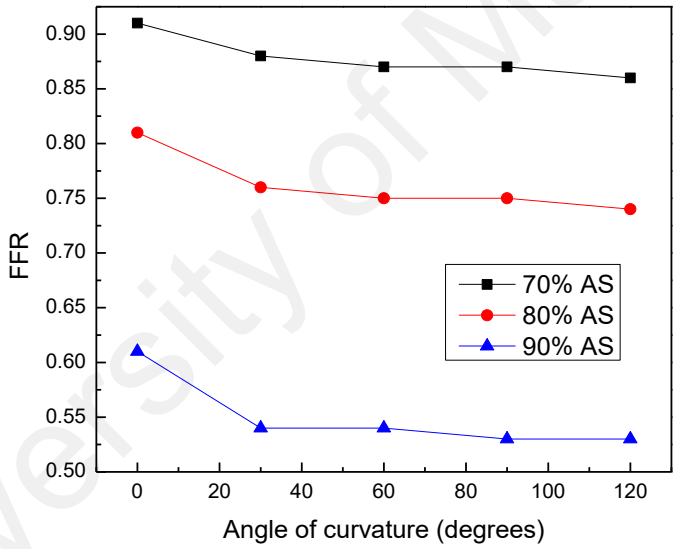

Figure 4.33: Variation of FFR with the angle of curvature in 70%, 80% and 90% AS models

.

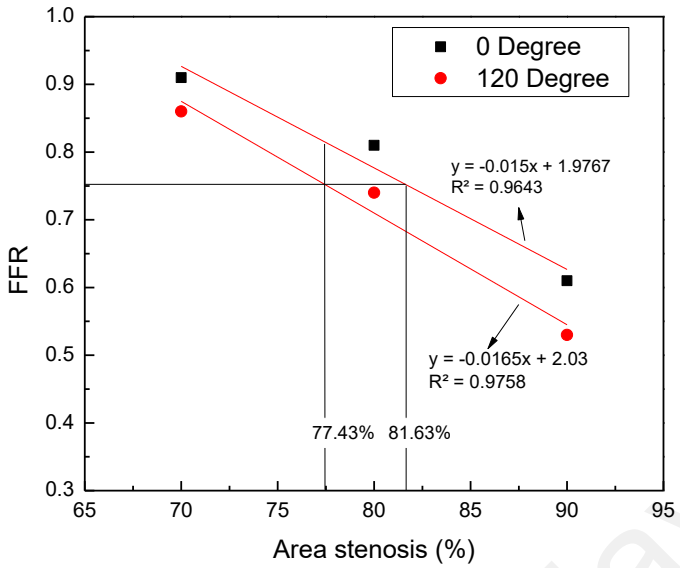

Figure 4.34: Variation of FFR value for straight and 120 degree models

The variation of Pressure drop coefficient (CDP) and Lesion flow coefficient (LFC) for the different angle of downstream curvature is depicted in figure 4.35 and figure 4.36 respectively. The CDP and LFC was calculated by using pressure difference, flow and stenosis geometry in all the severity models. It is observed that for a given percentage area stenosis, the CDP increases from 9.43 to 14.46, 20.35 to 29.87 and 89.86 to 119.71 in 70% 80% and 90%AS respectively, as the angle of downstream curvature increases from 0 to 120 degree. Whereas, it is found that the LFC value decreases from 0.76 to 0.61, 0.88 to 0.73 and 0.96 to 0.83 in 70%, 80% and 90% AS respectively as the angle of downstream curvature increases from 0 to 120 degree.

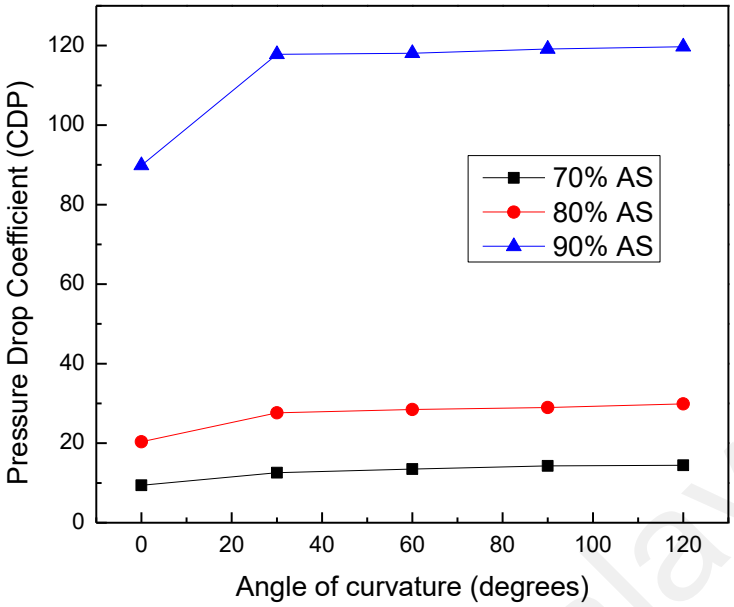

Figure 4.35: Variation of CDP with angle of curvature in 70%, 80% and 90% AS models

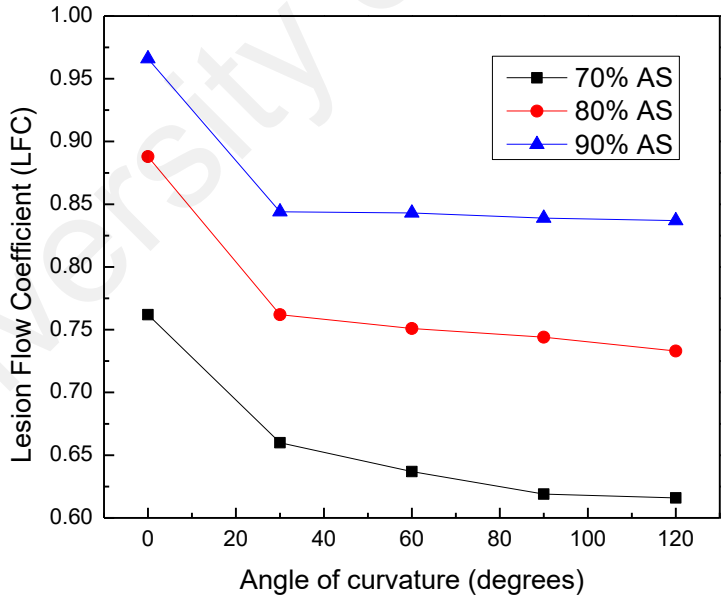

Figure 4.36: Variation of LFC with angle of curvature in 70%, 80% and 90% AS models

4.11 Influence of stenosis in realistic patient left coronary artery on hemodynamics

The following section describes the blood flow analysis of realistic coronary artery of 37 year old male patient suspected of coronary artery disease. A sample of multi-slice CT scan image acquisition was performed with 128-multislice scanner. The images were obtained by the producer described in detail as in section 3.7, of chapter 3. The DICOM images obtained from the patient was imported into the commercially available software MIMICS. By using the thresholding function and creating a 3D mask an optimized model of left coronary arteries with side branches were segmented. The surface models with and without stenosis was modelled by removing the soft tissues and saved in stereolithography (STL) for meshing. Further, the optimized meshed geometry was imported in CFX to analyze the flow behavior. The pulsatile pressure is applied at inlet and outflow boundary conditions was applied with the flow ratio through all the side-branches, following the Murry law. Figure 4.37 demonstrates the pressure variations in the normal and stenosed left coronary arterial segment during the systolic and diastolic period. The pressure contour shows the pressure distribution in normal coronary artery, ranging from 14630Pa to 13540Pa during the peak systole (1.2 s). A pressure drop was observed immediate after the stenosis area from 14360Pa to 14270Pa as compared with the normal coronary artery models during the peak systole. Similarly, a drop in pressure was found from 9905Pa to 9816Pa for the diastole period (1.51 s) during the cardiac cycle.

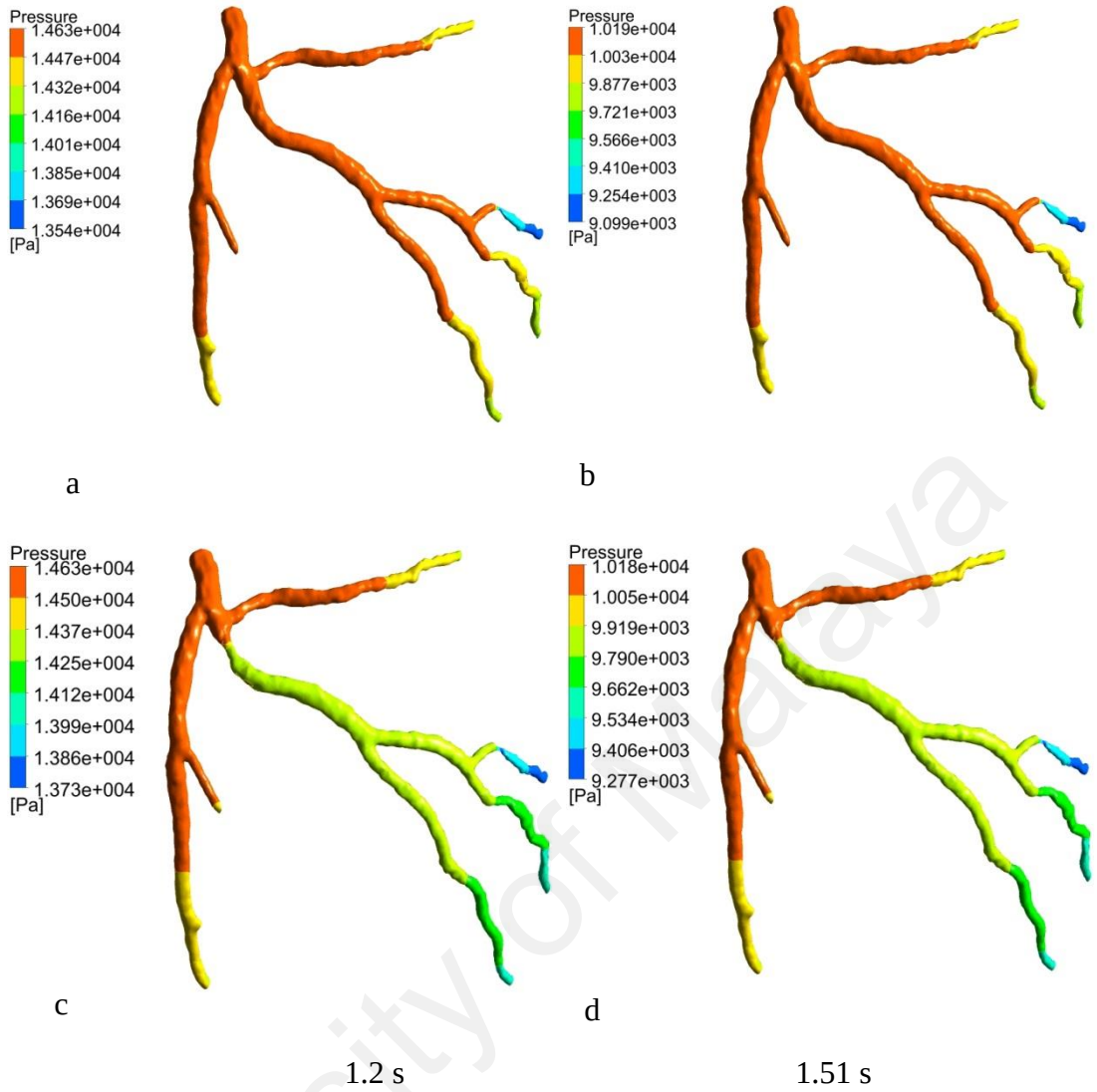

Figure 4.37: Pressure contour with and without stenosis coronary artery for the time a) and c) systole 1.2 s b) and d) diastole 1.51 s

The flow pattern in normal as well as stenosed left coronary artery is depicted in figure 4.38 during systolic and diastolic period of cardiac cycle. It can be clearly noticed that the velocity was found to increase across the stenosed region as compared to the normal left coronary artery. It is observed that flow velocity increased in the range from $4.0x10^{-1}$ m/s to $3.556x10^{-1}$ m/s in stenosed coronary artery as compared with the normal coronary artery ($1.778x10^{-1}$ m/s to $1.333x10^{-1}$ m/s). Similarly an increased flow pattern in the range from $4.0x10^{-1}$ m/s to $3.556x10^{-1}$ m/s was also seen in stenosis artery as

compared with the normal coronary artery across the plaque region during the diastole. A recirculation zone was also observed immediate after the stenosed region, which results in further development of the plaque, however a smooth velocity profile was observed in case of normal coronary artery.

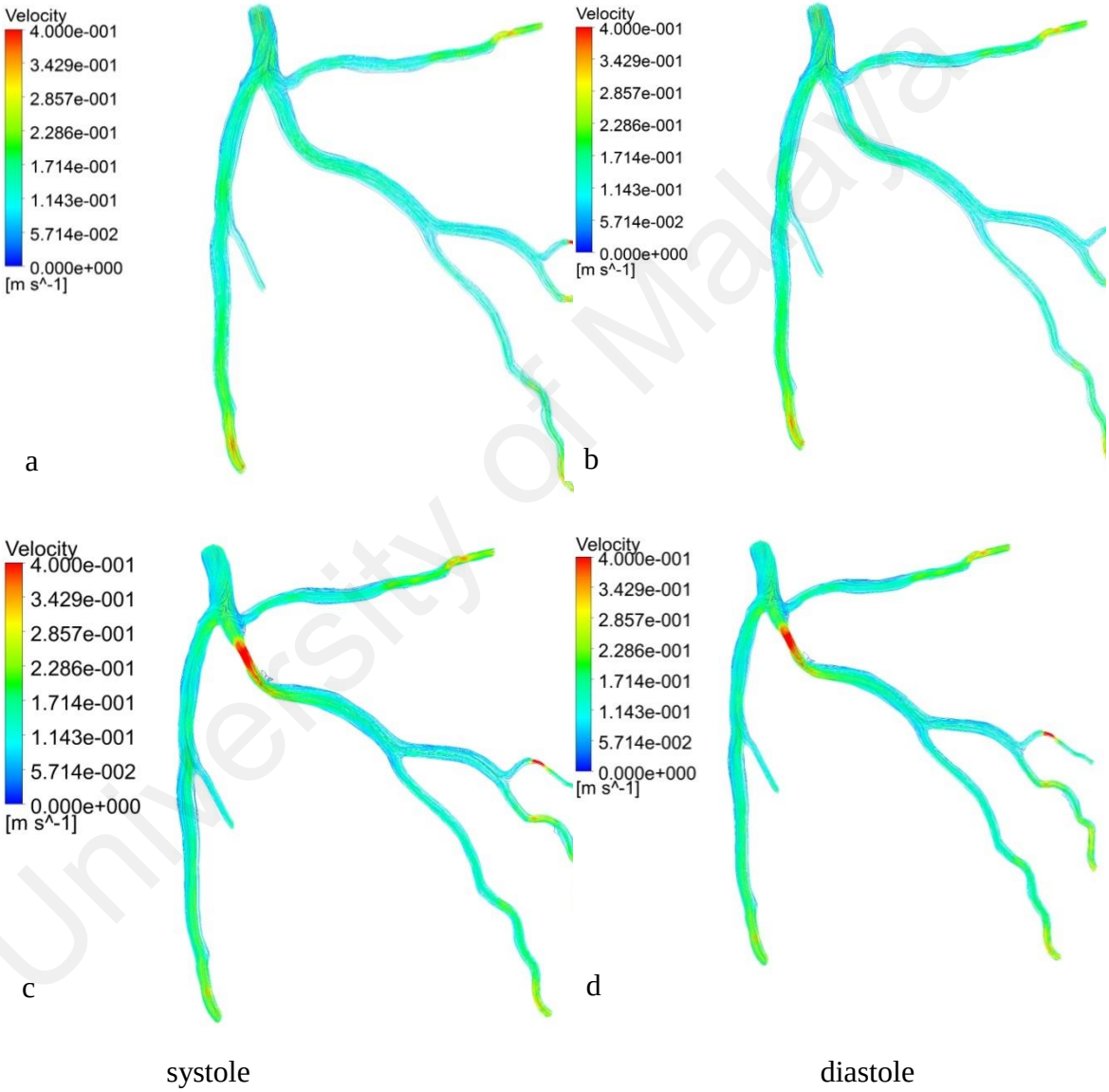

Figure 4.38: velocity contour with and without stenosis coronary artery for the time a) and c) systole 1.2 s b) and d) diastole 1.51 s

The distribution of wall shear stress in normal and stenosed left coronary artery models during the systolic and diastolic period is shown in figure 4.39. The wall shear stress across the stenosis is found to be increased as compared with the normal left coronary artery model. The wall shear stress in the normal artery is found to be within a range from 0 Pa to 3.5 Pa. However, the same region with stenosis is found to have wall shear stress in the range of 10.17 to 15.25 Pa. Similarly, for diastolic phase, the normal coronary artery has wall shear stress in the range from 0 Pa to 3.5 Pa which increased to the range from 10.17 Pa to 15.25 Pa for the stenosed artery. A high wall shear stress across the stenosis was due to the increase in the velocity at the stenosis that could lead to the aggravation of platelets activation, thinning of fibrous cap and the rupture of coronary artery (Chaichana et al., 2013a, 2013b; Feng et al., 2012).

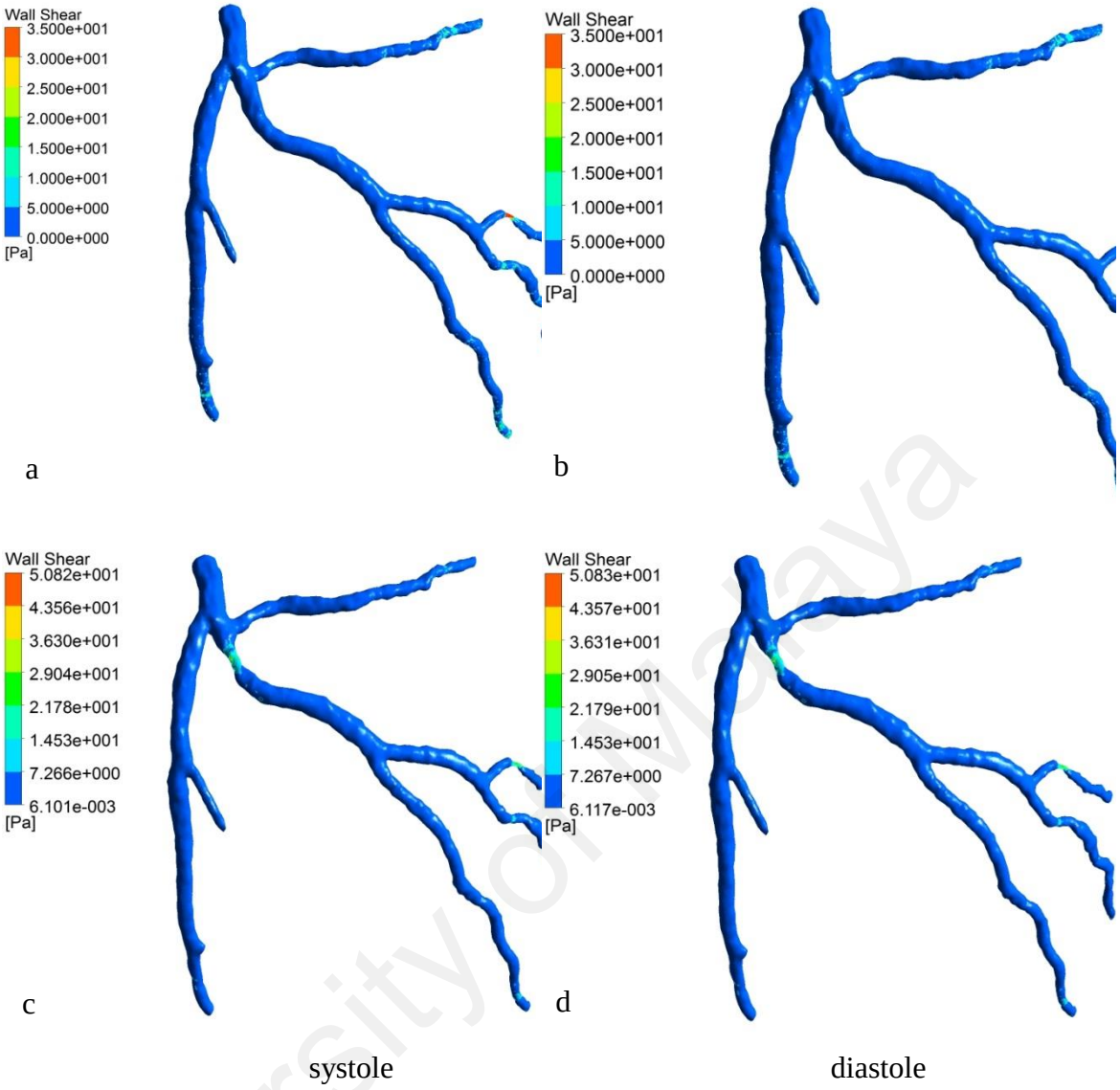

Figure 4.39: Wall shear stress contour with and without stenosis coronary artery for the time a) and c) systole b) and d) diastole

4.12 Influence of stenosis on pressure in various individual patients of coronary artery disease

The following section describes the blood flow analysis of realistic coronary artery of 4 patients. The models a,b,c and d in following figures belongs to patients 2,3,4 and 5 as shown in table 3.4. The four male patients, suspected of coronary artery disease of age between 39 to 49 year old were considered in this section. The location of stenosis more than 50% AS is shown in table 3.4. The CT scan data of four patients were obtained as described in section 3.7 of chapter 3. The images were saved in

DICOM format, and later imported to commercially available software MIMICS to study the blood flow behavior in these patients. Figure 4.40 illustrates the pressure variation in the left coronary artery of all four patients due to the stenosed area in the artery. It is evident from figure 4.40 that the pressure of the blood flow decreases in the post stenosed area, which is common phenomenon due to obstruction presented by presence of stenosis in the blood flow pathway. The stenotic resistance increases the pressure due to blockage effect in the area before stenosis whereas the pressure drops due to expansion after the stenosis. The pressure drop is one of the important parameter in assessing the severity of stenosis. The fractional flow reserve (FFR) which is used as judgment tool to assess the severity of blockage is based on pressure drop across the stenotic region. Higher the pressure drops, sever is the condition of patient. The variation of pressure depends on the blood flow rate dictated by various physiological conditions. The pressure drop across the stenosis at LAD branch is found to be in the range of 14300 Pa to 13670 Pa as shown in figure 4.40a. The pressure drop in figure 4.40b is in the range from 11490 Pa to 11230 Pa across the stenosis at LCX branch. Similarly, the pressure drop is found to be in the range of 10540 Pa to 10300 Pa and 11000 Pa to 10780 Pa respectively for the stenosis located at LAD as seen in figure 4.40c and 4.40d respectively.

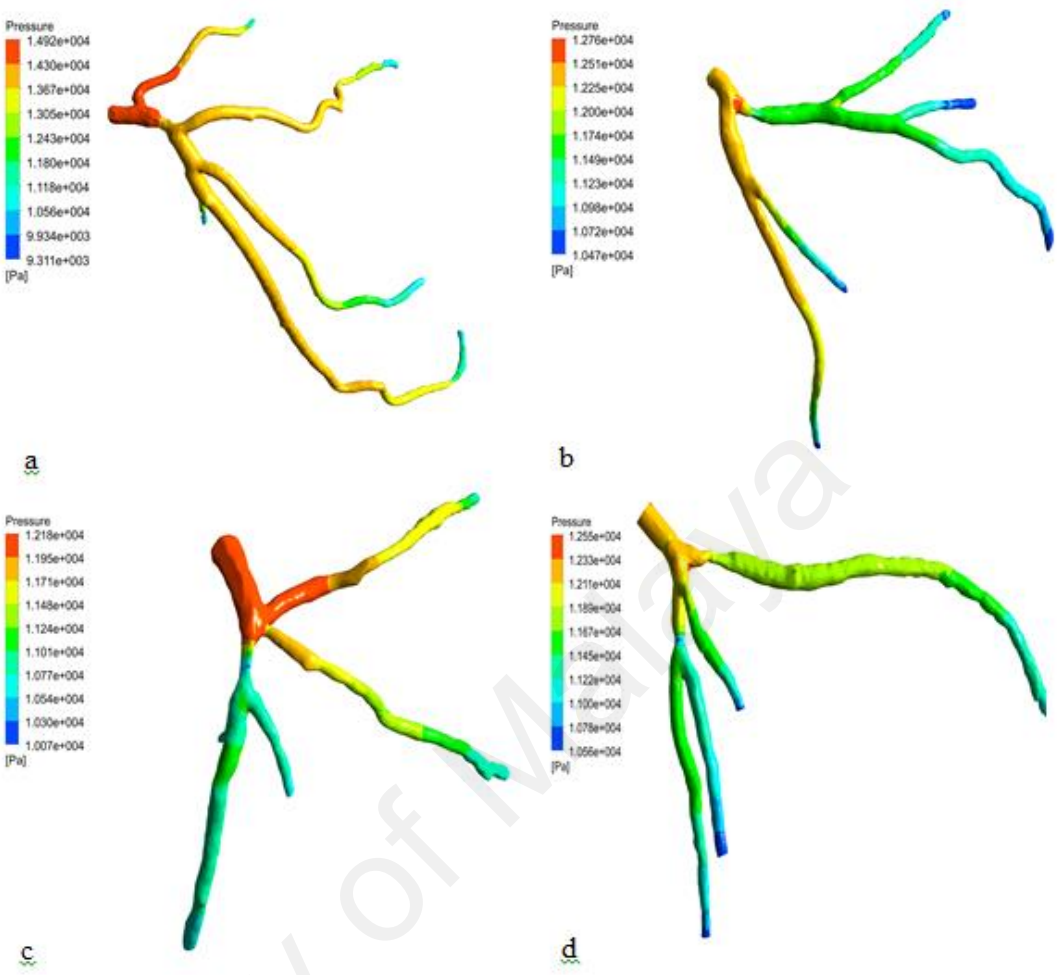

Figure 4.40: Visualization of pressure distribution of four patient in the left coronary artery for time step 1.2s

4.13 Influence of stenosis on velocity in various individual patients of coronary artery disease

Figure 4.41 demonstrates the change in velocity due to the stenosed area in the artery during the hyperemic conditions for 1.2s time step. It should be noted that the results are presented at 1.2s which is peak velocity phase in the cardiac cycle. The velocity increases at sharp rate at the stenosis region. This happens because of conversion of pressure energy into kinetic energy due to pressure drop. The velocity is

found to be affected beyond the stenosis region due to the reduction in the arterial area. The blood

velocity increased from 0.95 m/s to 1.67 m/s at the LAD (Figure. 4.41a), whereas the increment of 0.8 m/s to 1.6 m/s could be seen at the LCX as shown in figure 4.41b. In the same way the velocity increased from 0.94 m/s to 1.69 m/s at LCX figure (4.41c) and from 0.78 m/s to 1.4 m/s. at LAD (figure 4.41d). The increment of velocity is consistent with other studies being carried out for normal flow conditions (Chaichana et al., 2013a, 2013b; Chaichana, Sun, & Jewkes, 2013c). A recirculation area immediate to the stenosis was noticed which leads to low wall shear stress. The recirculation area is created due to low pressure zone thus having very low velocity blood flow pertinent to that particular area. The absence of sufficient blood flow hinders the cleaning of adhesives such as fat or calcification etc. in that particular region. Thus it renders the recirculation region into a safe place for deposition of undesirable material. According to the analysis it is found that low velocity region at post stenosis could lead to the formation of new stenosis.

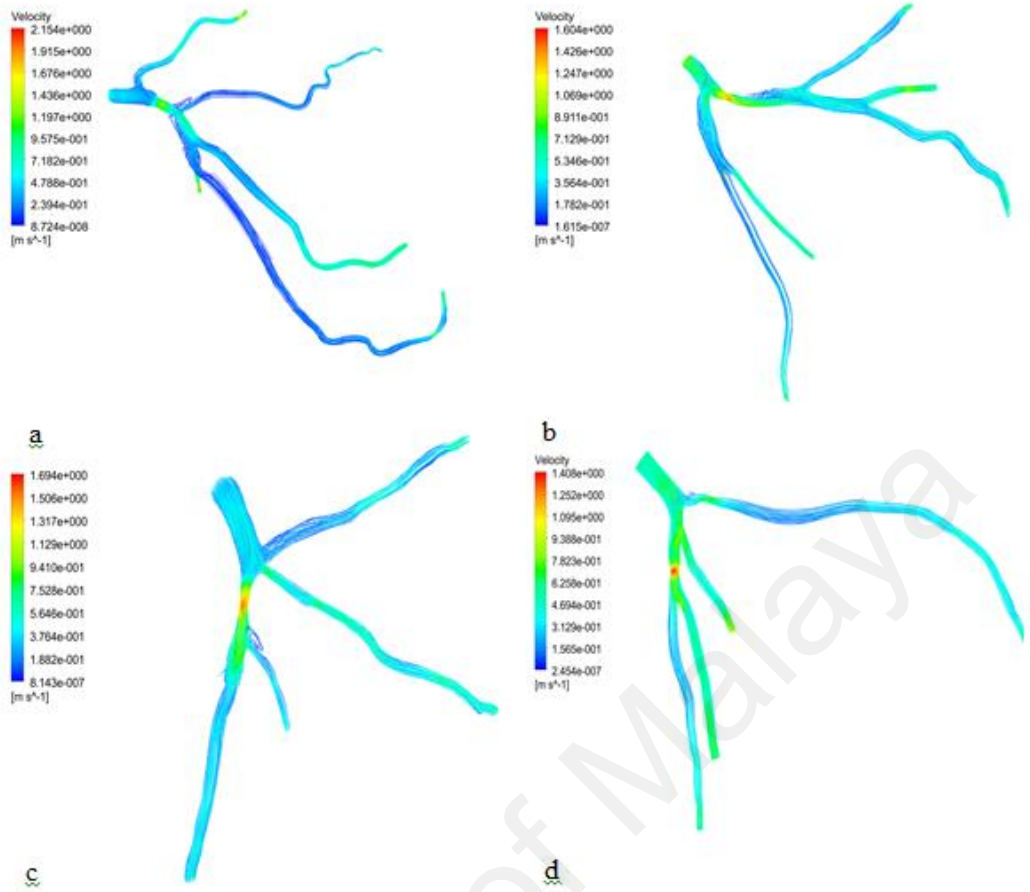

Figure 4.41: Visualization of velocity pattern of four patients in the left coronary artery for time step 1.2s

4.14 Influence of stenosis on wall shear stress in various individual patients of coronary artery disease

The effect of stenosis on the wall shear stress is depicted in figure 4.42 The wall shear stress has significance due to its role in determining the artery strength. The higher wall shear stress may lead bursting or rupturing the arterial wall. It is well known that the high wall stress may create ruptures and low wall stress helps in fatty or other undesirable substances to get deposited on arterial walls thus further increasing the

stenosis region. It is also reported that the normal LAD has a wall shear stress value of 12 Pa (Su et al., 2014)(Su et al., 2014). It is noted that the wall shear stress is also significantly increased across the stenosis at LAD and LCX branches. The maximum significant wall shear stress for four patients is found to be 91 Pa, 50 Pa, 65 Pa and 51 Pa respectively as illustrated in figure 4.42a, 4.42b, 4.42c and 4.42d respectively. The finding of this study could be useful in predicting the progression of atherosclerosis in the coronary arteries. The previous studies reported that stenosis frequently occurred near the bifurcation, due to the angulation between LAD and LCX and tortuosity which could lead to low wall shear region at bifurcations. The highest wall shear stress to be observed was that of 91 Pa at LAD model (figure 4.42a). This is very high value compare to the normal condition of no stenosis.

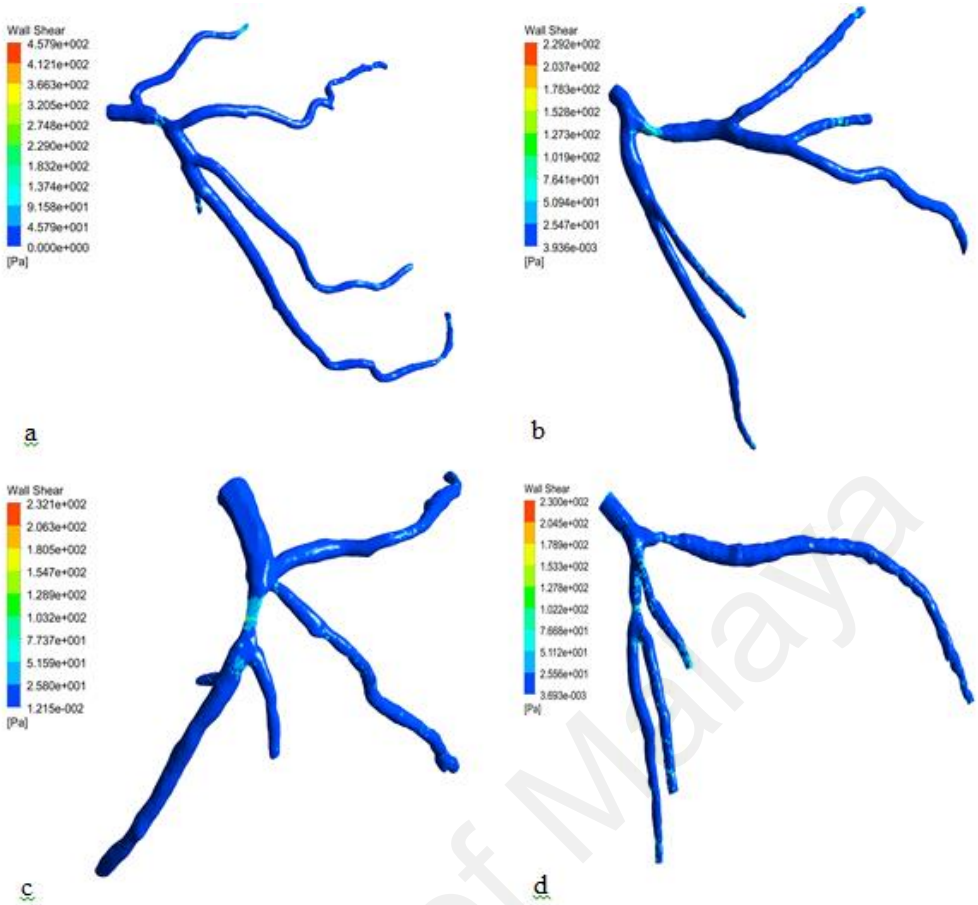

Figure 4.42: Wall shear stress distribution of four patient in the left coronary artery for time step 1.2s

4.15 Effect of various degree of stenosis on hemodynamic parameters in normal and stenosed left coronary artery

It is seen from various studies that the stenosis could be formed in various degrees of area blockage and also it may occur at different locations along the coronary artery. It is really hard to get the specific patient having a specified area of stenosis at a given location. Since the current study is focussed to study the influence of AS of 70%, 80% and 90%, we could not get the patient having exact above mentioned blockage area and also the desired location of those blockages. Thus we had to rely on Mimics software to create the stenosis of desired blockage area and location on real artery. Thus current section (section 4.15) is dedicated to investigate the blood flow of artery having stenosis at main stem. The artery in this model belongs to a male subject of age 46 as

shown at table 3.4(patient 3). Figure 4.43 illustrates the pressure distribution for normal and stenosed coronary artery with different percentage of stenosis during the cardiac cycle of 1.2s. The pressure drop in normal left coronary artery is in the range from 14650 Pa to 14160 Pa as shown in figure 4.40a. For a 70% area stenosis at the main stem as shown in figure 4.43b, the pressure drop across the stenosis is in the range from 11250 Pa to 10710 Pa. The pressure drop is increased as the percentage area stenosis at the main stem increases, in the range from 7772 Pa to 6267 Pa and -4029 Pa to -7662 Pa respectively for the 80% AS and 90%AS as shown in figure 4.43c and figure 4.43d respectively. The severity of stenosis is assessed by the pressure drop across the stenosis region by using a standard parameter such as fractional flow reserve (FFR). Figure 4.40d shows a higher pressure drop across the stenosis as its percentage areas stenosis is 90% AS, which results in severe condition for patient.

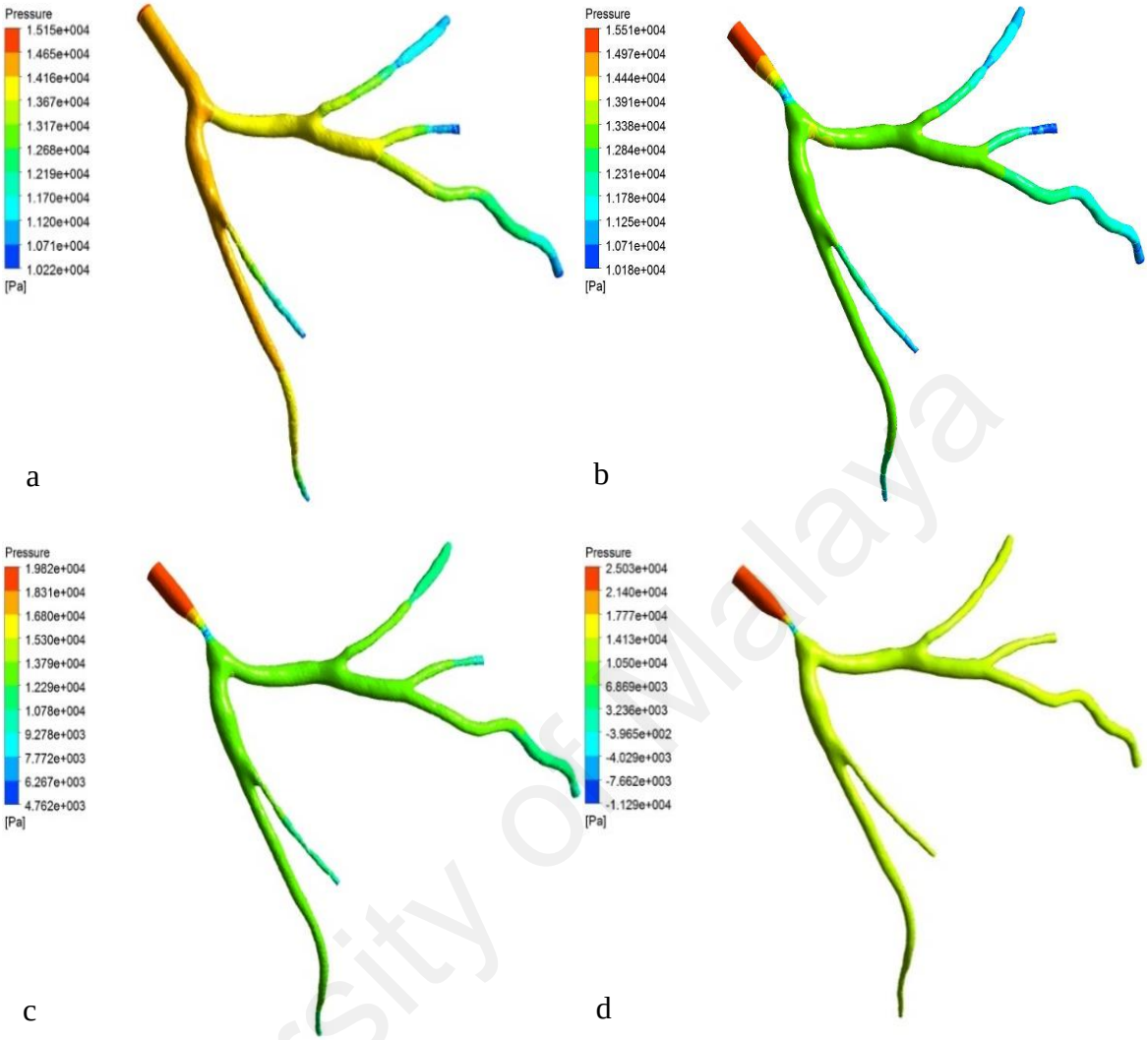

Figure 4.43: Pressure distribution in left coronary artery for 1.2s during the cardiac cycle a) Normal b) 70% AS c) 80% AS d) 90% AS

Figure 4.44 shows the pressure variation in 2D plane just before stenosis, at the center of stenosis and just after the stenosis area for normal artery suffering from, 70% AS, 80% AS and 90% AS respectively. It is very clear from figure 4.44 that the pressure in the converging region or just before stenosis increases significantly due to resistance offered to blood flow by narrowing area of stenosis. It is noted that the pressure near the start of stenosis increased by 70% for 90% AS, as compared to the case of normal artery. Similarly, the pressure for 90% as compared to normal artery at the middle of stenosis and just after stenosis has decreased by 131% and 10% respectively.

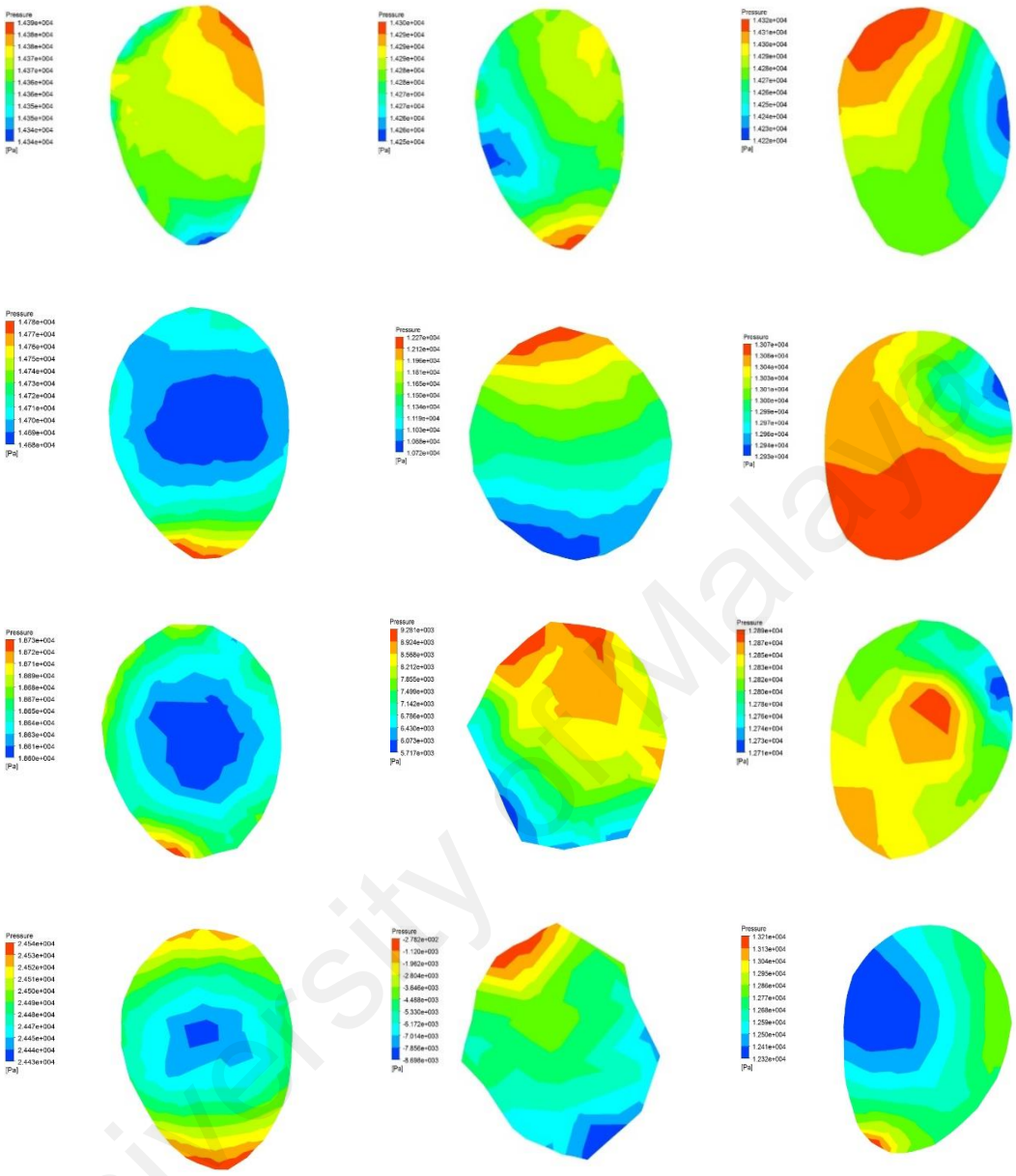

Figure 4.44: Cross sectional plane for 70%AS, 80%AS, and 90%AS at a) before stenosis b) mid stenosis and c) after stenosis

Figure 4.45 shows the velocity pattern for normal and stenosed coronary artery with various percentage area stenosis during the cardiac cycle for 1.2s. The velocity increases sharply across the stenosis region as compared with the normal coronary artery model. The blood velocity was observed for 70% AS model is in the range from

1.4m/s to 2.24m/s as shown in figure 4.45b. It is found from figure 4.45b and figure 4.45c that velocity further increases in the range from 1.6m/s to 2.5m/s and 2.6m/s to 4m/s respectively, as the percentage area stenosis increases from 70%AS to 80%AS across the stenosis. The higher velocity was seen for the 90% AS in the range from 4.2m/s to 7.1m/s as shown in figure 4.45d as compared to the other models. It should be noted that the hyperemic condition arises due to various reasons such as increased demand of blood as a result of exercises etc. that leads to higher blood flow rate by increasing the velocity. It further noted that a recirculation zone immediate to the stenosis is created as compared to the normal coronary artery model. This disturbed flow helps in fatty or other undesirable substances to get deposited on arterial walls thus further increasing the stenosis region.

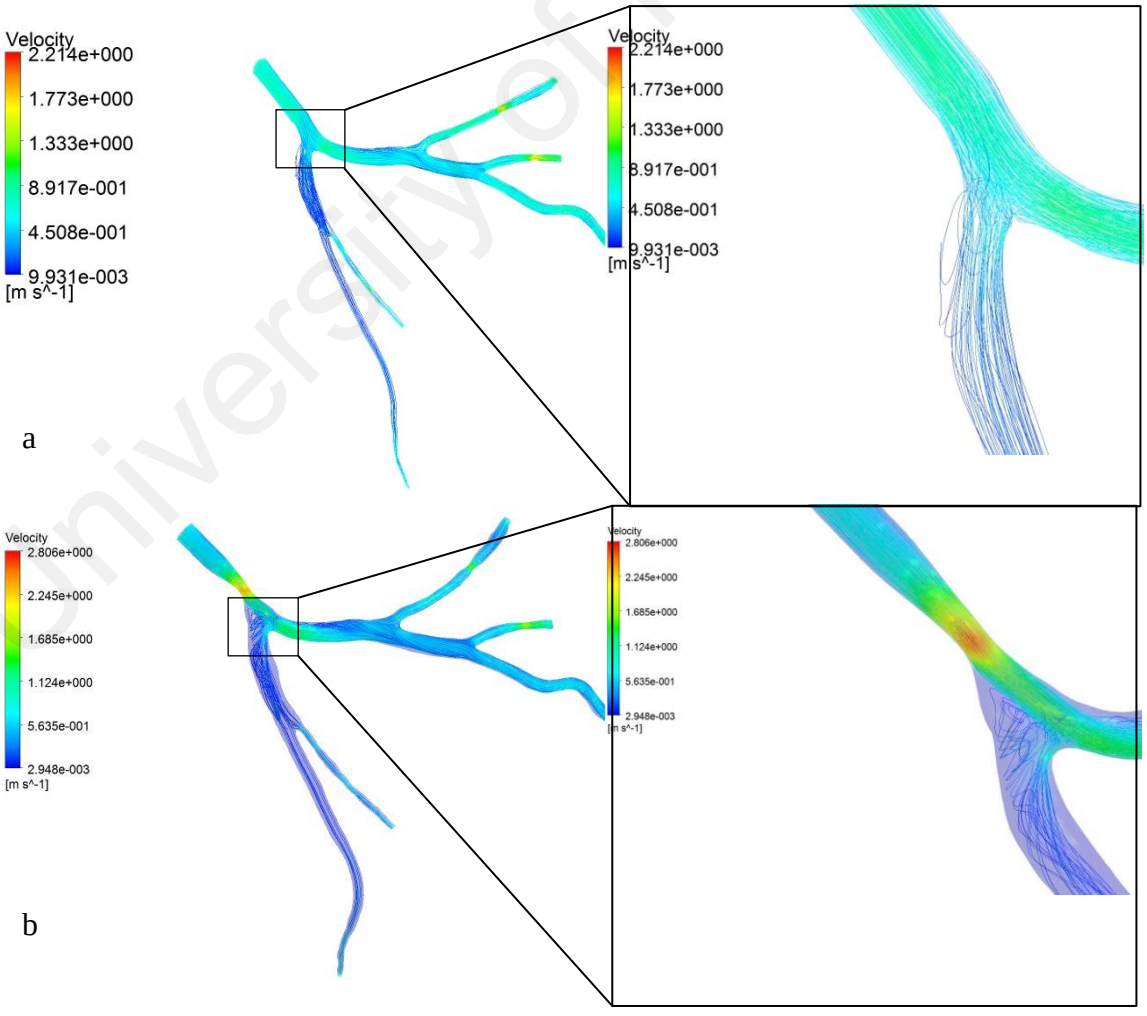

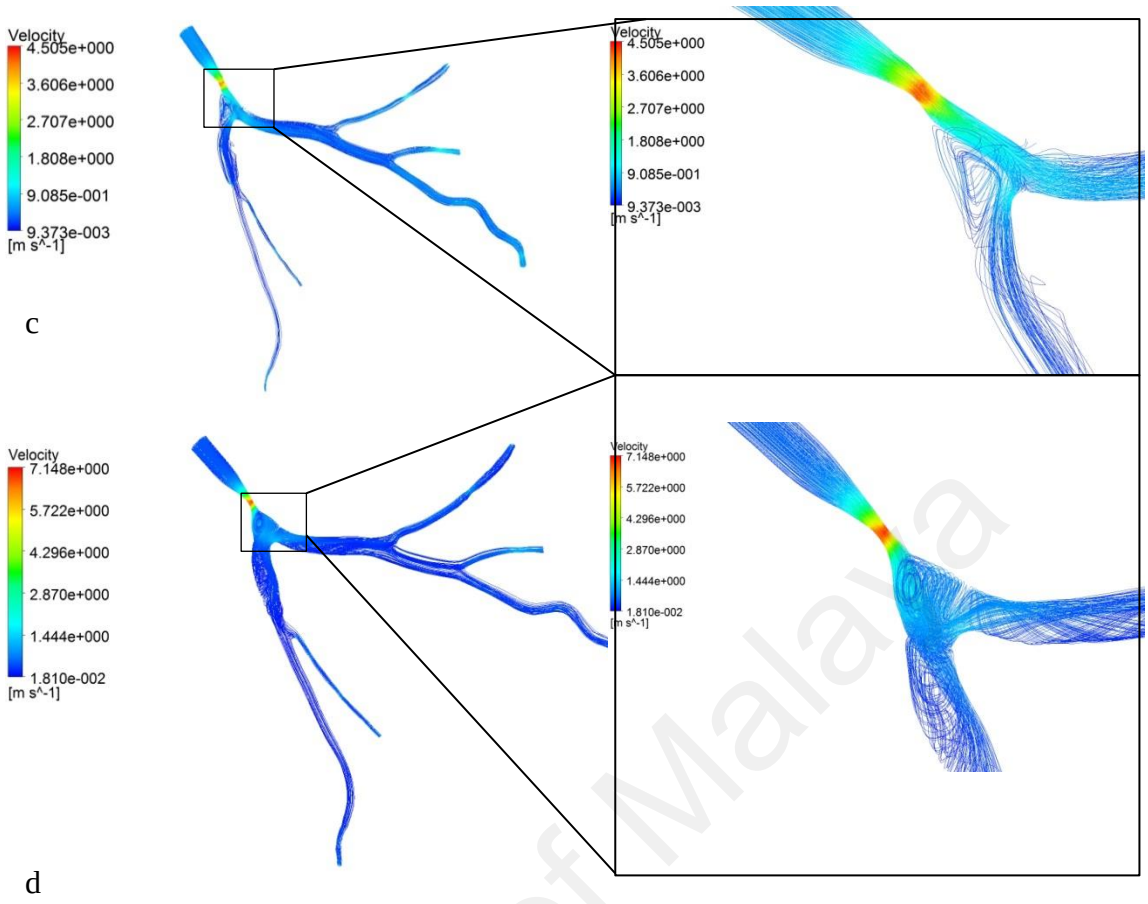

Figure 4.45: velocity distribution in left coronary artery during peak systole a) Normal b) 70% AS c) 80% AS d) 90% AS

Figure 4.46 depicts the effect of different degree of stenosis on the wall shear stress. The wall shear stress plays a significance role in determining the artery strength. Figure 4.46b shows the increase in wall shear stress in the range from 40 Pa to 163 Pa as compared with the normal coronary model which shows in the range from 40Pa to 125Pa (figure 4.46a). The wall shear stress further increase in the range from 299Pa to 598Pa and 403Pa to 807Pa, as the percentage AS increases to 80% AS and 90% AS, as sown in figure 4.46c and figure 4.46d respectively. Thus higher wall shear stress may lead bursting or rupturing the arterial wall. It is well known that the high wall stress may

help in rupture. This study shows that different degree stenosis in left coronary artery produces a significant effect on the flow pattern and wall shear stress.

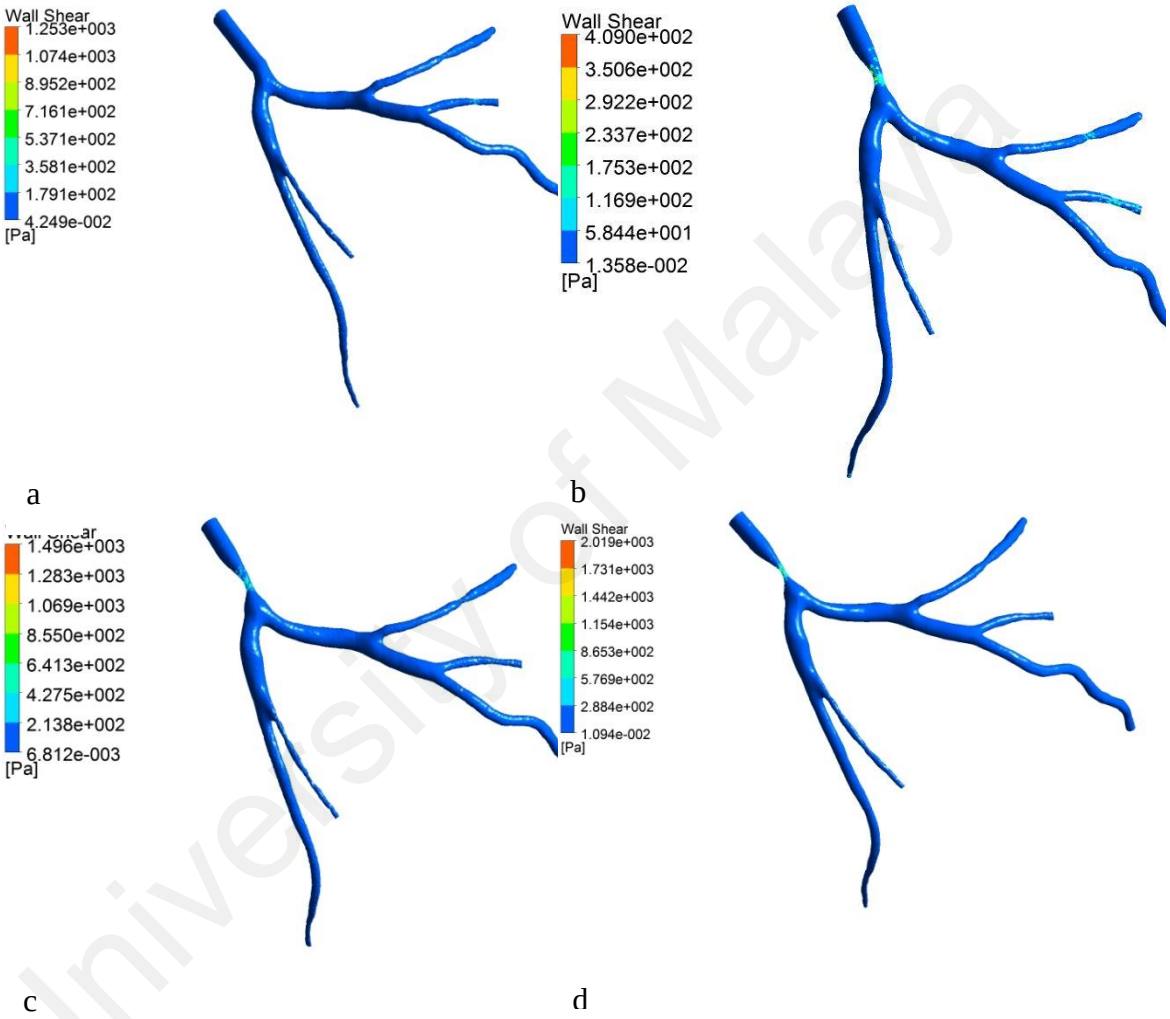

Figure 4.46: wall shear stress distribution in left coronary artery during cardiac cycle a) Normal b)70% AS c)80% AS d)90% AS

At hyperemic condition the time average pressure drop and pressure proximal to stenosis along with the Fractional Flow Reserve (FFR) values calculated and reported in table 4.1 The results of the current section provide the necessary information on the effect of various percentage of stenosis on the hemodynamic parameters in the left main stem. It is found that the FFR value significantly dropped to 0.69 for the case of 90% AS. The FFR value reflects the functional severity of stenosis. It is noted that a FFR of less than 0.8 is functionally significant. If FFR drops less than 0.75 then clinicians recommend an angioplasty or coronary artery bypass graft (CABG). For the cases of FFR values mora than 0.8, surgical procedure may not be required and the patient is advised to undergo a medical therapy. Thus, FFR can guide the clinicians as what type of medical treatment to be adopted. It is very clear from table 4.1 that 90% AS has very low (0.69) FFR value, indicating that the possible treatment required is that of interventional procedure instead of just medical therapy.

Table 4.1: Results calculated from the computational simulation for 70%AS, 80%AS, 90% AS

%Area Stenosis (AS)	Hyperemic flow Q (ml/min)	$\tilde{p}_a$ mmHg	($\Delta\tilde{p}$)	FFR
70%	175	95.8	6.7	0.92
80%	165	109.7	20.7	0.81
90%	115	131.0	40.5	0.69

4.16 Effect of multi-stenosis in left coronary artery on the hemodynamic parameters with different flow rates

It has been common observation for doctors that the stenosis may develop at multiple places in same patient. The existence of multiple stenosis endangers the life of

patient and it could lead to more severity than single stenosis. Thus the current section is aimed to study the presence of multiple blockages at various locations on coronary artery. The coronary artery in present section (section 4.16) belongs to patient 3 of table 3.4 and the stenosis is introduced at various locations with the help of Mimics software. In the case of multi stenosis left coronary artery different degree of multi-stenosis is placed at various locations across the bifurcations to investigate the effect of those stenosis on the hemodynamic parameters such as wall pressure, velocity and wall shear stress for the maximum velocity at 1.2s during the cardiac cycle.

4.16.1 Location of 70% AS at left main stem (LMS) and 80% AS at left circumflex (LCX) branch

Figure 4.47 illustrates the pressure distribution in a multi stenosed left coronary artery for various flow rate at 1.2s during the cardiac cycle. In the figure, Left Main Stem (LMS) of coronary artery has 70% AS and the Left Circumflex branch has 80% AS. It is observed that the pressure drops across the stenosis. The maximum pressure drop across the 70% AS at the LMS is in the range from 13300 Pa to 12730 Pa, 14250 Pa to 13460 Pa, 14280 Pa to 13250 Pa and 15140 Pa to 13840 Pa for 100, 125, 150 and 175ml/min respectively, whereas the pressure drop across the 80% area stenosis at the Circumflex branch is in the range from 12150 Pa to 11580 Pa, 11890 Pa to 11100 Pa, 12210 Pa 11180 Pa and 11260 Pa to 9971 Pa for 100, 125, 150 and 175ml/min respectively. As expected, the maximum pressure drops for the higher degree of stenosis. It is also noted that the pressure drop increases with the increase in the blood flow rate across the higher degree of stenosis. It should be noted that the presence of secondary stenosis in the Circumflex branch has further complicated the flow behaviour vindicated in terms of increased pressure drop at the main stem area. The pressure drop in the main stem has increased by 34% due to secondary stenosis as compared to similar

conditions of single stenosis (figure 4.43 b). Thus it can be conveniently said that the severity of patients substantially increases when multiple stenosis are developed.

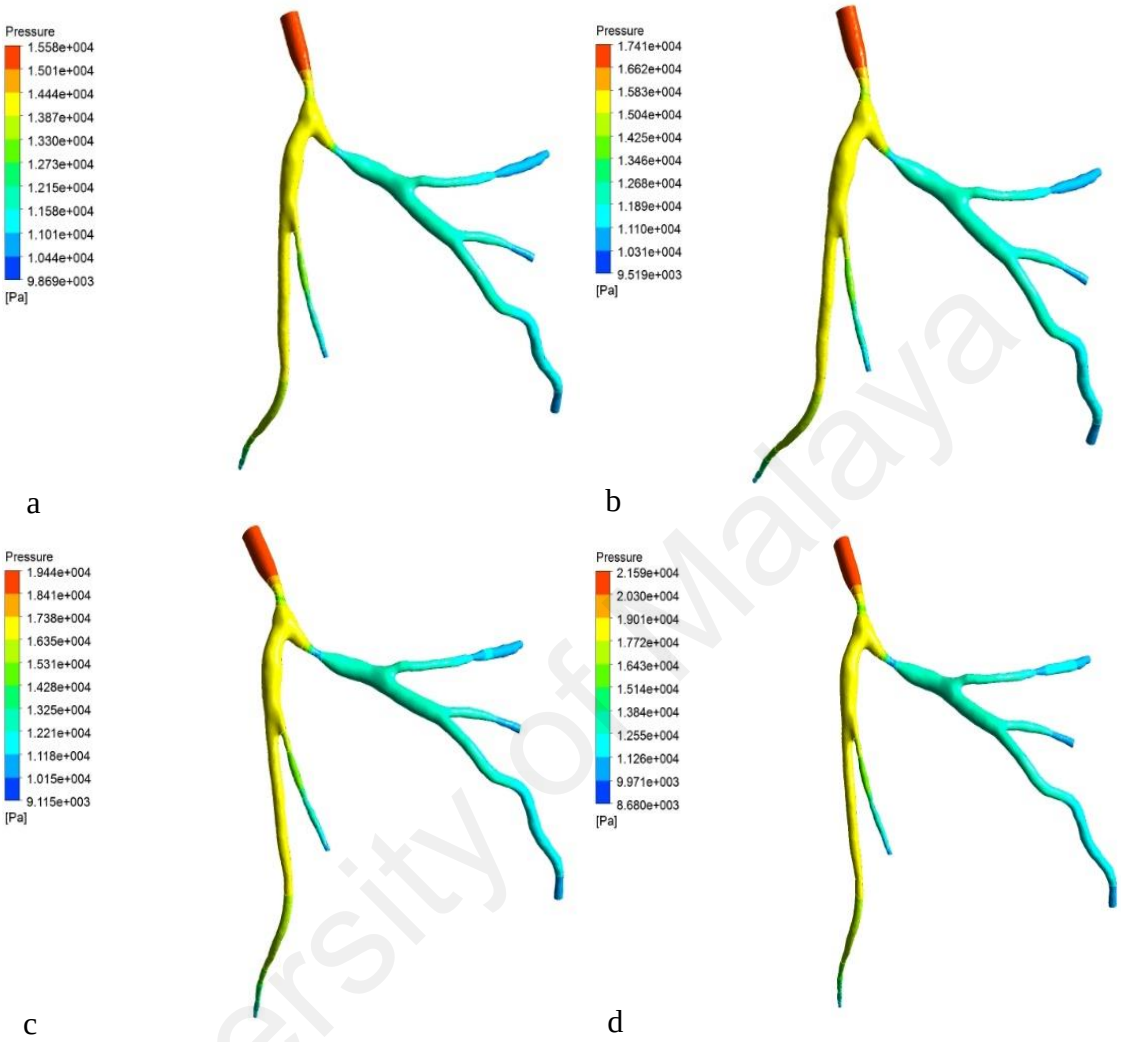

Figure 4.47: Pressure distribution in left coronary artery of 70% and 80%AS located at LMS and LCX respectively for 1.2s during the cardiac cycle for various flow rate a) 100ml/min b) 125ml/min c) 150ml/min d) 175ml/min

Figure 4.48 shows a velocity pattern in a multi stenosed left coronary artery for various flow rate at 1.2s during the cardiac cycle. It is seen that the velocity across the stenosis increased. The maximum velocity is found across the higher degree of stenosis that is across the LCX. The velocity across the 70% AS at the LMS is noted in the range from 0.76 m/s to 1.0 m/s, 0.95 m/s to 1.2 m/s, 1.1 m/s to 1.5 m/s and 1.3 m/s to 1.7 m/s for 100, 125, 150 and 175ml/min respectively. Similarly, the maximum velocity across

the 80% AS in the circumflex branch is in the range from 1.5 m/s 1.7 m/s, 2.2 m/s 2.5 m/s, 2.7 m/s to 3.0 m/s and 3.1 m/s to 3.5 m/s for 100, 125, 150 and 175ml/min respectively. It is noted that velocity increases with the increases in blood flow rate. A recirculation zone is also observed immediate after the stenosis.

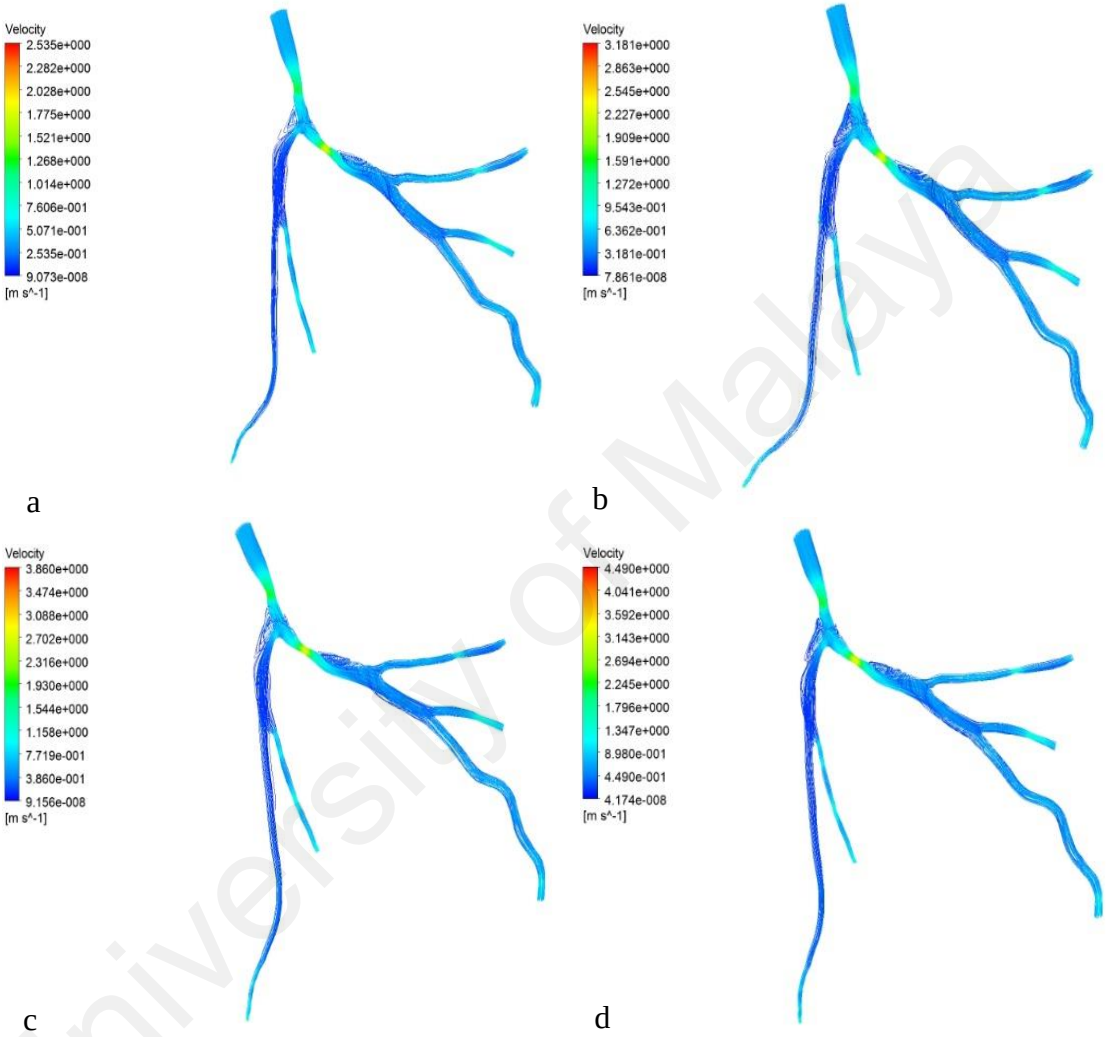

Figure 4.48: Velocity distribution in left coronary artery of 70% and 80%AS located at LMS and LCX respectively for 1.2s during the cardiac cycle for various flow rate a) 100ml/min b) 125ml/min c) 150ml/min d) 175ml/min

The wall shear stress distribution in a multi stenosed left coronary artery for various flow rate at 1.2s during the cardiac cycle is depicted in figure 4.49. The higher wall shear stress is found across the region of stenosis, and it is maximum for the higher degree of stenosis. The wall shear stress across the 70% AS at the LMS is noted in the range from 0 Pa to 105 0 to 139 Pa, 0 Pa 180 Pa and 0 Pa to 239 Pa for 100, 125, 150 and 175ml/min respectively. This is 1.21 times increase in the wall shear stress due to presence of secondary stenosis as compared to single stenosis. It is also found that the wall shear stress increases with the increases in blood flow rate due to the increases in velocity across the higher degree of stenosis.

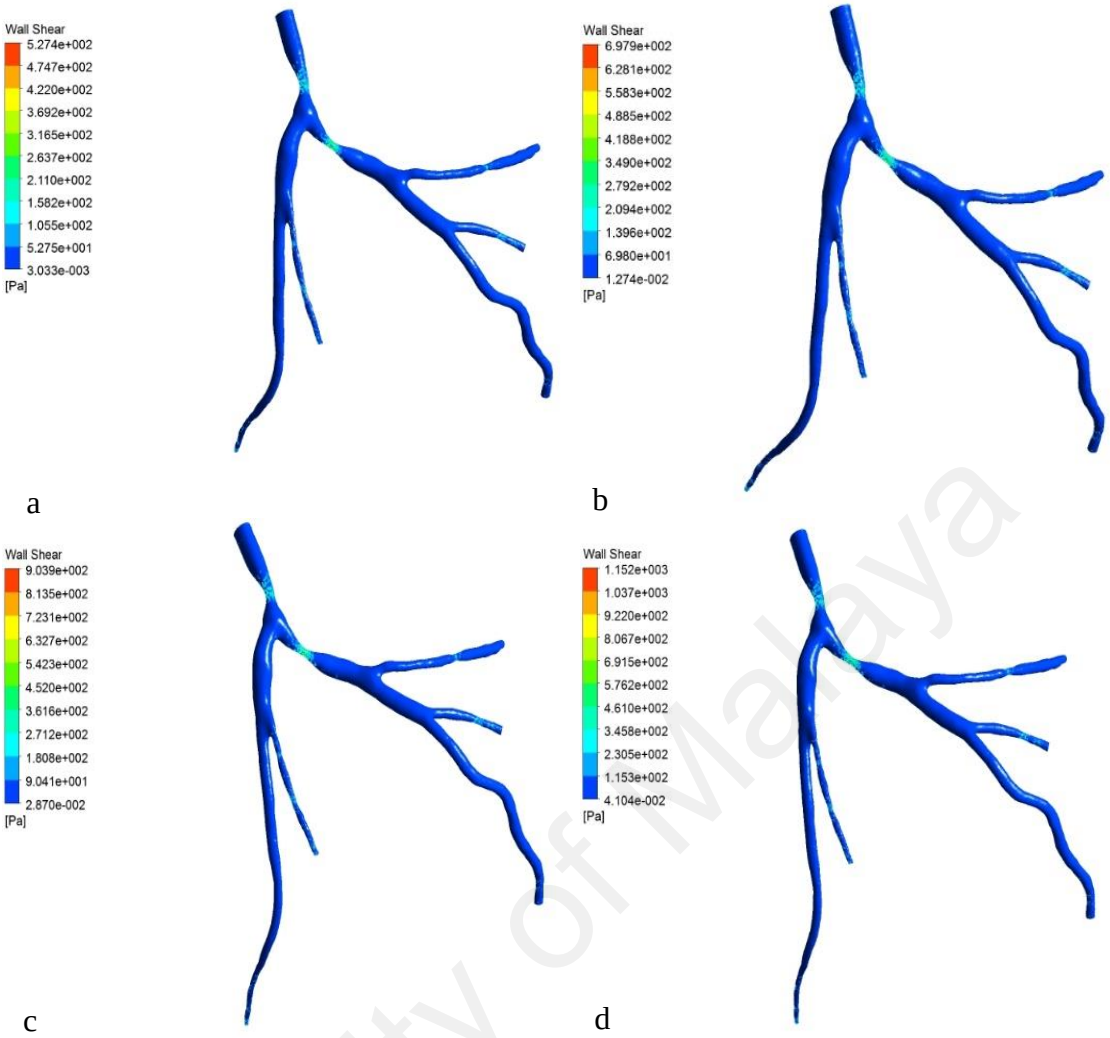

Figure 4.49: Wall shear stress in left coronary artery of 70% and 80%AS located at LMS and LCX respectively for 1.2s during the cardiac cycle for various flow rate a) 100ml/min b) 125ml/min c) 150ml/min d) 175ml/min

4.16.2 Location of 70% AS at left main stem (LMS) and 90% AS at left circumflex (LCX) branch

Figure 4.50 demonstrates the pressure distribution in a multi stenosed left coronary artery for various flow rate having 70% AS at the Left Main Stem (LMS) and 90% area stenosis at the Circumflex branch of coronary artery. It is observed that the maximum pressure drop is higher for stenosis of 90% blockage. The pressure drop across the 70% AS at the LMS is in the range from 13390 Pa to 12240 Pa, 15710 Pa to 13970 Pa, 18090 Pa to 15660 Pa and 20670 Pa to 17410 Pa for 100, 125, 150 and

175ml/min respectively, which is higher than that of secondary stenosis of 80% blockage. The pressure drop across the 90% area stenosis at the Circumflex branch is in the range from 5333 Pa to 4182 Pa, 3533 Pa to 1794 Pa, 1080 Pa -1350 Pa and -2127 Pa to -5383 Pa for 100, 125, 150 and 175ml/min respectively.

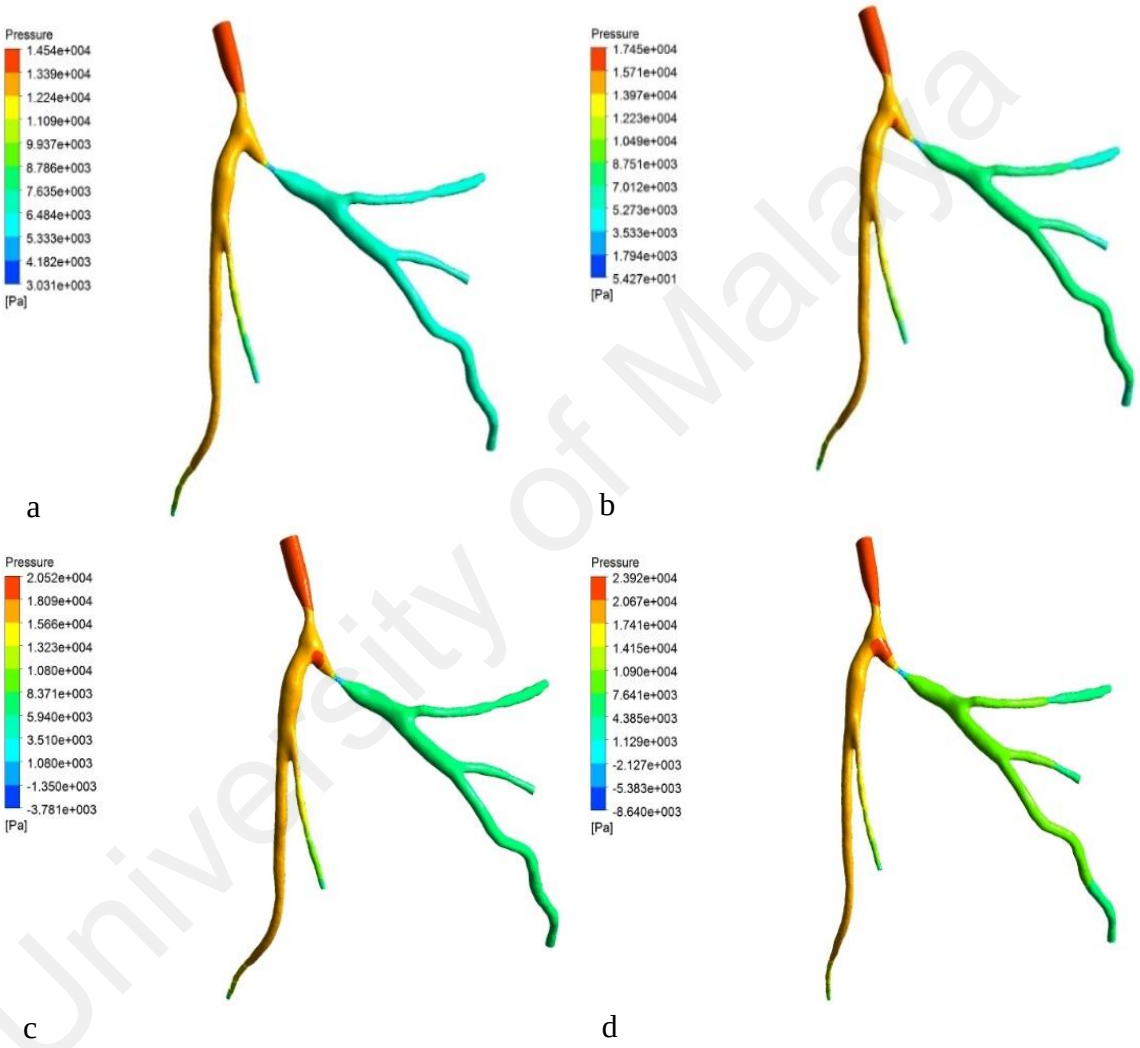

Figure 4.50: Pressure distribution in left coronary artery of 70% and 90%AS located at LMS and LCX respectively for 1.2s during the cardiac cycle for various flow rate a) 100ml/min b) 125ml/min c) 150ml/min d) 175ml/min

Figure 4.51 shows the effect of 90% secondary stenosis on velocity profile. The highest velocity is observed across the higher degree (90% AS) of stenosis. The velocity across the 70% AS at the LMS is observed in the range from 1.12m/s to 1.5m/s, 1.4m/s to 1.87 m/s, 1.68 m/s to 2.24 m/s and 1.95 m/s to 2.6 m/s for 100, 125, 150 and 175ml/min respectively. Similarly, the highest velocity across the 90% AS in the circumflex branch is in the range from 3.37m/s 3.75m/s, 4.21m/s 4.67m/s, 5.0m/s to 5.6m/s and 5.8m/s to 6.52m/s for 100, 125, 150 and 175ml/min respectively. This is higher than its corresponding values for 80% secondary blockage. The blood flow variation across the coronary artery could lead to detrimental effects and this is believed to play an important role in the biological mechanism that lead to the state of coronary artery disease. Especially the areas of low blood velocity and recirculation zones are potentially prone areas of further stenosis development (Chaichana et al., 2012, 2013b; Fuster, 1994). It is seen that the circulation zone increased due to increase in secondary blockage.

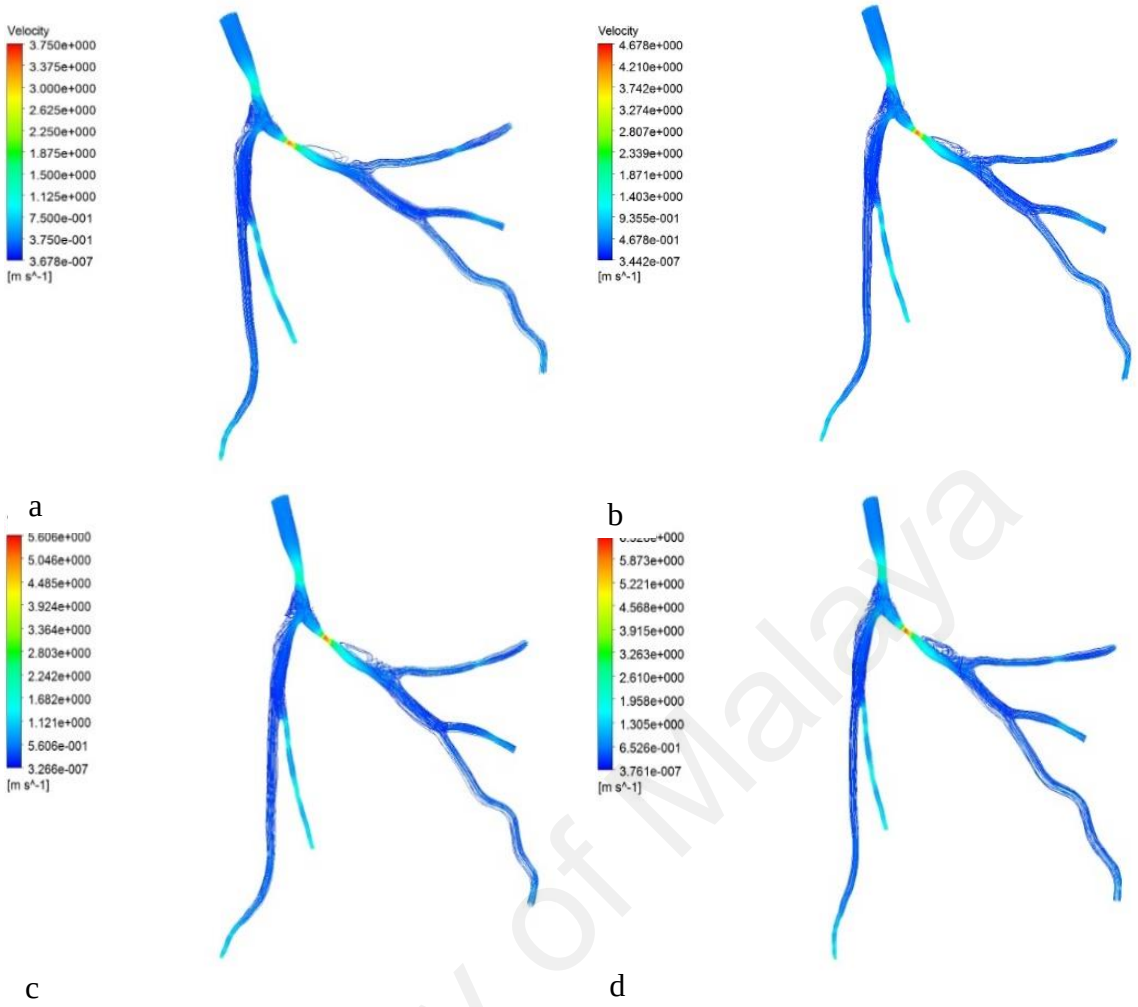

Figure 4.51: Velocity distribution in in left coronary artery of 70% and 90%AS located at LMS and LCX respectively for 1.2s during the cardiac cycle for various flow rate a) 100ml/min b) 125ml/min c) 150ml/min d) 175ml/min

Figure 4.52 shows the wall shear stress for 90% secondary stenosis. The maximum wall shear stress is found at the higher (90% AS) degree of stenosis. The wall shear stress at the region of artery is 0.02 Pa to 269 Pa, 0.011Pa to 339Pa, 0.029Pa to 405Pa and 0.04Pa to 470Pa for 100, 125, 150 and 175ml/min respectively. This is very clear that the increased blockage at secondary level has further increases the wall shear stress. This would be an alarming situation for patients having such condition due to high risk of artery rupture.

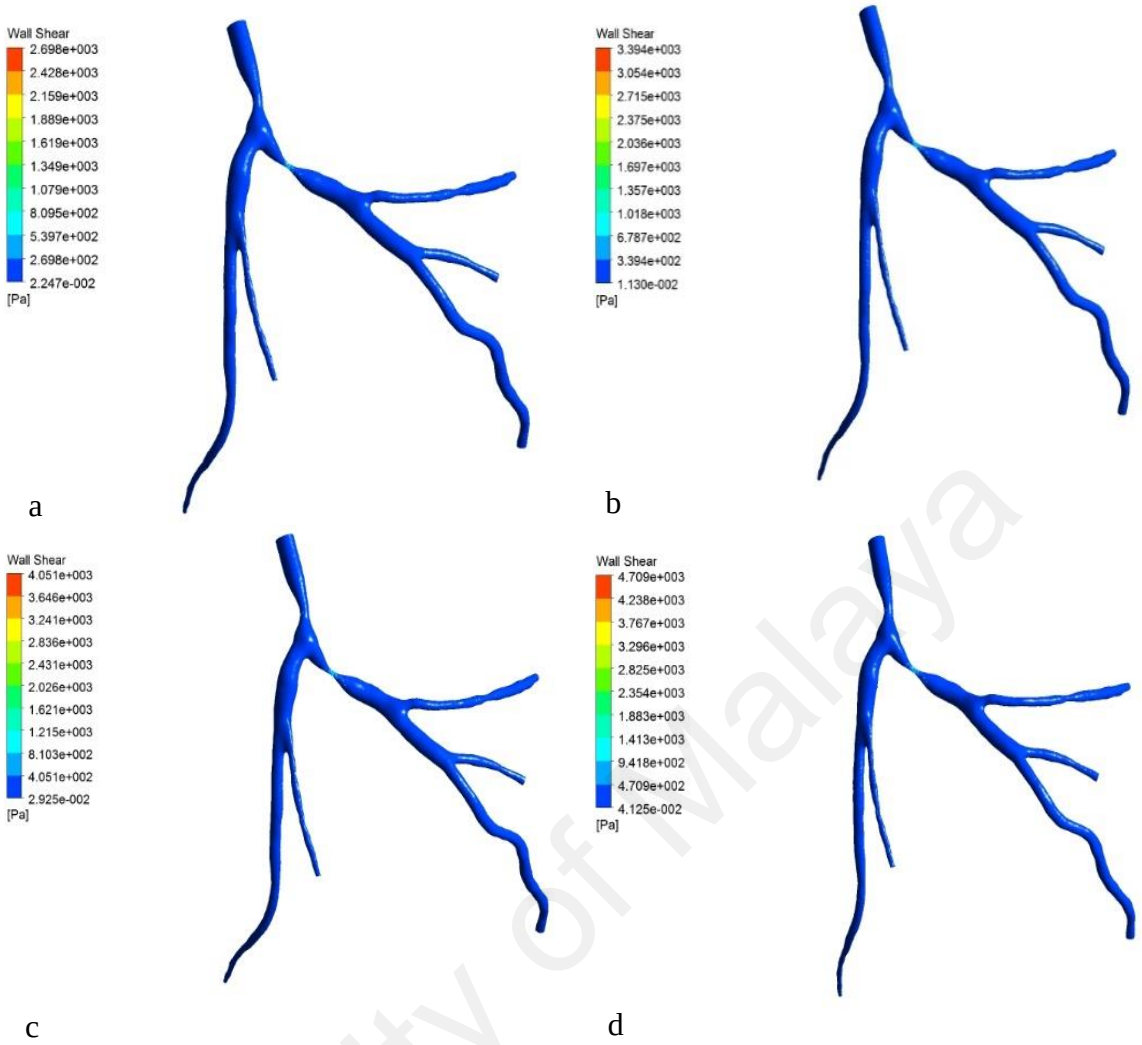

Figure 4.52: Wall shear stress in in left coronary artery of 70% and 90%AS located at LMS and LCX respectively for 1.2s during the cardiac cycle for various flow rate a) 100ml/min b) 125ml/min c) 150ml/min d) 175ml/min

4.16.3 Location of 70% AS at left anterior descending (LAD) and 90% AS at left circumflex (LCX) branch

It is seen in previous sections that the presence of secondary stenosis on branches of coronary artery can have significant effect on blood flow behaviour. It is well known that the location of stenosis has direct impact on the flow behaviour on artery. The effect of multiple stenosis on left anterior descending and circumflex branch of coronary artery is described in the following section. The artery in current study belongs to patient 3 as mentioned in table 3.4. Figure 4.53 represents the pressure

distribution in a multi stenosed left coronary artery for various flow rates at 1.2s during the cardiac cycle. Figure 4.53 shows 70% AS at the Left anterior descending (LAD) and 90% area stenosis at the left Circumflex (LCX) branch of coronary artery. This is different from previous section since both stenosis are present on branches of coronary artery rather than on main stem as deliberated in previous sections. As expected, the pressure drop across the stenosis is maximum for the 90% area stenosis as compared to the 70% area stenosis (AS). The wall pressure across the 70% AS is observed at the LAD is in the range from 13280 Pa to 12190 Pa, 15670 Pa to 14030 Pa, 18270 Pa to 15970 Pa and 21070 Pa to 17990 Pa for the 100, 125, 150 and 175ml/min respectively. Similarly the pressure drop across the 90% AS at the circumflex branch is in the range from 5656 Pa to 4567 Pa, to 4171 Pa to 2529 Pa, 2113 Pa to -196 Pa and -531 Pa to -3618 Pa for 100, 125, 150 and 175ml/min respectively. It is found that the LAD develops reasonably high pressure in comparison to that of LCX due to current stenosis size and location. As expected, the pressure drop across the blockages increases with the increases in the blood flow rate.

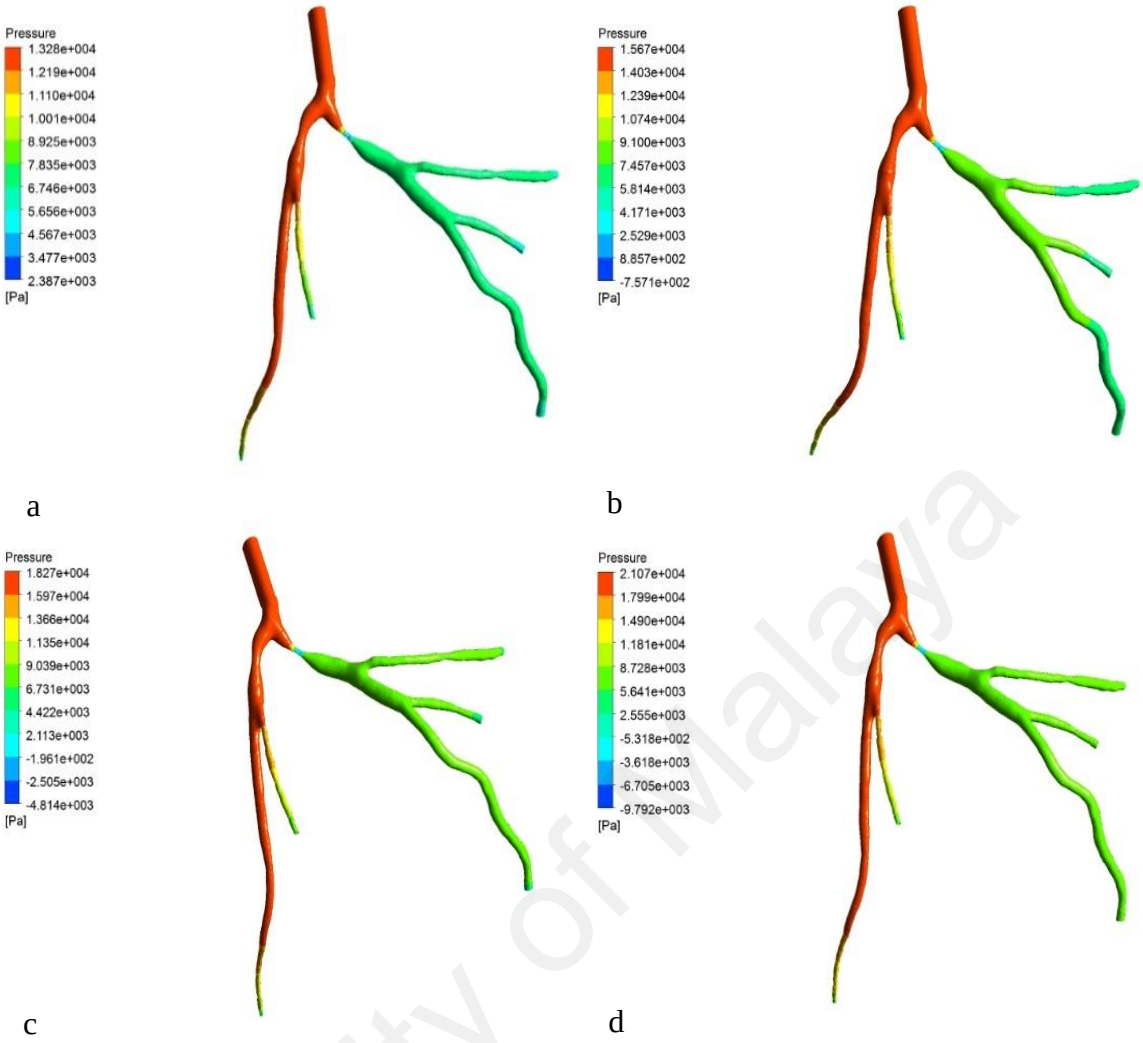

Figure 4.53: Pressure distribution in left coronary artery of 70% and 90%AS located at LAD and LCX respectively for 1.2s during the cardiac cycle for various flow rate a) 100ml/min b) 125ml/min c) 150ml/min d) 175ml/min

The velocity pattern in the multi stenosed left coronary artery is depicted in figure 4.54. It can be clearly seen from the figure 4.54 that the velocity increased across the stenosis, and it is maximum for the 90%AS at the left circumflex (LCX) branch of coronary artery. The velocity across the 70% AS at the LAD is observed in the range from 0.73m/s to 0.36m/s, 0.91m/s to 0.45m/s, 1.0m/s to 0.54m/s and 1.2m/s to 0.63m/s for 100, 125, 150 and 175ml/min respectively. Similarly the highest velocity across the 90% AS in the circumflex branch is in the range from 3.2m/s to 2.9m/s, 4.0m/s to

3.6m/s, 4.9m/s to 4.3m/s and 5.7m/s to 5.0m/s for 100, 125, 150 and 175ml/min respectively.

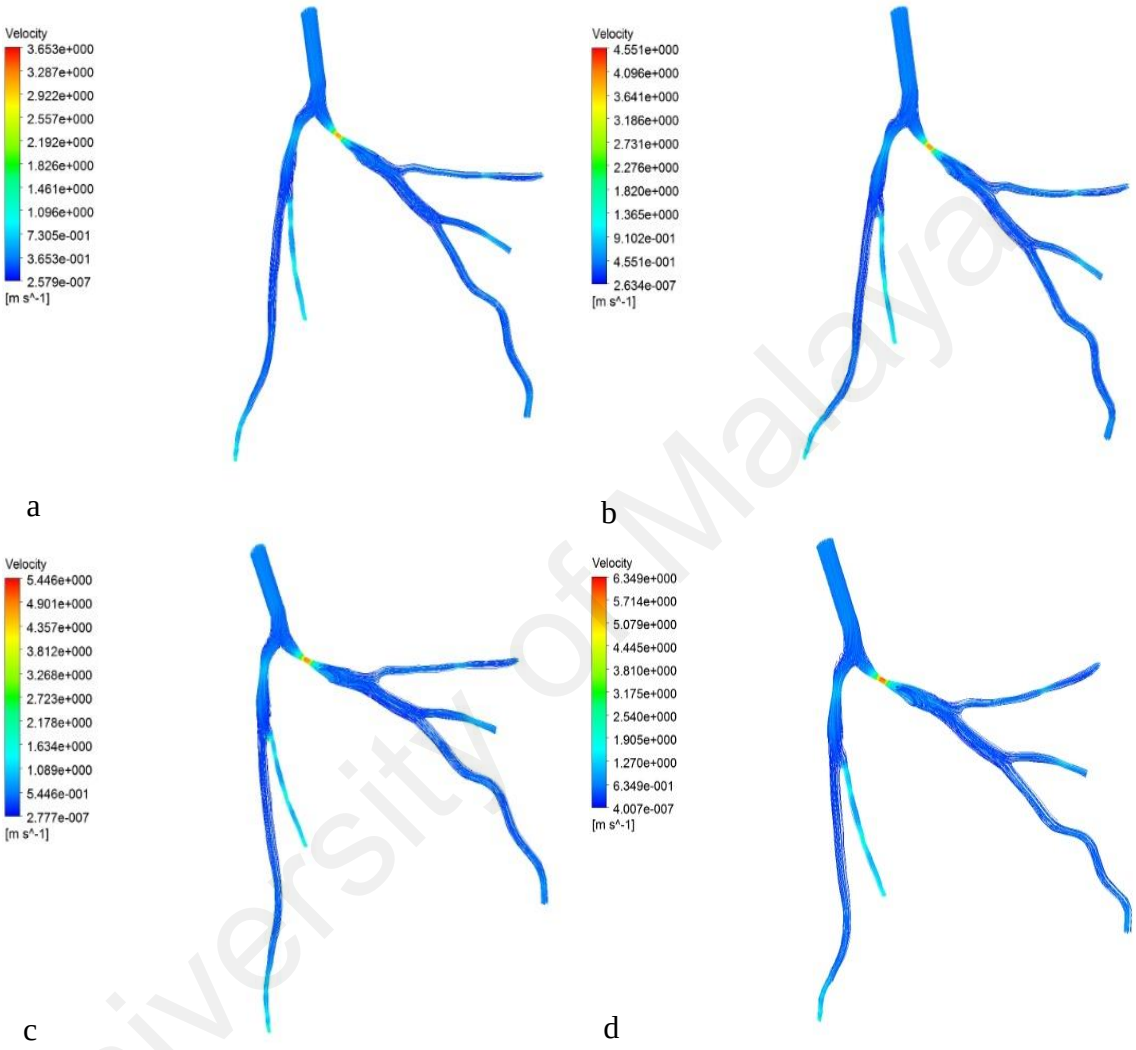

Figure 4.54: Velocity distribution in left coronary artery of 70% and 90%AS located at LAD and LCX respectively for 1.2s during the cardiac cycle for various flow rate a) 100ml/min b) 125ml/min c) 150ml/min d) 175ml/min

Figure 4.55 shows the wall shear stress distribution in the multi stenosed left coronary artery. It is observed that the maximum wall shear stress across the 90%AS at LCX as compared to the 70%AS at LAD. The wall shear stress across the 70% AS at the branch LAD is 127 Pa, 167 Pa, 208 Pa and 249 Pa for 100, 125, 150 and 175ml/min respectively. Similarly, the wall shear stress across the 90% AS at the branch LCX is in the range from 383 Pa, 503 Pa, 625 Pa and 747 Pa for 100, 125, 150 and 175ml/min respectively.

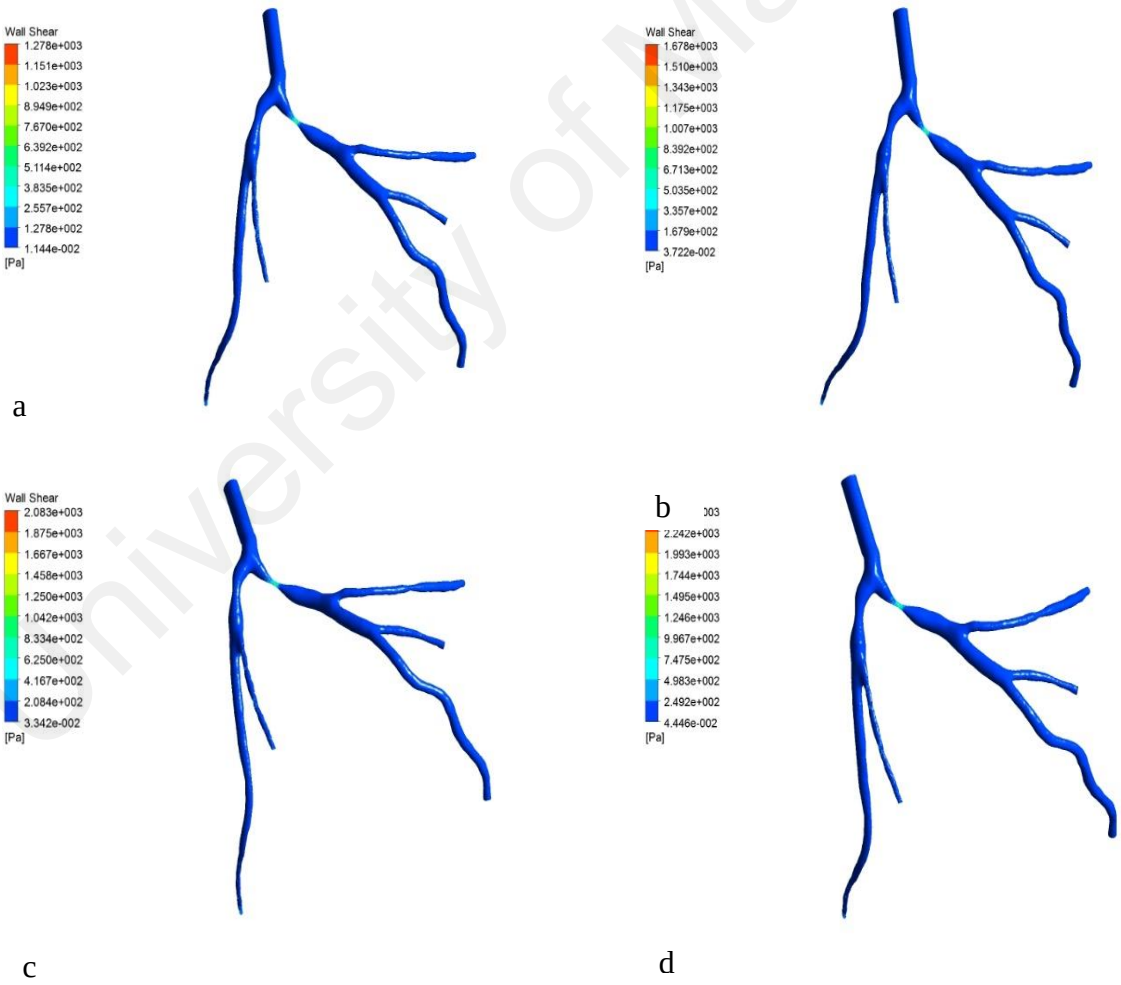

Figure 4.55: Wall shear stress in left coronary artery of 70% and 90%AS located at LAD and LCX respectively for 1.2s during the cardiac cycle for various flow rate a) 100ml/min b) 125ml/min c) 150ml/min d) 175ml/min

4.16.4 Location of 90% AS at left anterior descending (LAD) and 70% AS at left circumflex (LCX) branch

This section is aimed to investigate the effect of reversing the size of stenosis on LAD and LCX as compared to previous section i.e. section 4.16.3. Figure 4.56 shows the pressure distribution in a multi stenosis of left coronary artery located at LAD (90%AS) and LCX (70%AS) for various flow rate at 1.2s during the cardiac cycle. As expected, the pressure drops to greater extent at LAD than at the LCX. It should be noted that the LAD had very little pressure variations for reverse order of stenosis size on LAD and LCX (figure 4.53) as compared to present case (figure 4.55). This could be explained in a way that the angle of branching of LCX is higher than that of LAD for the artery being analysed. Thus the blood encounters relatively lesser resistance in LAD than LCX in current model. Thus the pressure variations in LCX are noticeable for LCX having 70% AS than LAD having 70% AS. It is observed that the angulation of bifurcation has an impact on blood flow characteristics (Chaichana et al., 2011). It is found that the pressure drop is higher for the 90%AS at the LAD branch as compared to the 70%AS at the LCX branch.

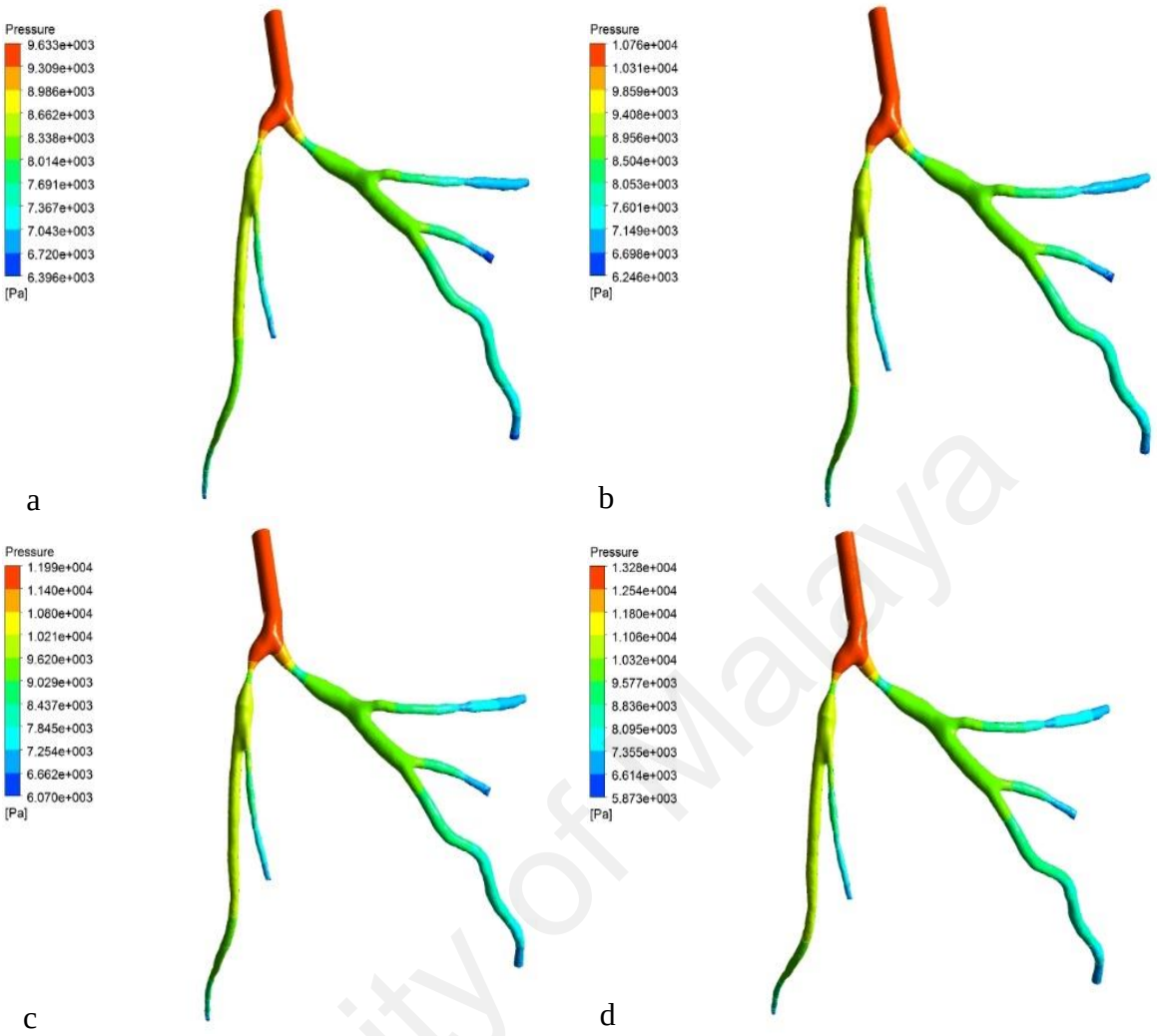

Figure 4.56: Pressure distribution in left coronary artery of 90% and 70%AS located at LAD and LCX respectively for 1.2s during the cardiac cycle for various flow rate a) 100ml/min b) 125ml/min c) 150ml/min d) 175ml/min

The velocity distribution in the multi stenosed left coronary artery for various flow rate is depicted in figure 4.57. It can be clearly seen from the figure 4.57 that the velocity increased across the stenosis, and it is maximum for the 90%AS at the left anterior descending (LAD) branch of coronary artery. As expected, the velocity across the higher degree (90%AS) stenosis increases with the increase in the blood flow rate.

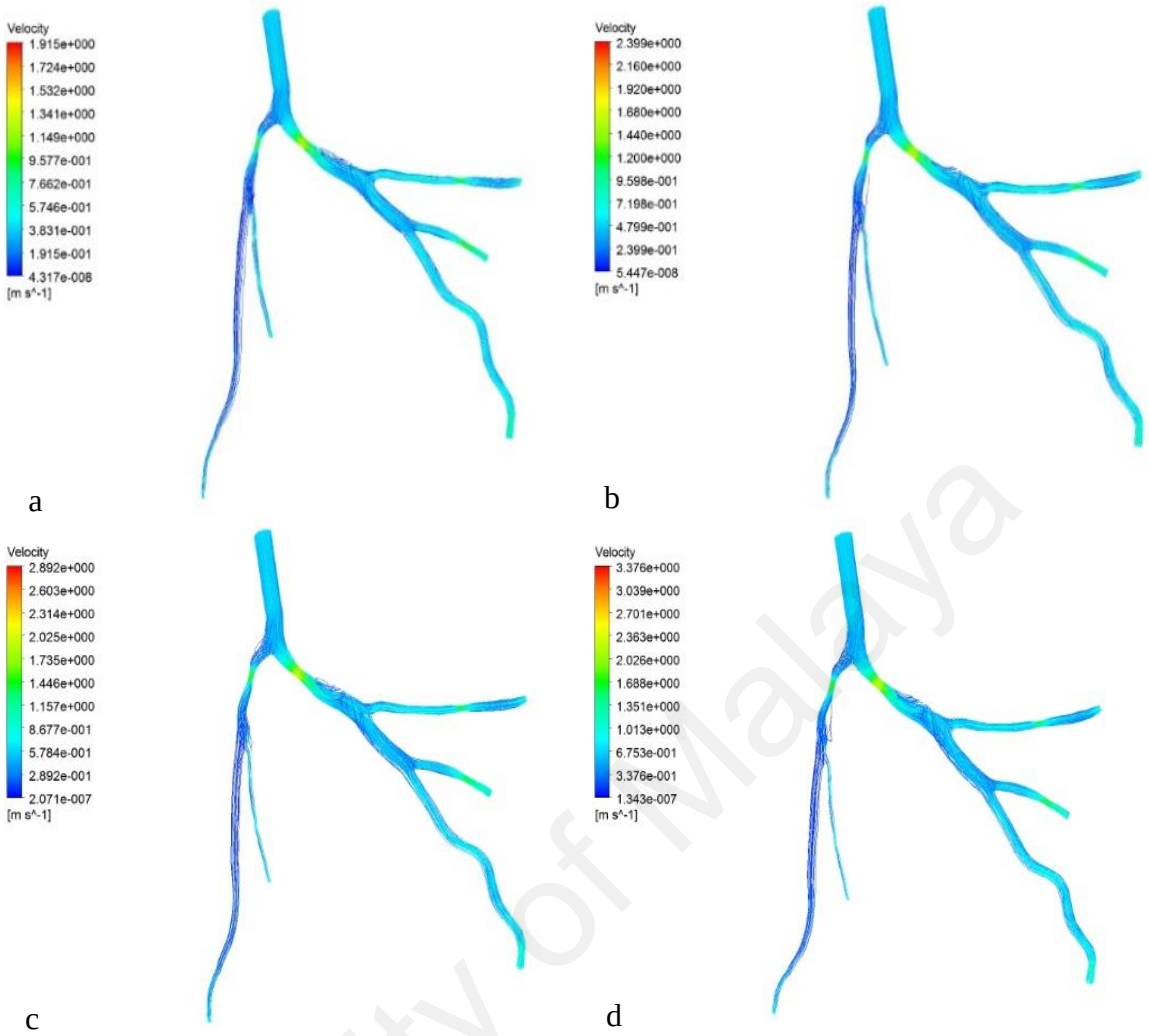

Figure 4.57: Velocity distribution in left coronary artery of 90% and 70%AS located at LAD and LCX respectively 1.2s during the cardiac cycle for various flow rate a) 100ml/min b) 125ml/min c) 150ml/min d) 175ml/min

The wall shear stress distribution in the multi stenosed left coronary artery for various flow rate is shown in figure 4.58. The maximum wall shear stress is found across the 90%AS at LAD as compared to the 70%AS at LCX. The wall shear stress across the 70% AS at the branch LCX is 92 Pa, 130 Pa, 170 Pa and 212 Pa for 100, for 100, 125, 150 and 175ml/min respectively. Similarly, the wall shear stress across the 90% AS at the branch LAD is 138 Pa, 195 Pa, 255 Pa and 318 Pa for 100, 125, 150 and 175ml/min respectively. It is obvious that the LAD has higher risk as compared to LCX. However, the wall shear stress in the non-stenotic region of artery is lesser for current

case as compared to its counterpart when LAD and LCX has 70% AS and 90% AS respectively. The wall shear stress can doubly dangerous. The higher wall shear stress may lead to rupture the artery. However, the low wall shear stress areas are known to be prone to development of stenosis (Delfino, Stergiopulos, Moore, & Meister, 1997; Dobrin, Littooy, & Endean, 1989; White et al., 1993)

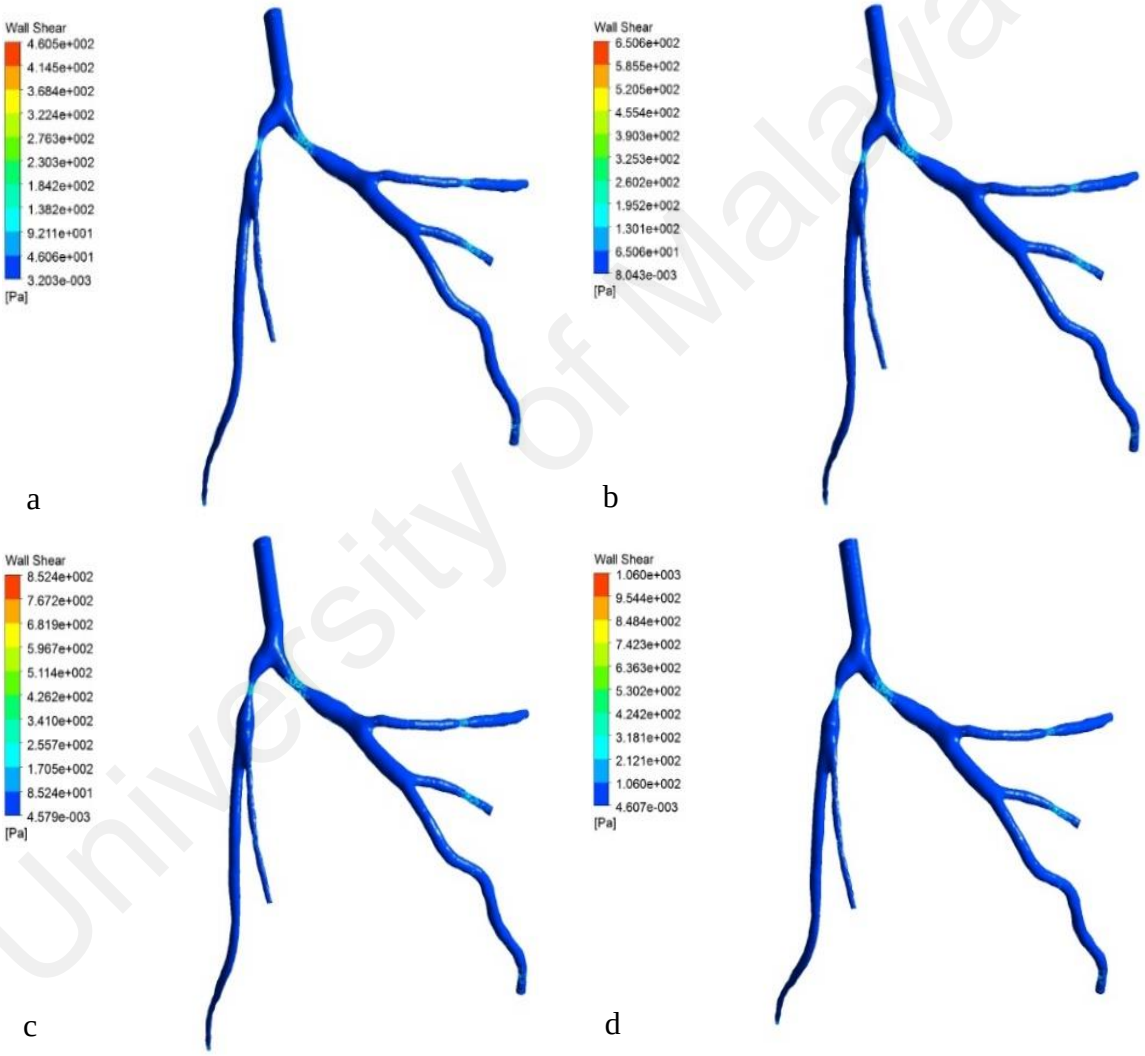

Figure 4.58: Wall shear stress in left coronary artery of 90% and 70%AS located at LAD and LCX respectively for 1.2s during the cardiac cycle for various flow rate a) 100ml/min b) 125ml/min c) 150ml/min d) 175ml/min

4.16.5 Severity analysis of different stenosis size and location

The previous sections have described the presence of two stenosis at various locations along the coronary artery. The study is further explored by varying the location of stenosis at branches and sub branches of left coronary artery. The current study comprised of 10 models having varying size and location of two stenosis. Figure 4.59 shows the locations of those 10 models considered along with table 4.1 showing the size and location of each model studied. It is known that the pressure drop in the artery due to presence of blockage areas can be taken as an indicator of the health of diseased artery. Thus the current study is focussed to assess the severity of artery based on pressure drop across various models being analysed. The models are rated according to the pressure drop with worse pressure drop getting the rank 1 in severity.

Table 4.2 shows the rating of 10 analysed models. The models were initially numbered sequentially as per the stenosis position away from main stem and then ranked according to the highest pressure drop. It is clear from table 4.2 that the model having 70% and 90% stenosis at Left Main Stem and just after the branching into LCX respectively is worst affected among all the models being investigated. This could be attributed to 90% blockage in the LCX that hinders the flow by offering extensive resistance. This is further vindicated by the fact that all the models that have 90% blockage at position two are among the worst affected as compared to other model being investigated. The change of blockage area from 90% to 80% has reduced the rating to 5. The least affected model among all, is the one having 90% and 70% stenosis at position 3 and 5 respectively which are located at LAD and sub branch of LCX. It is obvious from table 4.2 that the stenosis in the LCX has larger pressure drop as compared to stenosis at the LAD in the artery model belonging to patient 3. This could be attributed to the fact that the bifurcation angle of LCX is higher than that of LAD of coronary artery of patient 3. It is known that the atherosclerosis (a disease of the arteries

characterized by the deposition of plaques of fatty material on their inner walls) tends to develop at locations where disturbed flow patterns occur such as places where a coronary angulation is formed between the left anterior descending (LAD) and left circumflex (LCX). Wide angulation leads to significant flow disturbances in the artery that are directly related to the formation of plaques (Chaichana et al., 2011) .The LAD and LCX angles were approximately measured as 31^{o} and 39^{o} respectively. It should be noted that the severity rating may change in another patient due to change of bifurcation angle.

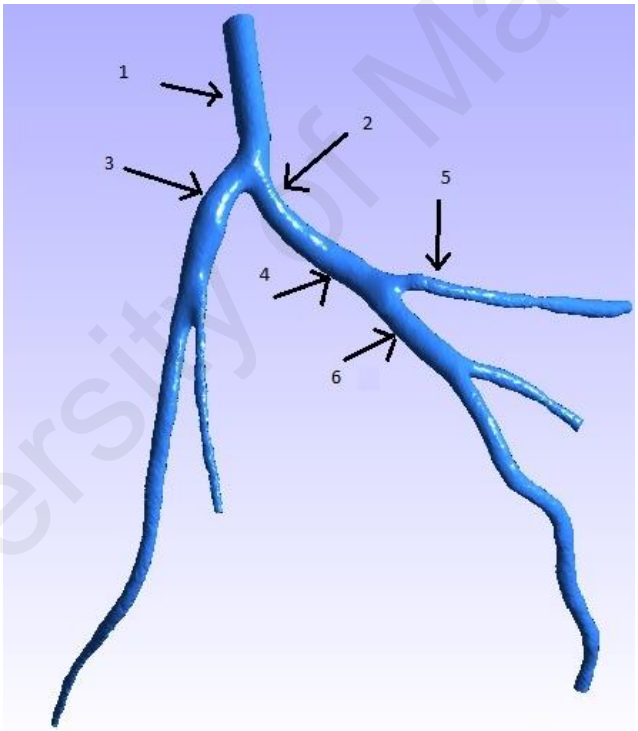

Figure 4.59: Various stenosis positions

Table 4.2: Size and location of stenosis in various models studies

Model No/Position	1	2	3	4	5	6
MODEL 1	70%	80%				
MODEL 2	70%	90%				
MODEL 3		90%	70%			
MODEL 4		90%	80%			
MODEL 5		70%	90%			
MODEL 6		90%			70%	
MODEL 7			90%		70%	
MODEL 8			70%			90%
MODEL 9		80%				70%
MODEL 10				70%		80%

Table 4.3: Severity ranking of different models

Severity Rating	Model No
1	MODEL 2
2	MODEL 3
3	MODEL 4
4	MODEL 6
5	MODEL 1
6	MODEL 8
7	MODEL 9
8	MODEL 10
9	MODEL 5
10	MODEL 7

Similarly, the 10 models being studied for multi-stenosis are analysed with respect to wall shear stress and ranked according to higher to lower wall shear stress being developed. It should be noted that the high wall shear stress is critical for the health of the artery wall and it may cause rupture. The various models under investigation are analysed for wall shear stress and rated according to highest to lowest shear stress as shown in in table 4.4. It is seen that model 2 that has 70% AS at Left main stem and 90% AS at LCX has highest wall shear stress development. It should be noted that this particular model is also ranked no 1 with respect to the severity of pressure drop (table 4.3). Thus it can be conveniently said that the combination of 70% AS and 90% AS on Left main stem and LCX can pose high risk to human life. Model 2 is followed by model 3, model 4 and model 6 in the severity of wall shear stress rating that also matches with pressure drop severity as well. However, model 9 has slightly higher wall shear stress as compared to model 1 but the pressure drop across model 1 is higher than that of model 9. Model 7 has least wall shear stress as compared to all other models considered.

Table 4.4: Severity Rating Based on Wall Shear Stress

Rank	Positions
1	MODEL 2
2	MODEL 3
3	MODEL 4
4	MODEL 6
5	MODEL 9
6	MODEL 8
7	MODEL 1
8	MODEL 5
9	MODEL 10
10	MODEL 7

The study is further explored to analyse the transient velocity variation at the main left stem (point 1) and near the branching point of main left stem into LAD and LCX (point 2). The transient velocity variation is studied for 4 blood flow rates such as 100ml, 125 ml, 150ml and 175 ml, as shown in figures 4.60 to 4.69. As expected, the velocity for higher flow rate is high in all the models studied. The trend of velocity variation is found to be similar for all the models corresponding to the cardiac cycle of 1.6 s. It is further observed that the velocity at point 1 which lies in left main stem is higher than that of the point near the bifurcation into LCX and LAD. This is due to the obstruction offered by the bifurcation region. It is seen that the velocity at point 1 does not vary much for different models. This happens because point 1 is near the inlet boundary of coronary artery. However, velocity at point 2 reduces significantly when stenosis is present in the branch and sub-branch of coronary artery.

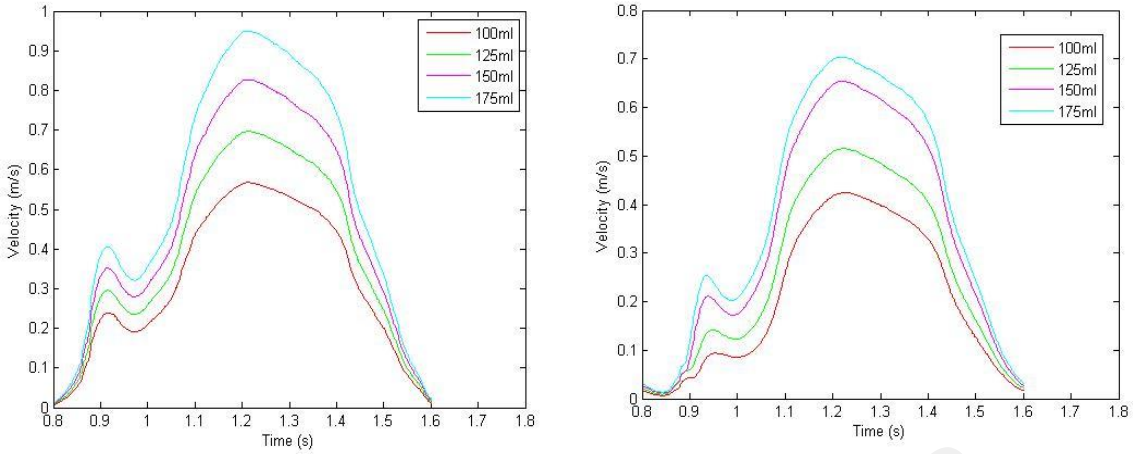

Figure 4.60: Velocity profile for model 1 at point 1 and point 2 for various flow rate

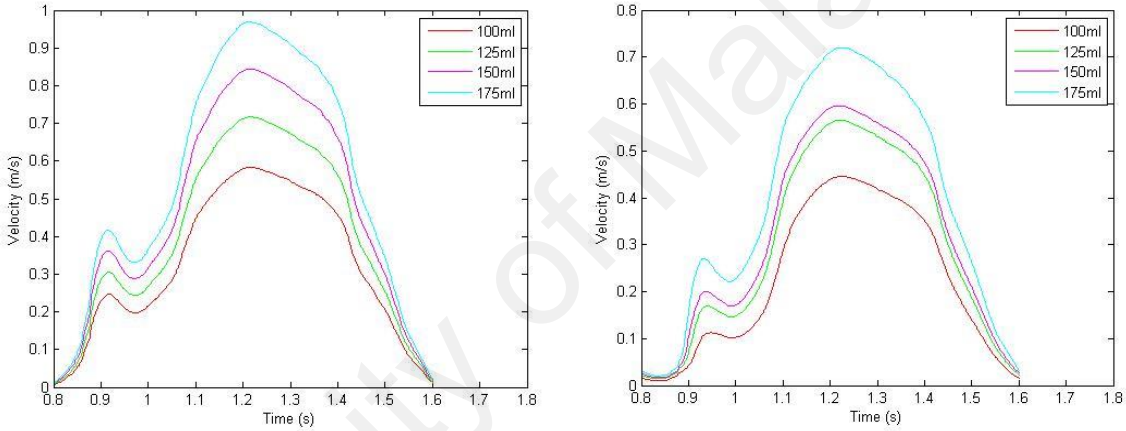

Figure 4.61: Velocity profile for model 2 at point 1 and point 2 for various flow rate

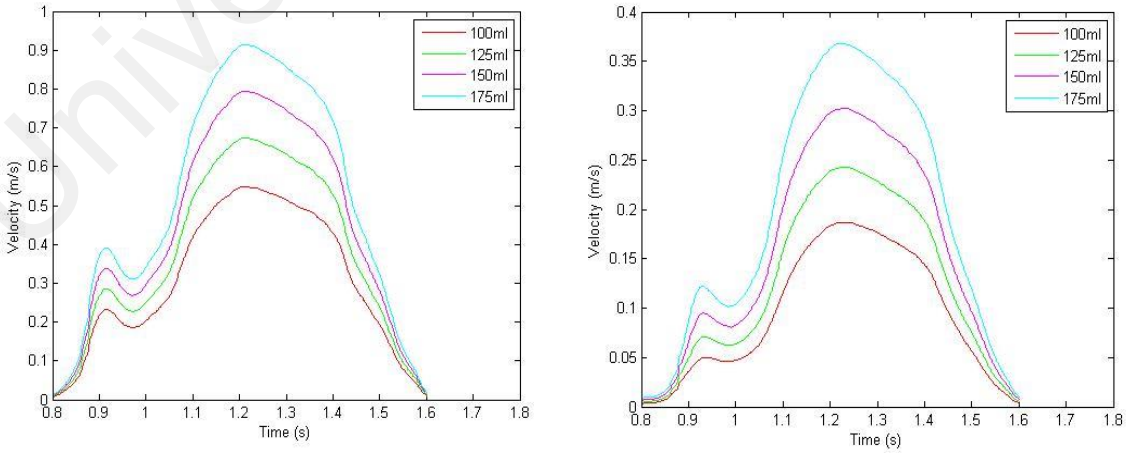

Figure 4.62: Velocity profile for model 3 at point 1 and point 2 for various flow rate

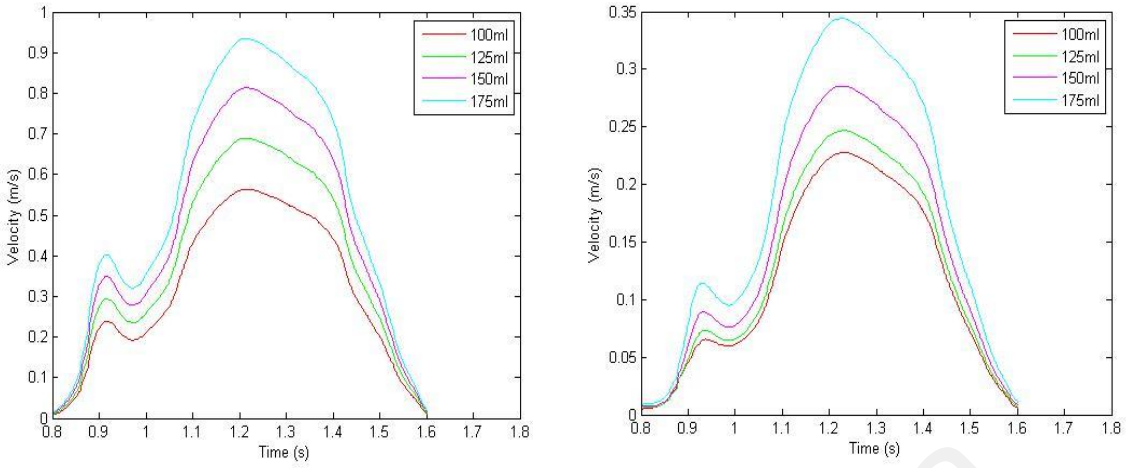

Figure 4.63: Velocity profile for model 4 at point 1 and point 2 for various flow rate

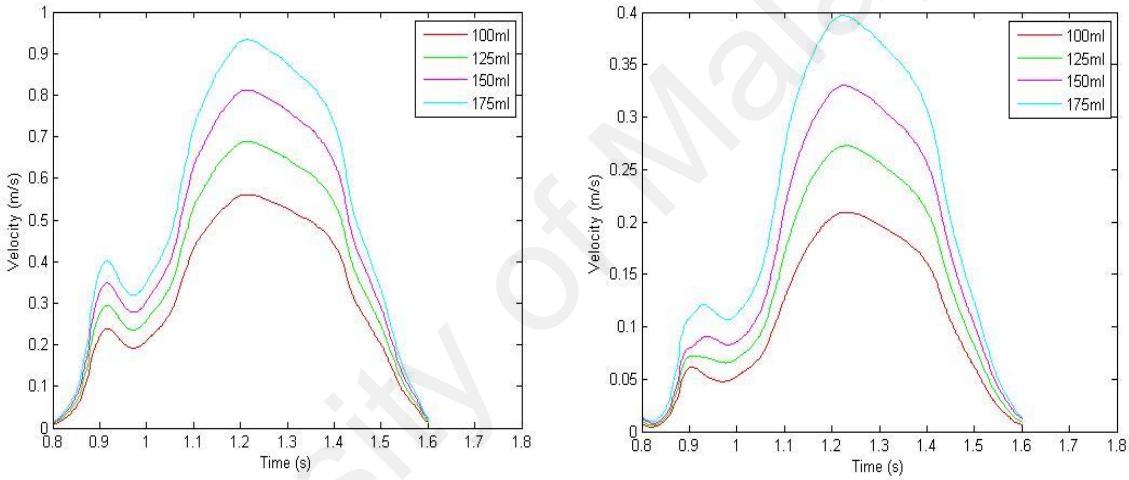

Figure 4.64: Velocity profile for model 5 at point 1 and point 2 for various flow rate

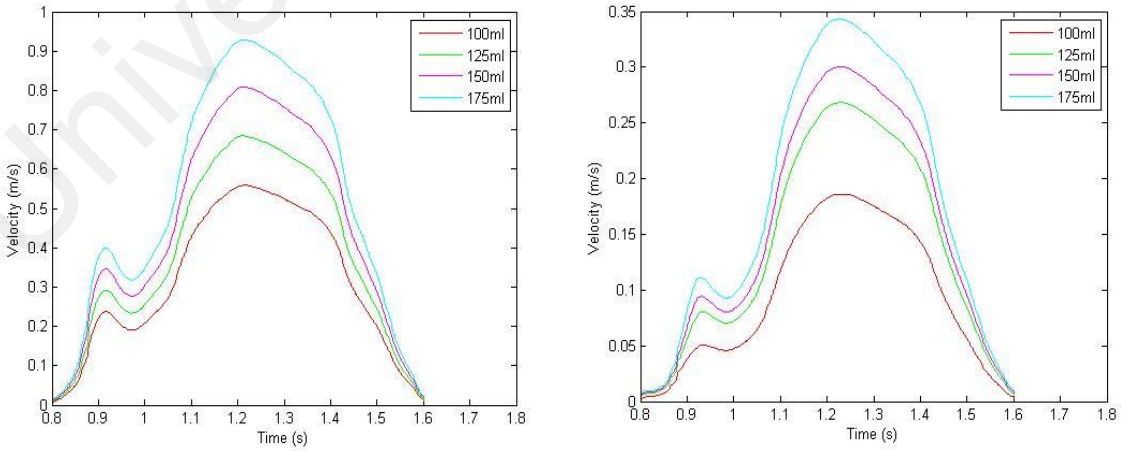

Figure 4.65: Velocity profile for model 6 at point 1 and point 2 for various flow rate

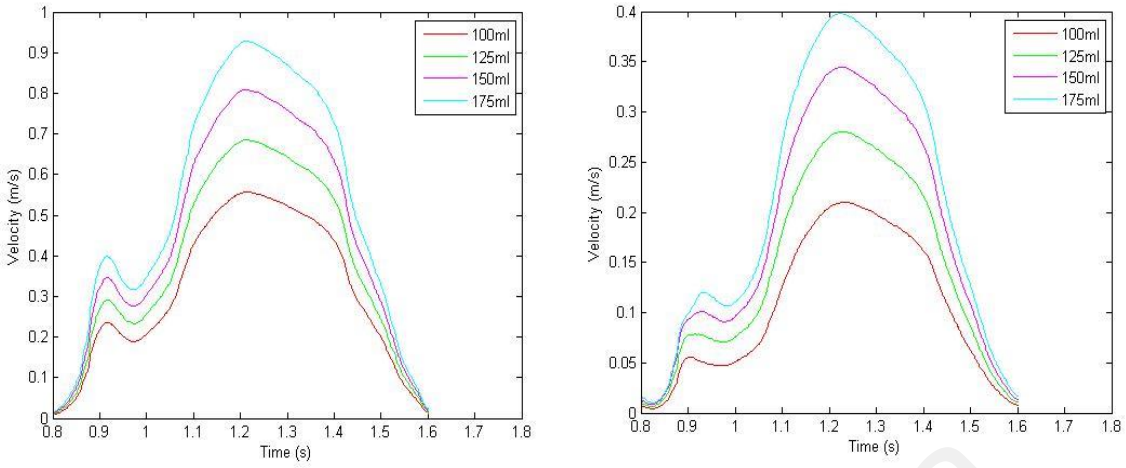

Figure 4.66: Velocity profile for model 7 at point 1 and point 2 for various flow rate

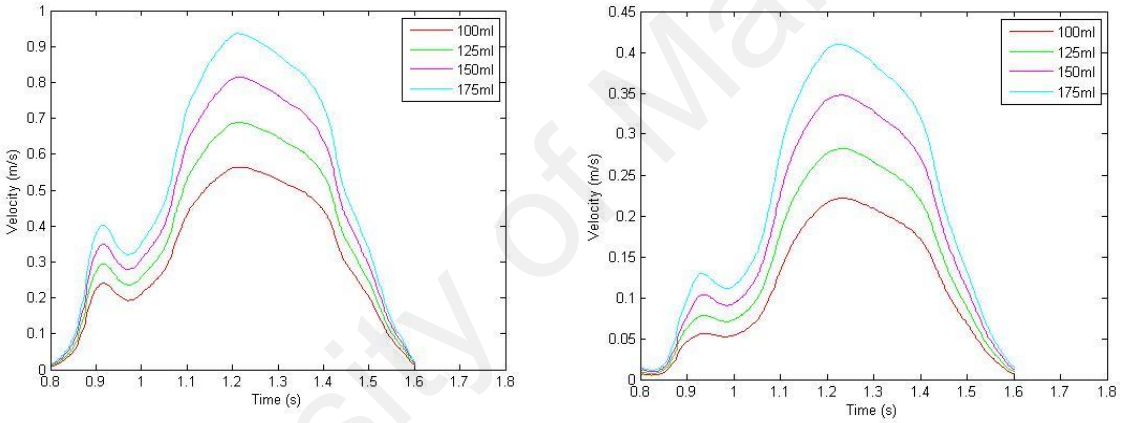

Figure 4.67: Velocity profile for model 8 at point 1 and point 2 for various flow rate

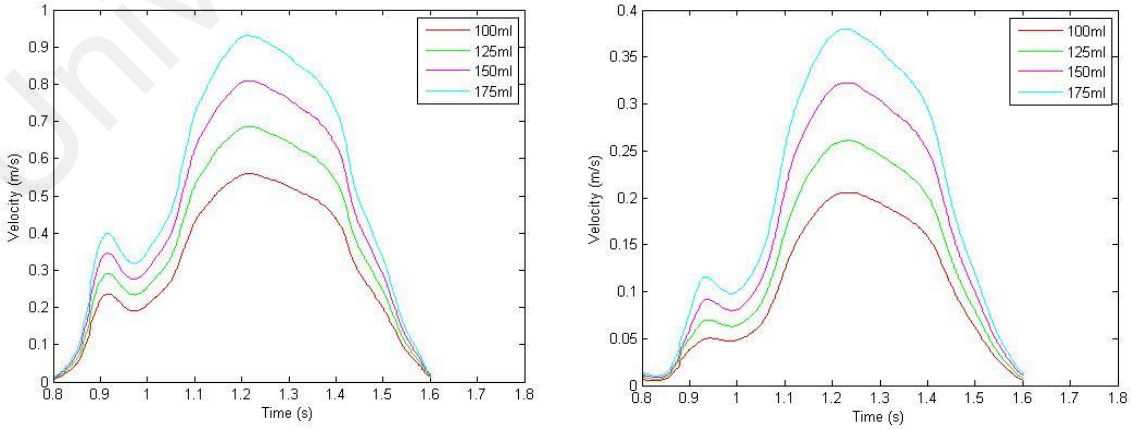

Figure 4.68: Velocity profile for model 9 at point 1 and point 2 for various flow rate

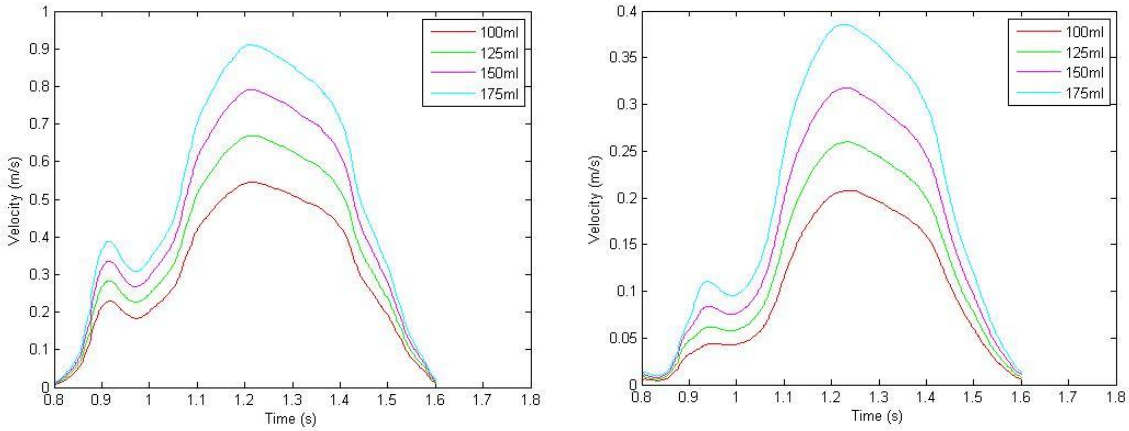

Figure 4.69: Velocity profile for model 10 at point 1 and point 2 for various flow rate

CHAPTER 5: CONCLUSION

5.1 Conclusions

For a given percentage area stenosis, the different shapes of stenosis affect the intraluminal flow and hence the changes in diagnostic parameter FFR were observed in all the three models (triangular, elliptical, and trapezium). The following conclusion are drawn from hemodynamic analysis of coronary artery model

- The increase in percentage area stenosis, increase the velocity profile inside the blockage region.
- The pressure drop is highest in case of trapezoidal stenosis and least for triangular shape for same area blockage due to stenosis thus the severity level of patients increases in case of trapezoidal geometry.
- The arterial wall is more prone to rupture due to trapezoidal stenosis than the elliptical or triangular shapes.
- The shape of stenosis has significant impact on the hemodynamic that should not be neglected in clinical decision making.

In case of the investigation of curvature angle, the following conclusion can be drawn from this study

- The blood behavior is substantially affected by the combined effect of stenosis and the curvature of artery.
- The presence of curvature provides low blood flow region at the lower wall of artery creating a potential stenotic region.
- The blood flow recovery is least for the smaller curvature angle

- The upper wall of artery after stenotic region is subjected to high shear stress due to curvature effect.

In case of study to investigate the effect of stenosis on the various hemodynamic parameters in 4 suspected patients in vivo models, the following conclusion could be drawn.

- The changes in the hemodynamic parameters would result in corresponding changes in the local blood flow conditions leading to the abnormalities in the coronary arterial conditions.
- The effect of the stenosis on the pressure variation could lead to the worsening of the atherosclerosis in the patients leading to the complications in the normal functioning off the heart.
- The high wall shear stress at the stenosis may increase the potential risk of stenosis rupture.
- The recirculation region at post stenosis could lead to the formation of stenosis.

For the case of different degree of multi stenosis present at various locations in the left coronary artery, the following conclusion can be drawn.

- The pressure drops is maximum across the higher degree of stenosis in multi stenosed models.
- The most affected model is that of having 70% and 90% area stenosis compared to other models studied.
- The least effect of stenosis on the pressure was found for the model having stenosis having 90% and 70% stenosis at position 3 and 5 respectively which are located at LAD and sub branch of LCX.

5.2 Recommendation for future research

In the current study, a computational fluid dynamic analysis on the idealistic and realistic patients specific left coronary artery models with the various parameters such as effect of different shapes of stenosis, angle of downstream curvatures, effects of various degree of stenosis and their locations in the patient specific left coronary artery models on the hemodynamic as well as on the diagnostic parameters have been studied and found important clinical information. The following proposals are put forward for future research work:

- The coronary artery models considered in the whole computational fluid dynamic studies as rigid artery wall rather than elastic, there for the simulation does not reflect the fully realistic physiological conditions. Hence in future the realistic patient's specific coronary artery models with elastic artery wall could be considered in future research.
- The study could be extended to right coronary artery

REFERENCES

Ahmed, Saad A. (1998). An experimental investigation of pulsatile flow through a smooth constriction. *Experimental Thermal and Fluid Science, 17*(4), 309-318. doi: http://dx.doi.org/10.1016/S0894-1777(98)00009-0

Ai, L., & Vafai, K. (2006). A coupling model for macromolecule transport in a stenosed arterial wall. *International Journal of Heat and Mass Transfer, 49*(9–10), 1568-1591. doi: 10.1016/j.ijheatmasstransfer.2005.10.041

Alberto Figueroa C. (2006). *A coupled-momentum method to model blood flow and vessel deformation in Human Arteries: Applications in disease research and Simulation-Based Medical Planning.* (Ph.D), Stanford University.

Alishahi, M, Alishahi, MM, & Emdad, H. (2011). Numerical simulation of blood flow in a flexible stenosed abdominal real aorta. *Scientia Iranica, 18*(6), 1297-1305.

Alishahi, M., Alishahi, M. M., & Emdad, H. (2011). Numerical simulation of blood flow in a flexible stenosed abdominal real aorta. *Scientia Iranica, 18*(6), 1297-1305. doi: 10.1016/j.scient.2011.11.021

Andersson, Helge I., Halden, Ragnhild, & Glomsaker, Terje. (2000). Effects of surface irregularities on flow resistance in differently shaped arterial stenoses. *Journal of Biomechanics, 33*(10), 1257-1262. doi: http://dx.doi.org/10.1016/S0021-9290(00)00088-9

Ashtekar, Koustubh D, Back, Lloyd H, Khoury, Saeb F, & Banerjee, Rupak K. (2007). In vitro quantification of guidewire flow-obstruction effect in model coronary stenoses for interventional diagnostic procedure. *Journal of Medical Devices, 1*(3), 185-196.

Banerjee, Rupak K., Peelukhana, Srikara V., & Goswami, Ishan. (2014). Influence of newly designed monorail pressure sensor catheter on coronary diagnostic parameters: An in vitro study. *Journal of Biomechanics, 47*(3), 617-624. doi: http://dx.doi.org/10.1016/j.jbiomech.2013.12.005

Banerjee, RupakK, Ashtekar, KoustubhD, Helmy, TarekA, Effat, MohamedA, Back, LloydH, & Khoury, SaebF. (2008). Hemodynamic diagnostics of epicardial coronary stenoses: in-vitro experimental and computational study. *BioMedical Engineering OnLine, 7*(1), 1-22. doi: 10.1186/1475-925x-7-24

Bernsdorf, Jörg, & Wang, Dinan. (2009). Non-Newtonian blood flow simulation in cerebral aneurysms. *Computers & Mathematics with Applications, 58*(5), 1024-1029.

Bluestein, D, & Einav, S. (1993). Spectral estimation and analysis of LDA data in pulsatile flow through heart valves. *Experiments in Fluids, 15*(4-5), 341-353.

Bluestein, Danny, Einav, Shmuel, & Hwang, Ned HC. (1994). A squeeze flow phenomenon at the closing of a bileaflet mechanical heart valve prosthesis. *Journal of biomechanics, 27*(11), 1369-1378.

Botar, C. C., Vasile, T., Sfrangeu, S., Clichici, S., Agachi, P. S., Badea, R., . . . Moldovan, R. (2009). CFD Simulation of the Portal Vein Blood Flow. In S. Vlad, R. V. Ciupa & A. I. Nicu (Eds.), *International Conference on Advancements of Medicine and Health Care through Technology* (Vol. 26, pp. 359-362).

Brosh, David, Higano, Stuart T., Lennon, Ryan J., Holmes Jr, David R., & Lerman, Amir. (2005). Effect of lesion length on fractional flow reserve in intermediate coronary lesions. *American Heart Journal, 150*(2), 338-343. doi: http://dx.doi.org/10.1016/j.ahj.2004.09.007

Brosig, Richard, Kowarschik, Markus, Maday, Peter, Katouzian, Amin, Demirci, Stefanie, & Navab, Nassir. (2014). Blood Flow Quantification using 1D CFD Parameter Identification. In S. Ourselin & M. A. Styner (Eds.), *Medical Imaging 2014: Image Processing* (Vol. 9034).

Byun, H. S., & Rhee, K. (2004). CFD modeling of blood flow following coil embolization of aneurysms. *Medical Engineering & Physics, 26*(9), 755-761. doi: 10.1016/j.medengphy.2004.06.008

Calfon, Marcella A, Vinegoni, Claudio, Ntziachristos, Vasilis, & Jaffer, Farouc A. (2010). Intravascular near-infrared fluorescence molecular imaging of atherosclerosis: toward coronary arterial visualization of biologically high-risk plaques. *Journal of biomedical optics, 15*(1), 011107-011107-011106.

Chaichana, Thanapong, Sun, Zhonghua, & Jewkes, James. (2011). Computation of hemodynamics in the left coronary artery with variable angulations. *Journal of Biomechanics, 44*(10), 1869-1878. doi: http://dx.doi.org/10.1016/j.jbiomech.2011.04.033

Chaichana, Thanapong, Sun, Zhonghua, & Jewkes, James. (2012). Computational fluid dynamics analysis of the effect of plaques in the left coronary artery. *Computational and mathematical methods in medicine, 2012*.

Chaichana, Thanapong, Sun, Zhonghua, & Jewkes, James. (2013a). Haemodynamic analysis of the effect of different types of plaques in the left coronary artery. *Computerized Medical Imaging and Graphics, 37*(3), 197-206. doi: http://dx.doi.org/10.1016/j.compmedimag.2013.02.001

Chaichana, Thanapong, Sun, Zhonghua, & Jewkes, James. (2013b). Hemodynamic impacts of left coronary stenosis: A patient-specific analysis. *Acta of Bioengineering and Biomechanics, 15*(3).

Chaichana, Thanapong, Sun, Zhonghua, & Jewkes, James. (2013c). Hemodynamic impacts of various types of stenosis in the left coronary artery bifurcation: A patient-specific analysis. *Physica Medica, 29*(5), 447-452. doi: http://dx.doi.org/10.1016/j.ejmp.2013.02.001

Chaichana, Thanapong, Sun, Zhonghua, & Jewkes, James. (2014). Impact of plaques in the left coronary artery on wall shear stress and pressure gradient in coronary side branches. *Computer methods in biomechanics and biomedical engineering, 17*(2), 108-118.

Chakravarty, Santabrata, & Mandal, Prashanta Kumar. (2000). Two-dimensional blood flow through tapered arteries under stenotic conditions. *International Journal of Non-Linear Mechanics, 35*(5), 779-793.

Chakravarty, Santabrata, & Mandal, Prashanta Kumar. (2005). Effect of surface irregularities on unsteady pulsatile flow in a compliant artery. *International Journal of Non-Linear Mechanics, 40*(10), 1268-1281.

Chakravarty, Santabrata, & Mandal, Prashanta Kumar. (2009). Effect of heat and mass transfer on non-Newtonian flow–Links to atherosclerosis. *International Journal of Heat and Mass Transfer, 52*(25), 5719-5730.

Chen, Jie, & Lu, Xi-Yun. (2004). Numerical investigation of the non-Newtonian blood flow in a bifurcation model with a non-planar branch. *Journal of biomechanics, 37*(12), 1899-1911.

Chen, Jie, & Lu, Xi-Yun. (2006). Numerical investigation of the non-Newtonian pulsatile blood flow in a bifurcation model with a non-planar branch. *Journal of Biomechanics, 39*(5), 818-832.

Cho, Young I, Back, Lloyd H, Crawford, Donald W, & Cuffel, Robert F. (1983). Experimental study of pulsatile and steady flow through a smooth tube and an atherosclerotic coronary artery casting of man. *Journal of Biomechanics, 16*(11), 933-946.

Dash, R. K., Jayaraman, G., & Mehta, K. N. (1999). Flow in a catheterized curved artery with stenosis. *Journal of Biomechanics, 32*(1), 49-61. doi: http://dx.doi.org/10.1016/S0021-9290(98)00142-0

Dash, RK, Jayaraman, G, & Mehta, KN. (1999). Flow in a catheterized curved artery with stenosis. *Journal of Biomechanics, 32*(1), 49-61.

De Bruyne, Bernard, Pijls, Nico H.J., Kalesan, Bindu, Barbato, Emanuele, Tonino, Pim A.L., Piroth, Zsolt, . . . Fearon, William F. (2012). Fractional Flow Reserve–Guided PCI versus Medical Therapy in Stable Coronary Disease. *New England Journal of Medicine, 367*(11), 991-1001. doi: doi:10.1056/NEJMoa1205361

Delfino, A, Stergiopulos, N, Moore, JE, & Meister, J-J. (1997). Residual strain effects on the stress field in a thick wall finite element model of the human carotid bifurcation. *Journal of biomechanics, 30*(8), 777-786.

Dobrin, PhB, Littooy, FN, & Endean, ED. (1989). Mechanical factors predisposing to intimal hyperplasia and medial thickening in autogenous vein grafts. *Surgery, 105*(3), 393-400.

Feng, Rui, Xenos, Michalis, Girdhar, Gaurav, Kang, Wei, Davenport, James W, Deng, Yuefan, & Bluestein, Danny. (2012). Viscous flow simulation in a stenosis model using discrete particle dynamics: a comparison between DPD and CFD. *Biomechanics and modeling in mechanobiology, 11*(1-2), 119-129.

Fung, Y.C. (1984). *Biodynamics* (1 ed.). New York: Springer Verlag.

Fuster, Valentin. (1994). Lewis A. Conner Memorial Lecture. Mechanisms leading to myocardial infarction: insights from studies of vascular biology. *Circulation, 90*(4), 2126-2146.

Goswami, Ishan, Peelukhana, Srikara V, Al-Rjoub, Marwan F, Back, Lloyd H, & Banerjee, Rupak K. (2013). Influence of Variable Native Arterial Diameter and Vasculature Status on Coronary Diagnostic Parameters. *Journal of biomechanical engineering, 135*(9), 091005.

Govindaraju, Kalimuthu, Kamangar, Sarfaraz, Badruddin, Irfan Anjum, Viswanathan, Girish N., Badarudin, A., & Salman Ahmed, N. J. (2014). Effect of porous media of the stenosed artery wall to the coronary physiological diagnostic parameter: A computational fluid dynamic analysis. *Atherosclerosis, 233*(2), 630-635. doi: http://dx.doi.org/10.1016/j.atherosclerosis.2014.01.043

Ha, Hojin, & Lee, Sang-Joon. (2014). Effect of swirling inlet condition on the flow field in a stenosed arterial vessel model. *Medical engineering & physics, 36*(1), 119-128.

Han, H-C. (2012). Twisted blood vessels: symptoms, etiology and biomechanical mechanisms. *Journal of vascular research, 49*(3), 185-197.

Huang, Rong Fung, Yang, Ten-Fang, & Lan, Y-K. (2010). Pulsatile flows and wall-shear stresses in models simulating normal and stenosed aortic arches. *Experiments in fluids, 48*(3), 497-508.

Ikbal, Asif. (2012). Viscoelastic blood flow through arterial stenosis—Effect of variable viscosity. *International Journal of Non-Linear Mechanics, 47*(8), 888-894.

Ikbal, M. A. (2012). Viscoelastic blood flow through arterial stenosis-Effect of variable viscosity. *International Journal of Non-Linear Mechanics, 47*(8), 888-894. doi: 10.1016/j.ijnonlinmec.2012.05.006

Ishikawa, Takuji, Guimaraes, Luis F. R., Oshima, Shuzo, & Yamane, Ryuichiro. (1998). Effect of non-Newtonian property of blood on flow through a stenosed tube. *Fluid Dynamics Research, 22*(5), 251-264. doi: http://dx.doi.org/10.1016/S0169-5983(97)00041-5

Ismail, Zuhaila, Abdullah, Ilyani, Mustapha, Norzieha, & Amin, Norsarahaida. (2008). A power-law model of blood flow through a tapered overlapping stenosed artery. *Applied Mathematics and Computation, 195*(2), 669-680.

Jhunjhunwala, P., Padole, P. M., & Thombre, S. B. (2015). CFD Analysis of Pulsatile Flow and Non-Newtonian Behavior of Blood in Arteries. *Molecular & Cellular Biomechanics, 12*(1), 37-47.

Johnston, Barbara M, Johnston, Peter R, Corney, Stuart, & Kilpatrick, David. (2006). Non-Newtonian blood flow in human right coronary arteries: transient simulations. *Journal of biomechanics, 39*(6), 1116-1128.

Jou, Liang-Der, Lee, Deok Hee, & Mawad, Michel E. (2010). Cross-flow at the anterior communicating artery and its implication in cerebral aneurysm formation. *Journal of biomechanics, 43*(11), 2189-2195.

Jozwik, Krzysztof, & Obidowski, Damian. (2010). Numerical simulations of the blood flow through vertebral arteries. *Journal of Biomechanics, 43*(2), 177-185. doi: http://dx.doi.org/10.1016/j.jbiomech.2009.09.026

Jung, Jonghwun, & Hassanein, Ahmed. (2008). Three-phase CFD analytical modeling of blood flow. *Medical Engineering & Physics, 30*(1), 91-103. doi: 10.1016/j.medengphy.2006.12.004

Kagadis, George C, Skouras, Eugene D, Bourantas, George C, Paraskeva, Christakis A, Katsanos, Konstantinos, Karnabatidis, Dimitris, & Nikiforidis, George C. (2008). Computational representation and hemodynamic characterization of< i> in vivo</i> acquired severe stenotic renal artery geometries using turbulence modeling. *Medical engineering & physics, 30*(5), 647-660.

Kagadis, George C., Skouras, Eugene D., Bourantas, George C., Paraskeva, Christakis A., Katsanos, Konstantinos, Karnabatidis, Dimitris, & Nikiforidis, George C. (2008). Computational representation and hemodynamic characterization of in vivo acquired severe stenotic renal artery geometries using turbulence modeling. *Medical Engineering & Physics, 30*(5), 647-660. doi: http://dx.doi.org/10.1016/j.medengphy.2007.07.005

Kanaris, AG, Anastasiou, AD, & Paras, SV. (2012). Modeling the effect of blood viscosity on hemodynamic factors in a small bifurcated artery. *Chemical Engineering Science, 71*, 202-211.

Kaye, E. K., Valencia, A., Baba, N., Spiro, A., 3rd, Dietrich, T., & Garcia, R. I. (2010). Tooth loss and periodontal disease predict poor cognitive function in older men. *J Am Geriatr Soc, 58*(4), 713-718. doi: 10.1111/j.1532-5415.2010.02788.xJGS2788 [pii]

Kenjereš, Saša. (2008). Numerical analysis of blood flow in realistic arteries subjected to strong non-uniform magnetic fields. *International Journal of Heat and Fluid Flow, 29*(3), 752-764.

Keshavarz-Motamed, Z, & Kadem, L. (2011). 3D pulsatile flow in a curved tube with coexisting model of aortic stenosis and coarctation of the aorta. *Medical engineering & physics, 33*(3), 315-324.

Koerselman, J., van der Graaf, Y., de Jaegere, P. P., & Grobbee, D. E. (2003). Coronary collaterals: an important and underexposed aspect of coronary artery disease. *Circulation, 107*(19), 2507-2511. doi: 10.1161/01.cir.0000065118.99409.5f

Konala, Bhaskar Chandra, Das, Ashish, & Banerjee, Rupak K. (2011). Influence of arterial wall-stenosis compliance on the coronary diagnostic parameters. *Journal of Biomechanics, 44*(5), 842-847. doi: 10.1016/j.jbiomech.2010.12.011

Koo, Bon-Kwon, Kang, Hyun-Jai, Youn, Tae-Jin, Chae, In-Ho, Choi, Dong-Joo, Kim, Hyo-Soo, . . . Tahk, Seung-Jae. (2005). Physiologic Assessment of Jailed Side Branch Lesions Using Fractional Flow Reserve. *Journal of the American College of Cardiology*, *46*(4), 633-637. doi: 10.1016/j.jacc.2005.04.054

Krams, R, Wentzel, JJ, Cespedes, I, Vinke, R, Carlier, S, Van Der Steen, AFW, . . . Slager, CJ. (1999). Effect of catheter placement on 3-D velocity profiles in curved tubes resembling the human coronary system. *Ultrasound in medicine & biology*, *25*(5), 803-810.

Kristensen, Thomas Skaarup, Engstrøm, Thomas, Kelbæk, Henning, von der Recke, Peter, Nielsen, Michael Bachmann, & Kofoed, Klaus Fuglsang. (2010). Correlation between coronary computed tomographic angiography and fractional flow reserve. *International Journal of Cardiology*, *144*(2), 200-205. doi: 10.1016/j.ijcard.2009.04.024

Kumar Mandal, P, Chakravarty, Santabrata, & Mandal, Arabinda. (2007). Numerical study of the unsteady flow of non-Newtonian fluid through differently shaped arterial stenoses. *International Journal of Computer Mathematics*, *84*(7), 1059-1077.

Lee, Seung E, Lee, Sang-Wook, Fischer, Paul F, Bassiouny, Hisham S, & Loth, Francis. (2008). Direct numerical simulation of transitional flow in a stenosed carotid bifurcation. *Journal of biomechanics*, *41*(11), 2551-2561.

Lefèvre, Thierry, Louvard, Yves, Morice, Marie-Claude, Dumas, Pierre, Loubeyre, Christophe, Benslimane, Abdeljabbar, . . . Piéchaud, Jean-François. (2000). Stenting of bifurcation lesions: classification, treatments, and results. *Catheterization and cardiovascular interventions*, *49*(3), 274-283.

Leguy, CAD, Bosboom, EMH, Hoeks, APG, & van de Vosse, FN. (2009). Assessment of blood volume flow in slightly curved arteries from a single velocity profile. *Journal of biomechanics*, *42*(11), 1664-1672.

Leuprecht, A., Perktold, K., Kozerke, S., & Boesiger, P. (2002). Combined CFD and MRI study of blood flow in a human ascending aorta model. *Biorheology*, *39*(3-4), 425-429.

Li, M. X., Beech-Brandt, J. J., John, L. R., Hoskins, P. R., & Easson, W. J. (2007). Numerical analysis of pulsatile blood flow and vessel wall mechanics in different degrees of stenoses. *Journal of Biomechanics*, *40*(16), 3715-3724. doi: http://dx.doi.org/10.1016/j.jbiomech.2007.06.023

Liu, Biyue. (2007). The influences of stenosis on the downstream flow pattern in curved arteries. *Medical Engineering & Physics, 29*(8), 868-876. doi: 10.1016/j.medengphy.2006.09.009

Long, Q, Xu, XY, Ramnarine, KV, & Hoskins, P. (2001). Numerical investigation of physiologically realistic pulsatile flow through arterial stenosis. *Journal of Biomechanics, 34*(10), 1229-1242.

Lorenzini, Giulio, & Casalena, Erminio. (2008). CFD analysis of pulsatile blood flow in an atherosclerotic human artery with eccentric plaques. *Journal of Biomechanics, 41*(9), 1862-1870.

Mandal, Prashanta Kumar. (2005). An unsteady analysis of non-Newtonian blood flow through tapered arteries with a stenosis. *International Journal of Non-Linear Mechanics, 40*(1), 151-164. doi: 10.1016/j.ijnonlinmec.2004.07.007

Manimaran, R. (2011). CFD simulation of non-Newtonian fluid flow in arterial stenoses with surface irregularities. *World Academy of Science, Engineering andTechnology, 73*, 957-962.

Meijboom, W. Bob, Van Mieghem, Carlos A. G., van Pelt, Niels, Weustink, Annick, Pugliese, Francesca, Mollet, Nico R., . . . de Feyter, Pim J. (2008). Comprehensive Assessment of Coronary Artery Stenoses: Computed Tomography Coronary Angiography Versus Conventional Coronary Angiography and Correlation With Fractional Flow Reserve in Patients With Stable Angina. *Journal of the American College of Cardiology, 52*(8), 636-643. doi: http://dx.doi.org/10.1016/j.jacc.2008.05.024

Melih Guleren, K. (2013). Numerical flow analysis of coronary arteries through concentric and eccentric stenosed geometries. *Journal of biomechanics, 46*(6), 1043-1052.

Menter, F., Kuntz, M., & Langtry, R. (2003). *Ten years of Industrial experience with the {SST} model.* Paper presented at the Turbulence, Heat and Mass Transfer 4.

Menter, Florian R. (2009). Review of the shear-stress transport turbulence model experience from an industrial perspective. *International Journal of Computational Fluid Dynamics, 23*(4), 305-316. doi: 10.1080/10618560902773387

Misra, JC, & Shit, GC. (2006). Blood flow through arteries in a pathological state: A theoretical study. *International journal of engineering science, 44*(10), 662-671.

Mustapha, Norzieha, Amin, Norsarahaida, Chakravarty, Santabrata, & Mandal, Prashanta Kumar. (2009). Unsteady magnetohydrodynamic blood flow through irregular multi-stenosed arteries. *Computers in Biology and Medicine, 39*(10), 896-906.

Mustapha, Norzieha, Mandal, Prashanta K., Johnston, Peter R., & Amin, Norsarahaida. (2010). A numerical simulation of unsteady blood flow through multi-irregular arterial stenoses. *Applied Mathematical Modelling, 34*(6), 1559-1573. doi: http://dx.doi.org/10.1016/j.apm.2009.09.008

Myer, Kutz. (2003). PHYSICAL AND FLOW PROPERTIES OF BLOOD *Standard Handbook of Biomedical Engineering & Design*: McGraw Hill Professional, Access Engineering.

Nadeem, S, Akbar, Noreen Sher, Hendi, Awatif A, & Hayat, Tasawar. (2011). Power law fluid model for blood flow through a tapered artery with a stenosis. *Applied Mathematics and Computation, 217*(17), 7108-7116.

Naruse, T, & Tanishita, K. (1996). Large curvature effect on pulsatile entrance flow in a curved tube: model experiment simulating blood flow in an aortic arch. *Journal of biomechanical engineering, 118*(2), 180-186.

Nichols, W.W., and O'Rourke M.F. (1998). *McDonald's blood flow in arteries: Theoretical, experimental and clinical principles*: Oxford University Press, New York.

Nissen, S. E., & Gurley, J. C. (1991). Application of intravascular ultrasound for detection and quantitation of coronary atherosclerosis. *Int J Card Imaging, 6*(3-4), 165-177.

Nissen, S. E., & Yock, P. (2001). Intravascular ultrasound: novel pathophysiological insights and current clinical applications. *Circulation, 103*(4), 604-616.

Park, Seung-Jung, Kang, Soo-Jin, Ahn, Jung-Min, Shim, Eun Bo, Kim, Young-Tae, Yun, Sung-Cheol, . . . Park, Seong-Wook. (2012). Visual-Functional Mismatch Between Coronary Angiography and Fractional Flow Reserve. *JACC: Cardiovascular Interventions, 5*(10), 1029-1036. doi: 10.1016/j.jcin.2012.07.007

Paul, Manosh C., & Larman, Arkaitz. (2009). Investigation of spiral blood flow in a model of arterial stenosis. *Medical Engineering & Physics, 31*(9), 1195-1203. doi: http://dx.doi.org/10.1016/j.medengphy.2009.07.008

Peelukhana, Srikara Viswanath, Back, Lloyd H., & Banerjee, Rupak K. (2009). Influence of coronary collateral flow on coronary diagnostic parameters: An in vitro study. *Journal of Biomechanics, 42*(16), 2753-2759. doi: 10.1016/j.jbiomech.2009.08.013

Pielhop, K, Klaas, M, & Schröder, W. (2012). Analysis of the unsteady flow in an elastic stenotic vessel. *European Journal of Mechanics-B/Fluids, 35*, 102-110.

Pijls, N. H., Van Gelder, B., Van der Voort, P., Peels, K., Bracke, F. A., Bonnier, H. J., & el Gamal, M. I. (1995). Fractional flow reserve. A useful index to evaluate the influence of an epicardial coronary stenosis on myocardial blood flow. *Circulation, 92*(11), 3183-3193.

Pijls, Nico H. J., Fearon, William F., Tonino, Pim A. L., Siebert, Uwe, Ikeno, Fumiaki, Bornschein, Bernhard, . . . De Bruyne, Bernard. (2010). Fractional Flow Reserve Versus Angiography for Guiding Percutaneous Coronary Intervention in Patients With Multivessel Coronary Artery Disease: 2-Year Follow-Up of the FAME (Fractional Flow Reserve Versus Angiography for Multivessel Evaluation) Study. *Journal of the American College of Cardiology, 56*(3), 177-184. doi: http://dx.doi.org/10.1016/j.jacc.2010.04.012

Pijls, Nico H. J., & Sels, Jan-Willem E. M. (2012). Functional Measurement of Coronary Stenosis. *Journal of the American College of Cardiology, 59*(12), 1045-1057. doi: http://dx.doi.org/10.1016/j.jacc.2011.09.077

Qiao, AK, Guo, XL, Wu, SG, Zeng, YJ, & Xu, XH. (2004). Numerical study of nonlinear pulsatile flow in S-shaped curved arteries. *Medical engineering & physics, 26*(7), 545-552.

Rajabi-Jaghargh, Ehsan, Kolli, Kranthi K, Back, Lloyd H, & Banerjee, Rupak K. (2011). Effect of guidewire on contribution of loss due to momentum change and viscous loss to the translesional pressure drop across coronary artery stenosis: An analytical approach. *Biomedical engineering online, 10*(1), 51.

Ramanathan, Tamilselvi, & Skinner, Henry. (2005). Coronary blood flow. *Continuing Education in Anaesthesia, Critical Care & Pain, 5*(2), 61-64. doi: 10.1093/bjaceaccp/mki012

Razavi, A, Shirani, E, & Sadeghi, MR. (2011). Numerical simulation of blood pulsatile flow in a stenosed carotid artery using different rheological models. *Journal of biomechanics, 44*(11), 2021-2030.

Seiler, C., Stoller, M., Pitt, B., & Meier, P. (2013). The human coronary collateral circulation: development and clinical importance. *Eur Heart J, 34*(34), 2674-2682. doi: 10.1093/eurheartj/eht195

Seiler, Christian. (2003). The human coronary collateral circulation. *Heart, 89*(11), 1352-1357.

Shipkowitz, Tanya, Rodgers, VGJ, Frazin, Lee J, & Chandran, KB. (2000). Numerical study on the effect of secondary flow in the human aorta on local shear stresses in abdominal aortic branches. *Journal of Biomechanics, 33*(6), 717-728.

Siebes, Maria, Chamuleau, Steven A. J., Meuwissen, Martijn, Piek, Jan J., & Spaan, Jos A. E. (2002). Influence of hemodynamic conditions on fractional flow reserve: parametric analysis of underlying model. *American Journal of Physiology - Heart and Circulatory Physiology, 283*(4), H1462-H1470. doi: 10.1152/ajpheart.00165.2002

Sinha Roy, Abhijit, Back, Lloyd H., & Banerjee, Rupak K. (2006). Guidewire flow obstruction effect on pressure drop-flow relationship in moderate coronary artery stenosis. *Journal of Biomechanics, 39*(5), 853-864. doi: 10.1016/j.jbiomech.2005.01.020

Soulis, Johannes V., Farmakis, Thomas M., Giannoglou, George D., & Louridas, George E. (2006). Wall shear stress in normal left coronary artery tree. *Journal of Biomechanics, 39*(4), 742-749. doi: 10.1016/j.jbiomech.2004.12.026

Stroud, JS, Berger, SA, & Saloner, D. (2000). Influence of stenosis morphology on flow through severely stenotic vessels: implications for plaque rupture. *Journal of biomechanics, 33*(4), 443-455.

Su, Boyang, Huo, Yunlong, Kassab, Ghassan S, Kabinejadian, Foad, Kim, Sangho, Leo, Hwa Liang, & Zhong, Liang. (2014). Numerical investigation of blood flow in three-dimensional porcine left anterior descending artery with various stenoses. *Computers in biology and medicine, 47*, 130-138.

Sun, Zhonghua, & Cao, Yan. (2011). Multislice CT angiography assessment of left coronary artery: Correlation between bifurcation angle and dimensions and development of coronary artery disease. *European Journal of Radiology, 79*(2), e90-e95. doi: http://dx.doi.org/10.1016/j.ejrad.2011.04.015

Sung, Kun Hyuk, Ro, Kyoung Chul, & Ryou, Hong Sun. (2009). Numerical investigation on the blood flow characteristics considering the axial rotation in stenosed artery. *Korea-Australia Rheology Journal, 21*(2), 119-126.

Takeshita, A., Koiwaya, Y., Nakamura, M., Yamamoto, K., & Torii, S. (1982). Immediate appearance of coronary collaterals during ergonovine-induced arterial spasm. *Chest, 82*(3), 319-322.

Tang, Dalin, Yang, Chun, Kobayashi, Shunichi, Zheng, Jie, Woodard, Pamela K., Teng, Zhongzhao, . . . Ku, David N. (2009). 3D MRI-Based Anisotropic FSI Models With Cyclic Bending for Human Coronary Atherosclerotic Plaque Mechanical Analysis. *Journal of Biomechanical Engineering, 131*(6), 061010. doi: 10.1115/1.3127253

Tashtoush, Bourhan, & Magableh, Ahmad. (2008). Magnetic field effect on heat transfer and fluid flow characteristics of blood flow in multi-stenosis arteries. *Heat and Mass Transfer, 44*(3), 297-304.

Tobis, Jonathan, Azarbal, Babak, & Slavin, Leo. (2007). Assessment of Intermediate Severity Coronary Lesions in the Catheterization Laboratory. *Journal of the American College of Cardiology, 49*(8), 839-848. doi: 10.1016/j.jacc.2006.10.055

Toloui, M., Firoozabadi, B., & Saidi, M. S. (2012). A numerical study of the effects of blood rheology and vessel deformability on the hemodynamics of carotid bifurcation. *Scientia Iranica, 19*(1), 119-126. doi: http://dx.doi.org/10.1016/j.scient.2011.12.008

Tonino, Pim A.L., De Bruyne, Bernard, Pijls, Nico H.J., Siebert, Uwe, Ikeno, Fumiaki, van `t Veer, Marcel, . . . Fearon, William F. (2009). Fractional Flow Reserve versus Angiography for Guiding Percutaneous Coronary Intervention. *New England Journal of Medicine, 360*(3), 213-224. doi: doi:10.1056/NEJMoa0807611

Torii, Ryo, Wood, Nigel B, Hughes, Alun D, Thom, Simon A, Aguado-Sierra, Jazmin, Davies, Justin E, . . . Xu, X Yun. (2007). A computational study on the influence of catheter-delivered intravascular probes on blood flow in a coronary artery model. *Journal of biomechanics, 40*(11), 2501-2509.

Tu, Cheng, & Deville, Michel. (1996). Pulsatile flow of non-Newtonian fluids through arterial stenoses. *Journal of biomechanics, 29*(7), 899-908.

van Werkhoven, Jacob M., Schuijf, Joanne D., Jukema, J. Wouter, Pundziute, Gabija, de Roos, Albert, Schalij, Martin J., . . . Bax, Jeroen J. (2009). Comparison of Non-Invasive Multi-Slice Computed Tomography Coronary Angiography Versus Invasive Coronary Angiography and Fractional Flow Reserve for the Evaluation of Men With Known Coronary Artery Disease. *The American Journal of Cardiology, 104*(5), 653-656. doi: 10.1016/j.amjcard.2009.04.045

Versteeg, Henk Kaarle, & Malalasekera, Weeratunge. (2007). *An introduction to computational fluid dynamics: the finite volume method*: Pearson Education.

Wang, Xiaohong, & Li, Xiaoyang. (2011). Biomechanical behaviors of curved artery with flexible wall: A numerical study using fluid–structure interaction method. *Computers in biology and medicine, 41*(11), 1014-1021.

White, SS, Zarins, CK, Giddens, DP, Bassiouny, H, Loth, F, Jones, SA, & Glagov, S. (1993). Hemodynamic patterns in two models of end-to-side vascular graft anastomoses: effects of pulsatility, flow division, Reynolds number, and hood length. *Journal of biomechanical engineering, 115*(1), 104-111.

Wilcox, David Alem. (1994). Simulation of Transition with a Two-Equation Turbulence Model. *AIAA Journal, 32*(2), 247-255. doi: 10.2514/3.59994

Wilson, R. F., Johnson, M. R., Marcus, M. L., Aylward, P. E., Skorton, D. J., Collins, S., & White, C. W. (1988). The effect of coronary angioplasty on coronary flow reserve. *Circulation, 77*(4), 873-885.

Yamashita, Takehiro, Nishida, Takahiro, Adamian, Milena G, Briguori, Carlo, Vaghetti, Marco, Corvaja, Nicola, . . . Tobis, Jonathan M. (2000). Bifurcation lesions: two stents versus one stent—immediate and follow-up results. *Journal of the American College of Cardiology, 35*(5), 1145-1151.

Zeev Vlodaver , Robert F. Wilson , Daniel J. Garry. (2012). *Coronary Heart Disease*.

Zendehbudi, GR, & Moayeri, MS. (1999). Comparison of physiological and simple pulsatile flows through stenosed arteries. *Journal of Biomechanics, 32*(9), 959-965.

Zhang, Chi, Xie, Sheng, Li, Shuyu, Pu, Fang, Deng, Xiaoyan, Fan, Yubo, & Li, Deyu. (2012). Flow patterns and wall shear stress distribution in human internal carotid arteries: the geometric effect on the risk for stenoses. *Journal of biomechanics, 45*(1), 83-89.

LIST OF PUBLICATION

1) **Sarfaraz Kamangar**, Govindaraju Kalimuthu, Irfan Anjum Badruddin, A. Badarudin, N. J. Salman Ahmed, and T.M. Yunus Khan. Numerical Investigation of the Effect of Stenosis Geometry on the Coronary Diagnostic Parameters. The Scientific World Journal, Volume 2014, Article ID 354946, 7 pages. doi.org/10.1155/2014/354946

2) **Sarfaraz Kamangar**, Irfan Anjum Badruddin, A. Badarudin, N. Nik-Ghazali, Govindaraju Kalimuthu, N. J. Salman Ahmed, and T.M. Yunus Khan. Influence of stenosis on hemodynamic parameters in the realistic left coronary artery under hyperemic conditions, **In Press** (http://dx.doi.org/10.1080/10255842.2016.1233402)